ISSN 2521-6376

Journal of Baku Engineering University

MECHANICAL AND INDUSTRIAL ENGINEERING

Volume 9
Number 1
2025

Journal is published twice a year
Number-1. June, Number-2. December

An International Journal

http://journal.beu.edu.az

Contact address

Journal of Baku Engineering University
AZ0102, Khirdalan city, Hasan Aliyev str. 120, Absheron, Baku, Azerbaijan

Tel: *00 994 12 - 349 99 66/78* ***Fax:*** *00 994 12 349-99-90/91*

e-mail: *journal@beu.edu.az*
web: *http://journal.beu.edu.az*
facebook: *Journal Of Baku Engineering University*

ISSN 2521-6376

ISSN 2521-6376

BMU
BAKI MÜHƏNDİSLİK UNİVERSİTETİ

Journal of Baku Engineering University

MECHANICAL AND INDUSTRIAL ENGINEERING

Baku - AZERBAIJAN

Journal of Baku Engineering University

MECHANICAL AND INDUSTRIAL ENGINEERING

2025. Volume 9, Number 1

CONTENTS

2025. Volume 9, Number 1 ***Pages 3-8***

UOT 536.77:547.442
DOI: https://doi.org/10.30546/09085.2025.01.001

THE INVESTIGATION OF THE PROPERTIES OF THERMAL WATER "KHACMAZ" (p, ϱ, T) IN KHACMAZ DISTRICT, AZERBAIJAN

M. M. BASHIROV

Baku Engineering University, Hasan Aliyev str., 120, Khirdalan, AZ0102, Azerbaijan
mbashirov@beu.edu.az

N. D. NABIEV

Baku Engineering University, Hasan Aliyev str., 120, Khirdalan, AZ0101, Azerbaijan
nnabiyev@beu.edu.az

N. S. RZAYEV

Baku Engineering University, Hasan Aliyev str., 120, Khirdalan, AZ0102, Azerbaijan
nrzayev@beu.edu.az

A. M. NAMAZOVA

Technical Humanitarian Lisey, Azerbaijan, Baku, Nasimi r, 20 January str.60, AZ 1102
aytan_namazova@yahoo.com

ARTICLE INFO

Article history:
Received: 2025-01-08
Received in revised form: 2025-01-08
Accepted: 2025-01-22
Available online

Keywords:
density, pressure, temperature, thermal waters.
JEL Classification: L95, Q25, Q51

ABSTRACT

The experimental laboratory, in which the properties of thermal water "Khachmaz" (p,ρ,T) in Khachmaz district, Azerbaijan were investigated, was air-conditioned at a constant temperature of T=293.15 K. The results obtained for the aqueous solution of water, toluene and NaCl (m=2.96661 mol·kg^{-1}) were compared with the data given in various sources. The obtained results are presented graphically in the figures. In article, the dependence of the density of Khachmaz thermal water of the Khachmaz region of Azerbaijan on the temperature of ρ/(kg · m^{-3}) was measured in the high-precision temperature range T = (278.15-468.15) in a tubular densimeter 5000M Anton-Paar DSA. Using experimental values at selected temperatures, analytical relationships of thermal water were established. The obtained values are described by mathematical equations.

1. Introduction

There are various geothermal technologies in the world with different levels of development, which are widely used in district heating systems, greenhouses and other applications. The technology of generating electricity from naturally high-conductivity hydrothermal tanks is also considered reliable. The majority of the geothermal power plants currently in operation in the world are based on dry steam turbines or "flash" devices (single, double and triple) and are used at 180 °C above hot water sources. Furthermore, new technologies are presently being developed, such as Enhanced Geothermal Systems (EGS)

Another option for a geothermal power plant uses natural geothermal resources, such as, water heated to a high temperature as a result of natural processes. However, the scope of such resources is limited. For example, in Russia, Kamchatka and Caucasian mineral water regions are among them. Otherwise, as a result of high geological pressure, water itself freely rises through a specially dug hole. This is a general operating principle that is applicable to almost all types of geothermal power plants.

Also, the substantial work is being carried out in this direction in Azerbaijan. By decision of the Republic of Azerbaijan dated October 21, 2004, the Ministry of Energy was instructed to ensure the implementation of the provisions of the State Program on "the Use of Alternative and Renewable Energy Sources". The State Program reflects the applications of energy sources that are convenient for our republic in this area, such as the use of wind energy, solar energy, geothermal waters, hydroelectric power of mountain rivers, canals, as well as the use of biomass energy. There are also fundamental possibilities of using the internal heat from the Earth's subsoil. According to the temperature, water or steam-water mixture can be used for hot water supply and heat supply, for the production of electrical energy, or for all of these purposes simultaneously. High-temperature heat of near-volcano areas and hot dry rocks are preferably used to generate electricity and heat. The potential total operating capacity of global geothermal power plants lags behind that of most other power plants using renewable energy sources. However, the high energy intensity of individual geographical regions where fuel and minerals are not available or relatively expensive, as well as government programs are developing in this direction.

2. The problem statement and solution

From 1950 to the present, the works of all researchers in Azerbaijan contain a lot of diverse and valuable information about the sources of mineral waters in different regions of the republic. Also, many questions of their formation and genesis are still insufficiently worked out and require in-depth study. This issue depends on solving the problems of prospecting and rational use of hydro-mineral resources. In hydrochemical and hydrodynamic approaches, the transition zone from less mineralized water to saline water, which is of greater interest in terms of the detection of different types of mineral waters, has not been studied yet.

The temperature of the mineral waters of Azerbaijan fluctuates between 4-65^{0}C. This applies only to natural water sources. At the same time, water with a temperature of 95°C is extracted from the bowels of the earth in Azerbaijan.

The investigated thermal waters were taken directly from their exit zones and prepared for experimental purposes by various chemical processing methods. These areas are rich in nitrogen and hydrogen sulfide thermal and cold mineral springs. Sodium (Na) constitutes the majority of the chemical elements of the "Khachmaz" geothermal power resource in Khachmaz district, Azerbaijan. It accounts for approximately 72.41÷90.12% of all chemical substances of the "Khachmaz" geothermal power resource in Khachmaz district, Azerbaijan. Before conducting the main experiments, the operating capacity of the experimental device to be used was confirmed by conducting verification experiments with materials that have high-quality experimental data. Since this vibrating tube method needs to be calibrated with at least two substances, water and aqueous NaCl solutions, methanol, ethanol and toluene were chosen as the main substances used for the calibration for this purpose. The process of

calibration was analyzed. After the calibration procedure, the calibrated items were repeatedly measured and the average error of the comparisons was analyzed. In a number of cases, the experiments were repeated 4-5 times at the same temperatures, and the operating capacity of the device was checked at different times, regardless of its charging difference and the experiment. The laboratory where the experiments were conducted was air conditioned at a constant temperature of T=293,15 K. The comparison of the results obtained for the aqueous solution of water, toluene and NaCl (m=2,96661mol·kg^{-1}) with the information given in the literature is shown in figures 1, 2 and 3.

3.Discussion of the research work and its results:

As shown in the figures below, the difference between the newly obtained density data and the data given in the literature does not exceed the estimated errors of the measurements on this device. Bi-distilled water was obtained in various laboratory facilities. NaCl, methanol and other reagents were purchased from Merck company (Germany). The results were always close to each other with small errors. All this testifies to the high accuracy of the developed experimental device.

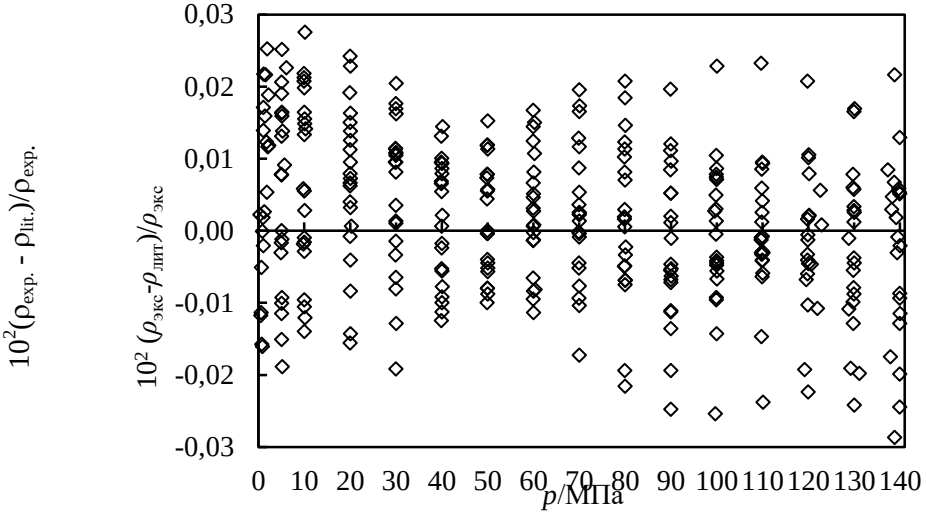

Fig. 1. Dependence of measured water density on pressure at temperature T=(278,15-468,15) K and difference from literature data IAPWS 95

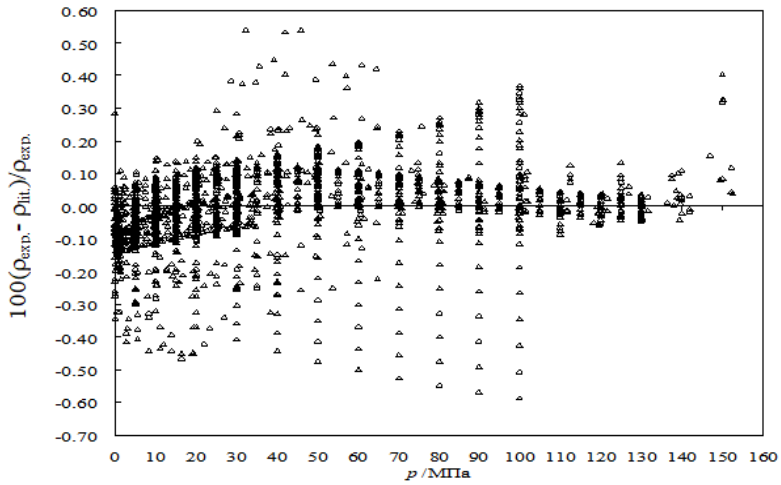

Fig. 2. Dependence of the measured density of toluene on pressure at a temperature of T=(278,15-468,15) K and the difference with data from various literature (data up to 2000).

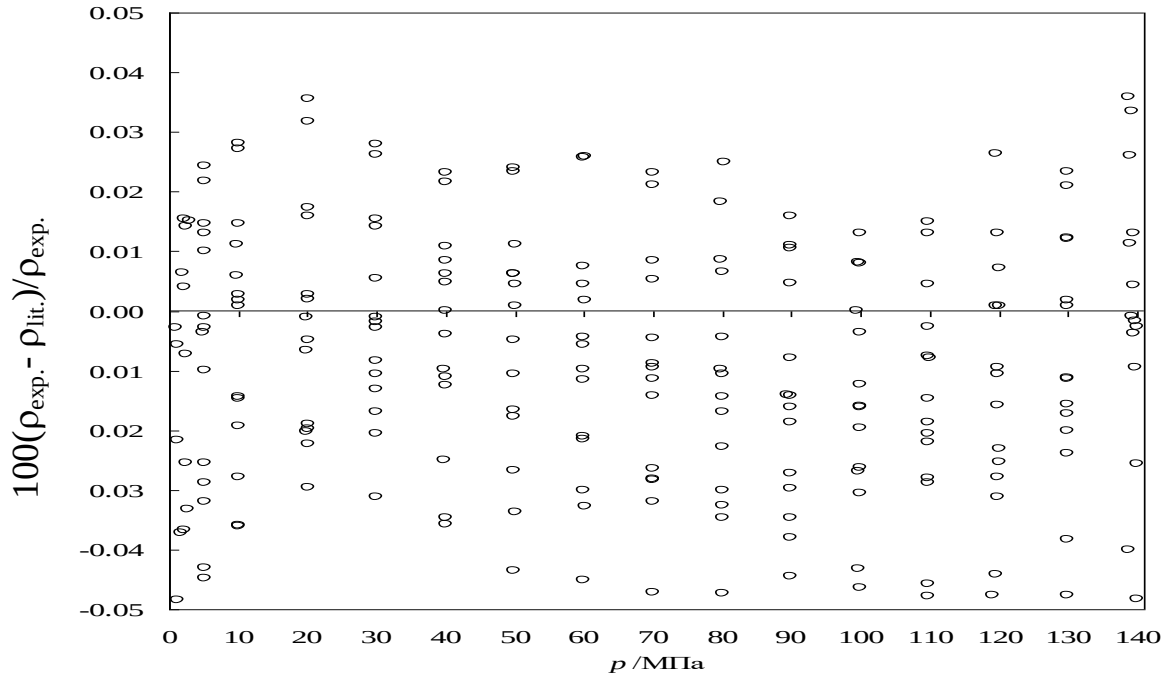

Fig. 3. Dependence of the measured density of aqueous NaCl solutions (m=2,96661 mol·kq¹) at temperature T=(278,15-468,15) K and difference with data from different literature (data up to 2000).

After testing water, NaCl, methanol, ethanol and toluene (p, ϱ, T), dependences (p, ϱ, T) of thermal water in Khachmaz district of Azerbaijan, as well as high pressure and experimental device where vibration tube method is implemented at different temperatures were measured.When measuring the dependences (p, ϱ, T) in each equilibrium state, it was sought to create as low pressure values as possible in order to obtain highly accurate density values using graphical extrapolation at atmospheric pressure, which were compared with the values of density measured on the DMA 4500 device. The data obtained by these different methods are in good agreement within ±0.02%. Each isotherm experiment was performed with pressure intervals of approximately 5 MPa. Researches for all studied objects were conducted at temperatures starting from T=(278.15÷373.15) K and pressures up to p=40 MPa. The obtained experimental parameters (p, ϱ, T) are given in table 1.

Table 1. **Experimental values of the density of thermal water "Khachmaz" in Khachmaz district, Azerbaijan at various pressures and temperatures**

$\frac{p}{MPa}$	$\frac{\rho}{kg \cdot m^3}$	$\frac{T}{K}$	$\frac{p}{MPa}$	$\frac{\rho}{kg \cdot m^3}$	$\frac{T}{K}$
0.624	1004.04	278.15	1.160	989.32	328.02
5.004	1006.21	278.15	5.024	990.99	328.04
10.023	1008.65	278.16	10.079	993.00	328.17
15.012	1011.05	278.15	15.576	995.38	328.18
20.035	1013.43	278.14	19.985	997.22	328.19
25.036	1015.76	278.15	25.527	999.61	328.17
30.054	1018.07	278.15	30.023	1001.50	328.14
35.124	1020.37	278.14	35.513	1003.58	328.12
40.021	1022.56	278.15	39.978	1005.37	328.06
0.539	1002.59	288.14	0.846	981.22	343.15
5.006	1004.66	288.16	5.097	983.06	343.16

9.855	1006.87	288.17	9.967	985.17	343.14
15.151	1009.25	288.17	15.525	987.55	343.15
20.064	1011.43	288.17	20.000	989.45	343.15
25.121	1013.64	288.16	25.586	991.82	343.14
30.103	1015.79	288.16	30.045	993.68	343.16
35.111	1017.92	288.16	35.514	995.98	343.15
40.145	1020.04	288.15	40.050	997.87	343.15
1.025	1000.15	298.27	0.846	974.29	354.24
5.079	1002.02	298.22	5.097	976.23	354.25
9.818	1004.22	298.22	9.967	978.33	354.27
15.593	1006.61	298.17	15.525	980.63	354.27
20.018	1008.46	298.13	20.000	982.58	354.27
25.104	1010.69	298.13	25.586	984.92	354.27
30.155	1012.85	298.12	30.045	986.83	354.28
35.089	1014.82	298.13	35.514	989.17	354.27
40.040	1016.88	298.13	40.050	991.07	354.27
0.898	995.52	313.08	1.626	962.02	372.90
4.995	997.25	313.10	5.059	963.59	372.90
9.972	999.20	313.15	10.042	965.73	372.96
15.563	1001.65	313.17	15.525	968.08	372.97
20.008	1003.42	313.20	20.014	970.00	372.99
25.534	1005.80	313.18	25.596	972.31	373.00
30.057	1007.65	313.19	30.001	974.44	372.90
35.586	1009.82	313.17	35.576	976.79	372.91
39.970	1011.52	313.15	40.013	978.53	372.92

Isotherms are plotted in p-ϱ coordinates in the pressure range of 0,1-40 MPa (Figure 4).

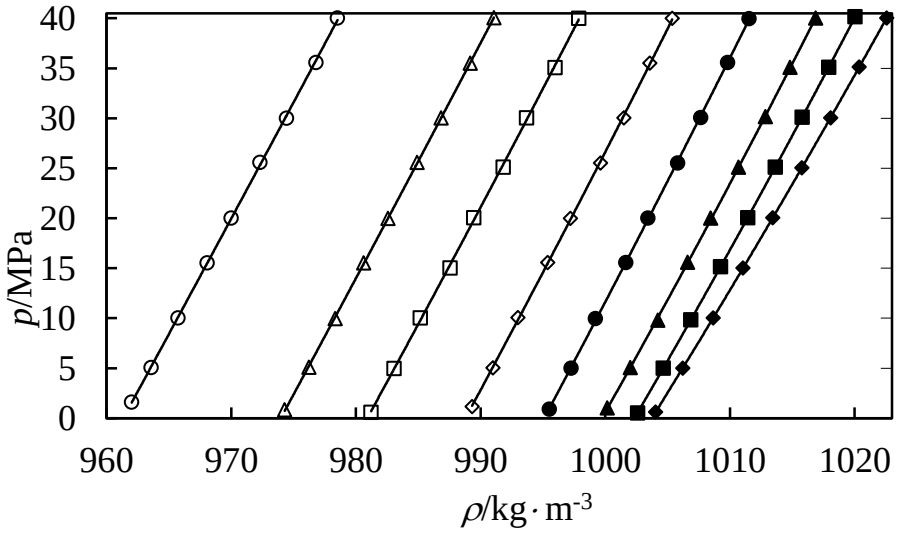

Fig. 4. Dependence of pressure (p) on density (ϱ) of thermal water "Khachmaz" in Khachmaz district, Azerbaijan, calculated according to formulas 1-2: ♦, 278,15 K; ■, 288,16 K; ▲, 298,17 K; •, 313,18 K; ◊, 328,18 K;□, 343,15 K; Δ, 354,27 K; ○, 372,96 K.

The measured density of thermal water "Khachmaz" in Khachmaz district, Azerbaijan was also calculated on the DMA 5000M device at atmospheric pressure with an accuracy of 0.01% (more precisely than at high pressures). This device allows accurate measurements at temperatures up to T = 363,15 K. The results obtained are written by the following equation of state:

$$p = A\rho^2 + B\rho^8 + C\rho^{12} \qquad (1)$$

It is proved that with an increase in the third limit of the Akhundov-Imanov equation, the error in the description of experimental data decreases to $\Delta\varrho/\varrho=\pm(0.001\div0.003)\%$. The coefficients A(T), B(T) and C(T) depend on temperature in polynomial form:

$$A(T) = \sum_{i=1}^{3} a_i T^i,\ B(T) = \sum_{i=0}^{2} b_i T^i,\ C(T) = \sum_{i=0}^{2} c_i T^i \qquad (2)$$

The values of the coefficients a_{ij}, b_{ij} və c_{ij} in equation (2) are given in table 2.

Table 2.

a_1= -3.9508587	b_0= 8322.6444921	c_0= -6583.286607275
a_2= 0.019210690563	b_1= -56.828468335	c_1= 45.23492762848
a_3= -0. 3685081337·10^{-4}	b_2= 0.103286734291	c_2= -0.07893862924

Equation (1) makes it possible to write down the experimental values of the dependence of thermal water "Khachmaz" (p, ϱ, T) with an average error of 0.007%, taking into account the values of the coefficients A(T), B(T) and C(T).

REFERENCE

1. State Program on the Use of Alternative and Renewable Energy Sources in the Republic of Azerbaijan (approved by Decree of the President of the Republic of Azerbaijan. No. 462 dated October 21, 2004.
2. N.D.Nabiev, M.M.Bashirov, J.T.Safarov, A.N.Shahverdiyev, E.P.Hassel. (2009). Thermodynamic properties of geothermal power resources (Khachmaz Sabir-Oba) of Azerbaijan. Journal of Chemical and Engineering data, Vol. 54,No.6.
3. N.D. Nabiyev (2011). "The investigation of thermal-physical properties of geothermal power resources in Khachmaz district, Azerbaijan". Dissertation submitted for the degree of Doctor of Philosophy in Technology, Baku, page 177.
4. Wagner W., Pruß A.(2002). The IAPWS formulation 1995 for the thermodynamic properties of ordinary water substance for general and scientific use //Journal of Physical Chemistry Reference Data, vol. 31, p. 387-535.
5. Yokoyama O., Uematsu M. (2003).Thermodynamic properties of {xCH_3OH+(1-x) H_2O} with x = (1.0000, 0.8005, 0.4002, and 0.3034) in the temperature range from 320 K to 420 K at pressures to 200 MPa // The Journal of Chemical Thermodynamics, vol.35, p. 813-823.

2025. Volume 9, Number 1 ***Pages 9-16***

UOT: 519.87; 62-50; 004.8; 681.3
DOI: https://doi.org/10.30546/09085.2025.01.005

ENHANCING DECISION-MAKING IN DYNAMIC SYSTEMS THROUGH SYSTEMATIC ANALYSIS AND TECHNOLOGICAL INTEGRATION

ELVIN E. NASIROV
Baku Engineering University, Hasan Aliyev str., 120 AZ0101,
Khirdalan, Absheron, Azerbaijan
enesirov7@std.beu.edu.az

ZAHRA V. ZARBALIYEVA

Baku Engineering University, Hasan Aliyev str., 120 AZ0101,
Khirdalan, Absheron, Azerbaijan

zzerbeliyeva1@std.beu.edu.az

ARTICLE INFO

Article history:
Received: 2025-01-24
Received in revised form: 2025-02-04
Accepted: 2025-03-04
Available online

Keywords:
Systematic analysis; Decision-making models; Dynamic systems; Operational efficiency; Artificial intelligence.
JEL Classification: C61, C63, O33

ABSTRACT

The focus of this paper is on systematic approaches towards effective decision-making in complex adaptive systems through the application of chosen tactics aimed at increasing the accuracy of the decision-making process and the efficiency of the operations. Decision-making in organizations is a daunting task in the face of complexity and unpredictability which is the defining feature of dynamic systems. This paper also surveys the literature in decision-making and estimation, in particular, multi-criteria decision analysis MCDA and system dynamics, as well as Pareto optimization. The goals of this paper are to show the readers how these models, in their practical application, have been enhanced through the integration of modern technologies such as AI or ML for optimized decision-making in fast evolving and volatile environments. The results indicate that if employed and executed properly, systematic analysis can do wonders in improving the manner in which decisions are made and the performance of the organization as a whole. The study further examines the tension when decisions are being made in real-time such as the interplay between the quality of information and the complexity of the model. In particular, this paper asserts that systematic analysis can be effectively utilized across industries.

INTRODUCTION

Dynamic systems are essential in a number of industries and sectors namely, production, logistics, health care, environmental, and financial. Such systems are also very sophisticated and have a very high level of tolerance meaning that the decision makers are always at the case and have to be on the move to make decisions. Considering the high level of competition in the market, there are a number of variables that organizations have to deal with such as demand and supply, proper management of supply chains, technological

development and also legal requirements.[2] A clear characteristic of dynamic systems is that they are connected to one another. So, when one part is altered, it has a chain effect to the other parts of the system and vice versa, making the whole system even more complex and unpredictable than it already is.[3] For example, in international logistics when freight is delayed in one area it results to inefficiency and increased cost in other places. Such situations point out the issue of selective modification required not only to tackle present concerns but also future dynamics regarding the workings of the system. Systematic analysis emerges as a pertinent mechanism of addressing concerns arising from dynamic systems. It addresses systems theory and use system problems and relations between the parts of the system. In order to solve complex problems, decision makers need a systematic analysis, which enables them to determine patterns, assess tradeoffs and optimize outcomes by breaking down problems into parts.[5] This type of decision making is used greatly in industries where effective optimization of operations along with accurate decision makes the business able to sustain competition in the marketplace. Participation of other multi criteria decision making models, for instance, system dynamics, and Pareto optimization have also made the systematic analysis more useful.

The models add quantitative and qualitative data to system dynamics to allow an organization to make decisions that can prioritize different pressures and still be effective. For instance, there are low scales of optimization of the production schedules and use of the MCDA in the manufacturing sector to target waste cutting and energy use. The introduction of the modern technologies like AI, ML, and big data analytics has made it possible to systematically analyze data at a different level. With these technologies data can be processed and modeled in real time and also scenarios can be simulated in a way that provides insights that are so critical for making decisions. The modern societies are hostile or rapid changing environments, the systematic analysis and the advanced technology will assist the structures of motivation and the selection of strategies that help reduce the effective change volatility.[1] The primary purpose of this paper is to identify in a general manner as to how systematic analysis can enhance the systems decision making. Thus, while presenting an analysis of theoretical backgrounds, applications of descriptive norms, and the problems encountered in implementation, this research aims to contribute to the development of practical recommendations for practitioners and future studies. [4] Further, the study examines the possibility of concrete parallelism in auspices for sustainable initiatives, especially for rising business sectors struggling with challenges of financial profitability on the one hand and environmental stewardship on the other hand. In conclusion, it is the intent of this study to show that if the concept of systematic analysis is to remain relevant to the ever-evolving fields of study the systematic analysis needs to be a reality in the current world. Proper use of systematic analysis places companies in a more favorable light to cope with complexity thus delivering both operational efficiency and strategic value.

LITERATURE REVIEW

The application of systematic analysis for dynamic systems has been studied extensively in different fields among them in the industrial, logistical and service industries. Research has well pointed out that decision making is an obscure terrain particularly in a stochastic environment whereby contending components interact in a given system. The application of systematic analysis in these contexts provides the state-of-the-art approach for decision-making in order to enhance the quality of decisions and the effectiveness of the processes as well as management of means. The relevance of this approach is most apparent in industries concerned with tangible

products like manufacturing and logistics sectors, as well as the healthcare industry where the deployment of decisions made yields considerable consequences for cost, time and general system characteristics. The systematic analysis of the WSN design comprises one of the most popular and efficient methods that are referred to as Multi-Criteria Decision Analysis (MCDA). MCDA has been most used in the scheduling of production, the transportation networks and managing inventories. In the case of the logistics sector, for instance, MCDA has been employed to analyze supply chain management where the utilization of resources must balance need to meet clients demand. Likewise, System Dynamics which is another major methodology in systematic analysis has used for predicting the dynamics of the systems with time underpinning the feedbacks and interactions. SD has been useful in the implementation and projection of the unforeseeable results of decisions made in areas like energy, transport and the environment. Pareto Optimization of objectives along with the systematic analysis or decision-making that seeks to identify the best tradeoff between two conflicting objectives is also a large tool in the field of systematic analysis. This method has been implemented to effective decision making on resource deployment, production scheduling, and even on sustainability opportunities in industries running into the problem of the profit-loss equation and its impact on the environment and social responsibility. Nevertheless, there is still a significant gap between these systematic models and real-time decision-making systems, to which they are too often apply.

It is, therefore, clear that most of the current studies have focused more on theoretical models, or offline optimization methods that do not capture the dynamic and fast-evolving systems in the current world. For example, simulations and optimization mean so much but they heavily rely on non-real time data or heinous assumptions of the dynamic environment. In addition, there appears to be a dearth of literature on the use of more advanced technologies in performance modeling, including Artificial Intelligence (AI) and Machine Learning (ML).[7] In order to fill these gaps, this paper will center its discussion on the combination of systematic analysis with real-time decision-making systems, using AI and ML. These technologies can improve the accuracy of systematic models, and improve the ability of decision-makers to address changes in real time. For instance, AI and ML can analyze large amounts of data at a very fast rate, but also to recognize patterns in data, and provide insights that can improve the decision-making process in contexts characterized by risk and volatility. In addition, integration of the approaches can improve questions that may be associated with data quality, model capacity, and scalability of the systems used in making decisions. In this paper, the author aimed at synthesizing previous findings on the systematic models and an attempt to examine the existing issues' strengths and limitations while discussing the implications of AI and ML. It aims at present a systematic information-sharing approach for illustrating how these sophisticated technologies can enhance decision-making in the complex system, thus enhancing the systemic effectiveness, productivity, and viability of organizations, all vying in uncertain contexts.[6]

THEORETICAL BACKGROUND

An approach to conducting a systematic analysis for decision-making in dynamic systems comes from systems theory which in turn considers elements of the systems as intricately linked to one another. As Ludwig von Bertillon, the father of general systems theory has it, the behavior of any given system is a product of the interactions between elements of the system and not the interactions between the parts. This integrated approach is critical in describing complex and open systems with far reaching consequences where tweaks in one part may cause disruption to the whole system.[10]

1) Key Decision-Making Models

Several models are integral to systematic analysis in dynamic systems:

- Multi Criterion Decision Analysis (MCDA) aids in the assessment of multiple conflicting factors in a single decision-making process. It is now applied in such sectors like manufacturing, logistics and environmental to facilitate right decision making within the specified factors such as cost, risk and time.[8]
- System Dynamics (SD) is a method that was designed to show how systems behave within frameworks of positive feedback feedback loops, and time lags. Hence it is especially handy in modeling future repercussions of some decisions, say in logistics or medicine.[8]
- Pareto Optimization is that the process of making decisions which means that ranking objectives and balancing the positive results against the negative impacts of change to avoid worsening any goal, while seeking to enhance the other. It is deemed appropriate for deciding efficient use of the resources in a changing environment.[8]

2) Use of modern technology in production line

AI and ML improves systematic analysis through real time data processing, predictive data analytics and automated decision making where necessary. Applications of AI and ML models enhance decision-making since they provide highly accurate solutions in situations where there is ambiguity and fluctuating conditions more so in the supply chain and production. [8]

3) Challenges in Decision-Making

However, it has been known that systematic analysis has certain limitations such as data quality, complexity of the model, and incorporation of real time data. Even if data is not entirely accurate or complete, the decisions made using the data may be flawed, on the other hand, complex models make understanding and acceptance of their conclusions hard.[8]

4) Role in Decision-Making

Decision-making is well-coordinated when there are a flow, feedback, trade-offs, and other factors are considered systematically as encompassed by systematic analysis. The integration of AI and ML further enhances decision-making in dynamic environments, improving both efficiency and adaptability.

RESEARCH METHOD

The approach taken by this paper is that of qualitative research with a view of extending the application of systematic analysis in dynamic systems. The reason why the qualitative approach is selected is that this approach takes into account the factors that characterize decision making processes and the context in which they occur in practice. The research mainly focuses on action research, case studies and simulations with respect to decision making models and its actual application in working organizations especially in manufacturing and service sectors. Management decision-making models used in this study are Multi-Criteria Decision Analysis (MCDA) and Pareto Optimization. [7] MCDA is applied in order to evaluate and rank more than one solution simultaneously when trade-offs are present: all criteria are considered leveraged to the expected extent. For instance, in manufacturing the MCDA can be used to assess the best manufacturing procedure by comparing the cost, time and resource use. For organizations in service delivery, it assists in the distribution of resources in an efficient manner whilst at the

same time delivering desirable satisfaction levels among customers. Pareto Optimization is used to take decisions on the tradeoff between two objectives where one wants to optimize one objective while keeping other objectives as low as possible in order not to harm other aspects. In specific, logistics can try by use of Pareto Optimization where one tries to provide the best outcome in two elements such as the cost of transport and time for delivery.[9] Furthermore, there are simulations to detect and compare decision making approaches under actual circumstances. As the research explores plausible situations it analyses present decisions on future system behaviors taking feedbacks and system dynamics into consideration. The simulations also demonstrate how decision support systems CDRSS can be supported using technological assets of AI and proximate learning systems in real time decision support. The use of these methodologies is to show the effectiveness of systematic analysis in enhancing decision making of dynamic systems for effective performance hence sustainable results.

CHALLENGES IN DYNAMIC SYSTEMS

Systems are dynamic, and this in itself creates a number of issues with regard to decision making, firstly they are unpredictable, secondly, they are constantly changing. These are due to coupling between the elements of the system, risk and the necessity for synchronization of the decision making.[9]

1) Uncertainty and Complexity

The systems dynamics models are very responsive to changes and variations and this implies that-even if a slight change is made – a big difference is noticed. For instance, in the manufacturing industry, slight variations in the manufacturing procedures cause significant disturbances affecting the supply systems and chain both in terms of time and costs.

2) Data Quality and Availability

Timely and relevant information is important in the decision making of an organization. However, dynamic systems have related issues such as, data inconsistencies, incomplete data and delays which limits the applicability of decision models including MCDA or System Dynamics.

3) Feedbacks and non-linear coupling

Complex adaptive systems are yet intertwined by feedback and present nonlinear relations. Little negatives or positives may build up over time as they are magnified creating confusion, where decision makers need to consider both the proximate gains or losses and the ultimate impact of their decisions.

4) Decision Support and Flexibility in Real Time

Implementation of real-time decision support is relatively difficult as information flow may be slower and environments dynamic. The structure of decision-making models has to be very adaptable to changes because of the high dynamic nature of the system.

5) Decision making models provide the opportunity to scale up decision making within an organization.

Decision making models are the cornerstone of an enterprise's success, but as systems continue to grow more massive, the model's scalability becomes problematic. For extended structures like global supply chains, more sophisticated models are needed on account of the growing quantity of parameters and interrelations.

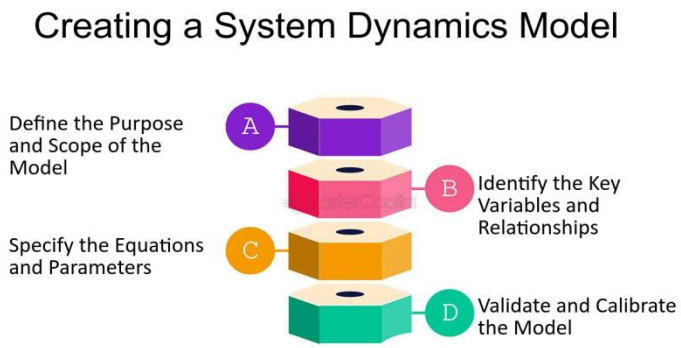

Figure 1: Creating a System Dynamics Model [9]

TECHNOLOGICAL INTEGRATION IN DECISION-MAKING

In dynamic environment the application of advanced technologies like artificial intelligence and machine learning, big data analytics has enhanced decision making processes. They provide capability to analyze large, big data sets, detect and understand patterns, and make optimized decisions in near-real time, thus improving overall flexibility in heavily kinetic landscapes. [2]

1) Role of AI and ML

AI and ML are core enablers of technological solution deployment in decision making. Machine learning algorithms continuously mine extensive data and then estimate the best course of action. For example, in the supply chain sector, it generates demand forecasts, determines the best way to deliver goods, and avoid excessive expenses. While, Machine Learning, gets adapted to data and learns progressively to make better predictions and better decisions in the future. In the field of healthcare, the use of ML is to try to predict the status of a patient which will lead to efficient usage of resources and increase in the right measure of treatment.

2) Big Data Analytics

Dynamic systems produce massive volumes of data known as big data which cannot be processed by conventional decision-making tools. Big Data Analytics ensures that organizations are able to manage this incoming and outgoing information to find out significant trends existing within an organization. For instance, in the financial sectors, big data analytic is applied in risk evaluation d and formulation of preventive measures.

3) Decision-making models are one of AEP's strengths; integrating them is its weakness.

AI and ML supplement conventional decision-making frameworks including the Multi Criterial Decision Analysis (MCDA) and System Dynamics (SD). AI-integrated MCDA enhances decision making under conditions of risk and uncertainty, while AI-based SD simulations give decision makers insights into the future consequences of their strategies, and insights into system behavior.

Table -1: Programmability [2]

	Low Task Programmability		High Task Programmability	
	Low Asset Specificity	High Asset Specificity	Low Asset Specificity	High Asset Specificity
Low Non-separability	1. Spot Market	2. Long-Term Contract	5. Spot Market	6. Joint Venture
High Non-separability	3. Relational Contract	4. Clan	7. Inside Contract	8. Hierarcy

DISCUSSION

The conclusion of this investigation supports that systematic analysis contributes towards an improved quality and utility of decisions in complex and unsteady environments. Therefore, if organizations apply other models like the Multi-Criteria Decision Analysis (MCDA), System Dynamics (SD), and Pareto Optimization, it will ease decision making processes in organizations facing more challenging environments. These methodologies enable the decision-makers to compare different contribution factors, probabilistic estimates and optimize the resources adequately.

However, there remain problems in its utilization. Information quality still remains a challenge because inefficient data creates a major problem in making decisions. Furthermore, due to the complexity of many models such as SD and MCDA, they are not easily applicable, especially in large and more complicated systems. Real-time decision-making systems are another challenge, where technologies compatible with the actual infrastructure for performing fast data analysis are integrated.

Every one of these challenges has an opportunity to be addressed by technological solutions like; Artificial Intelligence (AI) and Machine Learning (ML). These tools allow one to make the analysis and optimal decisions rather quickly as well as improve the flexibility of systematic analysis in rapidly changing conditions. Nevertheless, it is crucial to ensure a proper mix of technologies and people because contextual information and ethical concerns remain crucial drivers for the choices made in the organization.

CONCLUSION

Another significant finding apparent from literature synthesis is that the systematic analytical method is a valuable tool in making decisions in organizations operating in dynamic environment, where conditions are volatile, complex and organizations experience change at high rates. Structured models like Multi-Criteria Decision Analysis (MCDA), System Dynamics (SD) and Pareto Optimization when applied can increase accuracy of an organization decision-making, increase organizational effectiveness and reduce organizational susceptibilities. They offer effective strategies for analysis of prospects, treatment of results as well as the maximization of resources in various settings.

The advancement in technology, such as, Artificial Intelligence (AI), Machine Learning (ML), Big Data Analytics have brought the potential of systematic analysis to the next level. These technologies provide users with the ability to process data in real-time, make forecasts and adjust to various conditions, which is possible to achieve due to support of organizations. For instance,

AI and ML can improve production planning, supply chain demand forecasting and improve decision-making in rapidly dynamic environment.

Nevertheless, data quality, model and framework's complexity, and the scalability of using decision-making frameworks are still big issues. Each of these challenges will need more improvements in data governance, generating better and easily interpretable models, and funding for training professionals equipped with adequate legal knowledge to manage such technologies. In addition, decision-makers need to adopt sustainable decision-making frameworks to address organizational performance with sustainable standards and responsibilities.

Thus, the findings of this study make a valuable contribution to the literature for illustrating that incorporations of technology into the processes of marketing and new product development should be combined with human consideration to avoid a negative impact. Though systematic analysis and particularly AI can offer quantifiable analysis, it is the end user who is individually in charge of crucial discernment of the issue at stake, its cultural background, and the values that govern solutions in sectors such as healthcare, environmental science or political science.

REFERENCES

1. Gharajedaghi, J. (2011). *Systems thinking: Managing chaos and complexity: A platform for designing business architecture* (3rd ed.). Elsevier.
2. Hanseth, O., & Bygstad, B. (2018). *Designing dynamic systems: Lessons from sociotechnical theory.* Palgrave Macmillan.
3. Meadows, D. H., & Wright, D. (2011). *Thinking in systems: A primer.* Chelsea Green Publishing.
4. Sterman, J. D. (2020). *Business dynamics: Systems thinking and modeling for a complex world.* MIT Press.
5. Richmond, B. (2014). Systems thinking: A crucial tool for managing complex systems. *Journal of Systems Research, 12*(3), 215–230.
6. Lane, D. C. (2015). Qualitative system dynamics: A new era in modeling. In *Advances in system dynamics modeling* (pp. 45–63). Springer.
7. Kim, D. H., & Senge, P. (2019). Applying system dynamics in smart cities. In *Proceedings of the System Dynamics Society Conference, 2019* (pp. 120–130).
8. Sterman, J. D., & Rahmandad, H. (2017). Modeling feedback in complex systems. *System Dynamics Review, 33*(4), 307–310.
9. Oliva, R., & Sterman, J. D. (2013). Structural dominance in complex systems. In *Handbook of Systems Engineering and Management* (pp. 435–440). Wiley.
10. Borshchev, A., & Filippov, A. (2020). From system dynamics to agent-based modeling: A modern transition. *Simulation Modelling Practice and Theory, 95,* 101–113.

JOURNAL OF BAKU ENGINEERING UNIVERSITY- MECHANICAL AND INDUSTRIAL ENGINEERING
2025. Volume 9, Number 1 ***Pages 17-28***

UOT: 539
DOI: https://doi.org/10.30546/09085.2025.01.011

THE ORGANIZATION OF CATERING SERVICES BASED ON INFORMATION TECHNOLOGY

Z. A. DJAFAROV

Azerbaijan Technical University, H.Javid ave 25, AZ 1073 Baku, Azerbaijan.
zafar.cafarov@aztu.edu.az

M. R. ABBASZADA

Azerbaijan Technical University, H.Javid ave 25, AZ 1073 Baku, Azerbaijan.
abbaszademurad3@gmail.com

ARTICLE INFO

Article history:
Received: 2025-03-05
Received in revised form: 2025-03-05
Accepted: 2025-04-02
Available online

Keywords:
Xcode, Swift, Apple, Food, Order, Navigation Controller, Bar button items, Root changing, User Defaults, File Manager, JSON
JEL Classification: L81, O33, L86

ABSTRACT

The article is dedicated to the use of information technologies in the process of ordering food through a mobile application. Here, users can get information about certain food items, learn their prices, and add their favorite dishes to the cart. Additionally, users must go through login and registration processes to use the application. The profile screen will display the details associated with the user's login. On the Food screen, users can complete the process by pressing the button on the dish they want to add to the cart. This application also provides users with fast delivery and payment options. Meals are divided into various categories, making the selection process easier. Each dish comes with detailed descriptions and reviews. Users can save their favorite dishes and reorder them later. The notification system keeps users informed about the status of their orders. The mobile application uses modern technologies to offer an intuitive and user-friendly interface. Ordering food is easy, fast, and secure. These features make the application stand out.

1. Introduction

Xcode—Xcode is a powerful integrated development environment (IDE) designed by Apple for the macOS platform. It is used to develop applications for iOS, macOS, watchOS, and tvOS. Xcode is intended for both beginner and experienced developers and is one of the most essential tools within the Apple ecosystem.

Key features of Xcode include:

• **Programming language support** – Supports languages such as Swift, Objective-C, Ruby, Python, C++, and C;

• **Simulators** – Allows testing applications on virtual devices for iPhone, iPad, Apple Watch, and Apple TV;

• **Interface Builder** – Works with storyboard and XIB formats;

• **Debugging** – An essential tool for identifying and fixing errors and bugs in real-time.

Xcode is the most optimal environment for developing Apple applications. It can be downloaded for free from the Mac App Store.

Xcode is an indispensable tool for development in the Apple ecosystem, offering powerful features that meet the needs of modern developers.

II. DESCRIPTION OF THE PROCESSING SYSTEM

First, to start the project, we need to download Xcode to our system. After the download process is complete, we open Xcode, click on "Create a new project," and select the "Single App" option. At this point, Xcode generates several functions and classes in the background to enable us to use the simulator and implement the code we will write. The stages of application development can be outlined as follows:

A. Configuring the login and registration screens.

B. Creating a custom class for the main (home) screen and using a collection view.

C. Creating helper classes.

D. Utilizing a JSON file.

E. Preparing the cart and profile screens using a navigation item.

A. Configuration of login and register screens

There are two methods for creating a login screen: using **storyboard** or implementing it programmatically. However, in this article, I will focus on extensive use of storyboard and XIB files. First, we add a view controller to the storyboard. To link this controller to a file, we create a separate view controller class. To establish the connection between the storyboard and the class, we navigate to the **Identity Inspector** section in the storyboard and assign the name of the created class to our screen. The same process can also be applied to the register screen. The register screen will require basic user information, such as the user's name, email, email password, and mobile number. Once the user provides this information, they can navigate to the login screen, where the data entered in the register screen will also be visible. This process is called **data transformation** and can be implemented using closures. Alternatively, it can also be achieved by creating a separate protocol and using a delegate. The information entered by the user during registration will be stored in a separate file, which will be used to verify the accuracy of the login details. If the entered login data does not match the information in the existing file, an error alert will appear on the screen. If the data is correct, the user will be redirected to the main (home) screen.To achieve this, the following UI elements will be used:

UITextField: For entering text inputs like username, email, and password.

- **UIButton**: For actions such as login and register.
- **UIView**: For creating custom animations.

To incorporate animations, one of the most optimal methods is using **Lottie files**. On the Lottie Files website, you can search for and find custom animations that suit your app's needs and integrate them into your code. To use Lottie in Xcode, you can download the Lottie package manager from GitHub. Once the Lottie library is integrated into your project, you can utilize it to enhance your application with custom animations. *(Fig. 1)*

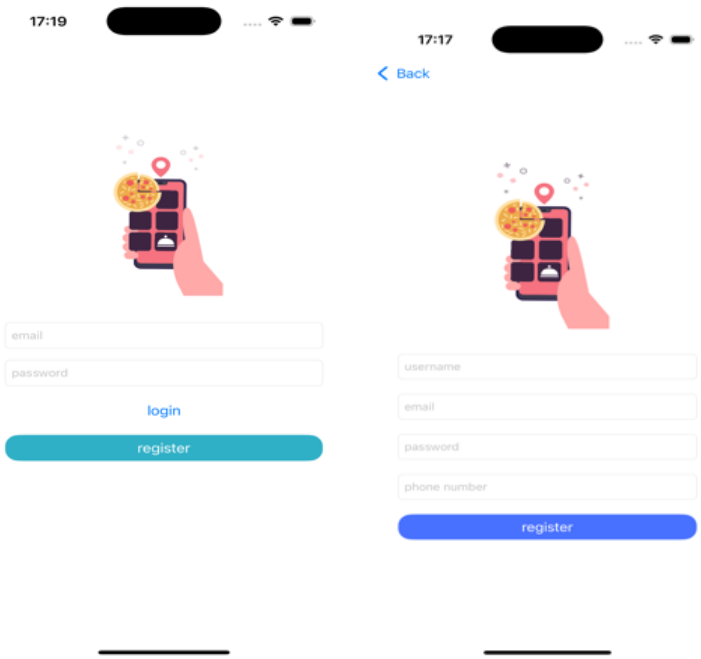

Fig 1. Login and register screens

B. Creating a Custom Class for the Main (Home) Screen and Using Collection View

A **collection view** is used on Apple devices to display multiple images or data items either side-by-side or top-to-bottom. Examples of collection views can be found in market applications or apps for selling clothing or goods. For the home screen, we assign a collection view to the controller in the storyboard. However, we create a **custom class** for the cells and define the cell size and the data to be displayed within that custom class. In addition to the custom class, we also create a **XIB file** for the cell. This XIB file will be used across two screens. One of the advantages of using XIB files is that if the same cell is required on multiple screens, creating it once is sufficient. After creating the cell class, we register it to the collection view on the home screen and call certain protocols to configure it. *(Fig. 2)*

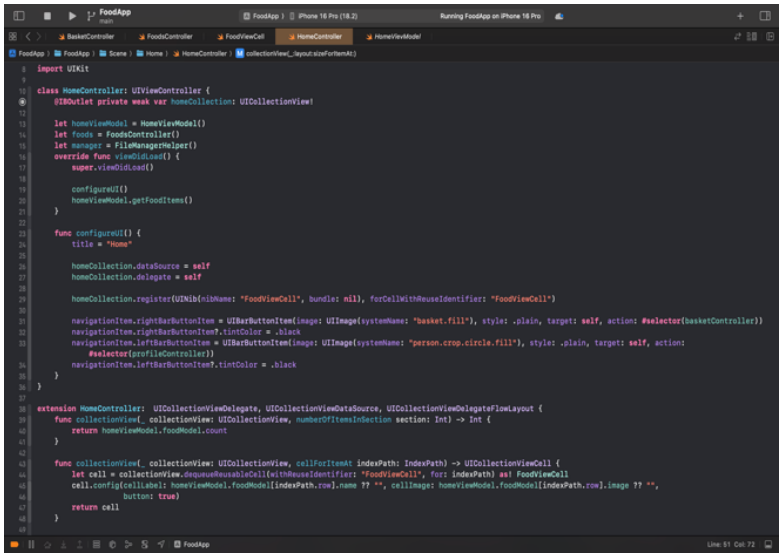

Fig 2. Home controller code description

To keep the code clean and organized in this controller, the following steps can be taken:

• Create a separate function to handle the logic inside **viewDidLoad** and call that function within **viewDidLoad**.

• To avoid cluttering the HomeController class, write an **extension** for it.

• In the extension, call the necessary protocols required for the HomeController. These protocols were mentioned above. Once we conform to these protocols in the extension, some functionalities will need to be integrated into the code. These functionalities are numberOfItemsInSection and cellForItemAt. With the help of these functions, we can display data on the screen and handle navigation between screens.

• Navigation between screens is configured using the didSelectItemAt function. This function allows us to display data and details on the food screen based on the cell clicked on the Home screen.

The Home screen consists of 6 cells, and the **navigation bar** contains 2 items. *(Fig. 3)*

Fig 3. Home controller

When a user clicks on a cell in this view, the corresponding food items will be displayed, and with each click on the button within the food item, that food will be added to the basket screen. In this controller, we will use the same **XIB file** that was used in the Home screen. The only difference is that this XIB file will be registered with the collection view in the **FoodController**. Additionally, as mentioned above, we will conform to the necessary protocols via an extension. This setup will ensure proper functionality for the food selection and basket actions. *(Fig. 4)*

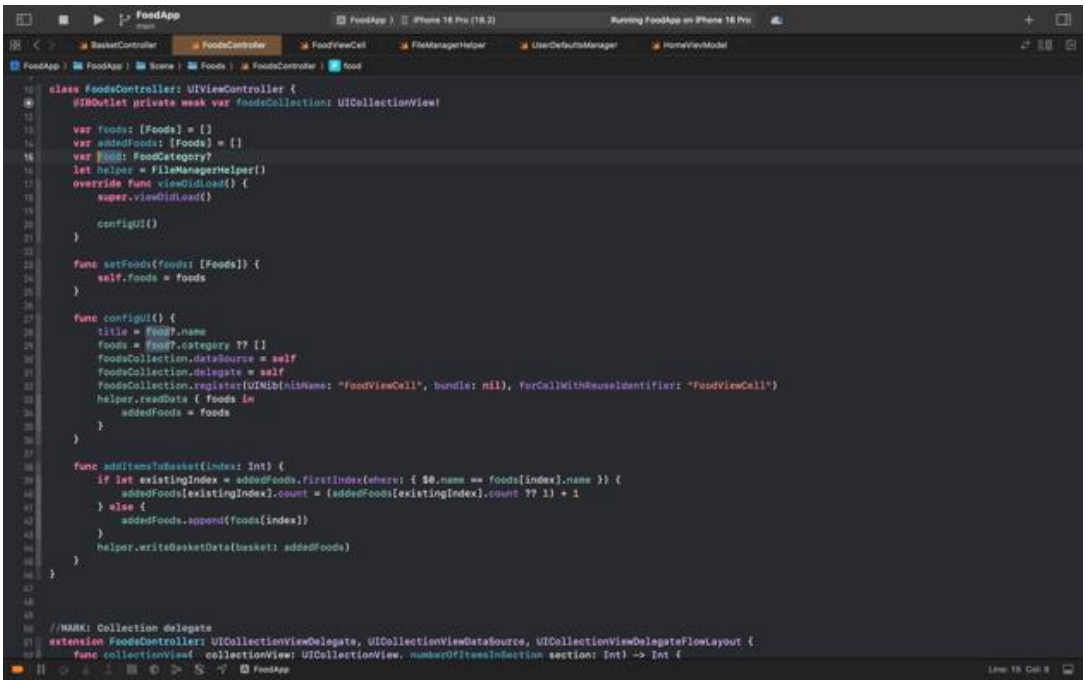

```
class FoodsController: UIViewController {
    @IBOutlet private weak var foodsCollection: UICollectionView!

    var foods: [Foods] = []
    var addedFoods: [Foods] = []
    var food: FoodCategory?
    let helper = FileManagerHelper()
    override func viewDidLoad() {
        super.viewDidLoad()

        configUI()
    }

    func setFoods(foods: [Foods]) {
        self.foods = foods
    }

    func configUI() {
        title = food?.name
        foods = food?.category ?? []
        foodsCollection.dataSource = self
        foodsCollection.delegate = self
        foodsCollection.register(UINib(nibName: "FoodViewCell", bundle: nil), forCellWithReuseIdentifier: "FoodViewCell")
        helper.readData { foods in
            addedFoods = foods
        }
    }

    func addItemsToBasket(index: Int) {
        if let existingIndex = addedFoods.firstIndex(where: { $0.name == foods[index].name }) {
            addedFoods[existingIndex].count = (addedFoods[existingIndex].count ?? 1) + 1
        } else {
            addedFoods.append(foods[index])
        }
        helper.writeBasketData(basket: addedFoods)
    }
}


//MARK: Collection delegate
extension FoodsController: UICollectionViewDelegate, UICollectionViewDataSource, UICollectionViewDelegateFlowLayout {
    func collectionView(_ collectionView: UICollectionView, numberOfItemsInSection section: Int) -> Int {
```

Fig 4. FoodController class

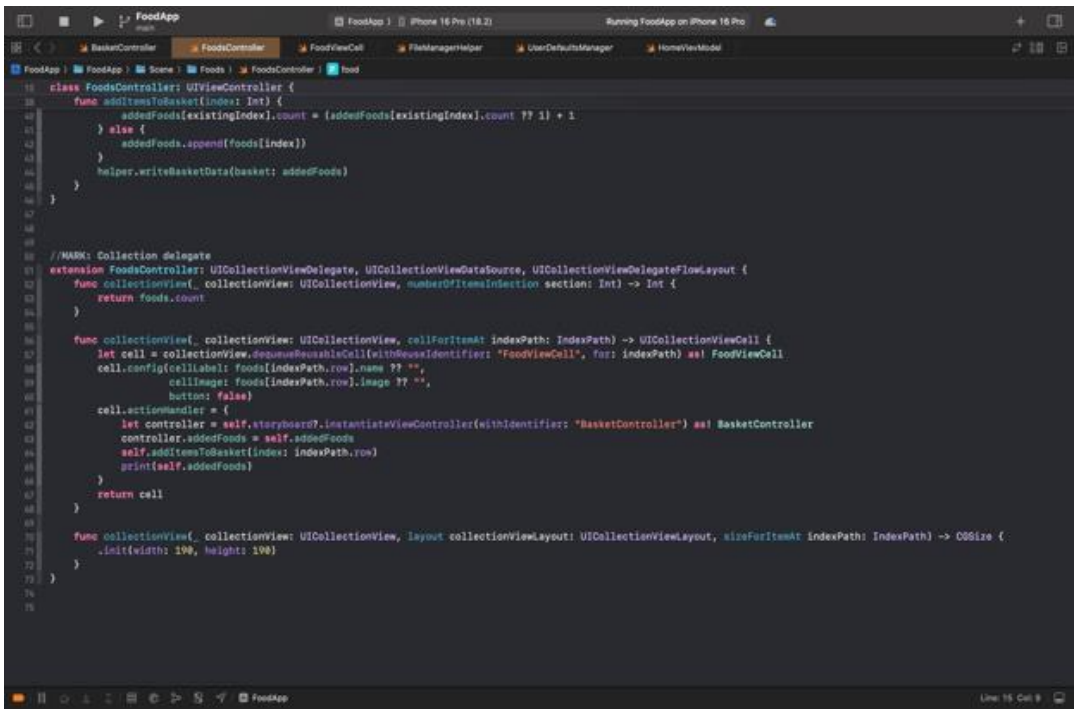

```
class FoodsController: UIViewController {
    func addItemsToBasket(index: Int) {
            addedFoods[existingIndex].count = (addedFoods[existingIndex].count ?? 1) + 1
        } else {
            addedFoods.append(foods[index])
        }
        helper.writeBasketData(basket: addedFoods)
    }
}


//MARK: Collection delegate
extension FoodsController: UICollectionViewDelegate, UICollectionViewDataSource, UICollectionViewDelegateFlowLayout {
    func collectionView(_ collectionView: UICollectionView, numberOfItemsInSection section: Int) -> Int {
        return foods.count
    }

    func collectionView(_ collectionView: UICollectionView, cellForItemAt indexPath: IndexPath) -> UICollectionViewCell {
        let cell = collectionView.dequeueReusableCell(withReuseIdentifier: "FoodViewCell", for: indexPath) as! FoodViewCell
        cell.config(cellLabel: foods[indexPath.row].name ?? "",
                    cellImage: foods[indexPath.row].image ?? "",
                    button: false)
        cell.actionHandler = {
            let controller = self.storyboard?.instantiateViewController(withIdentifier: "BasketController") as! BasketController
            controller.addedFoods = self.addedFoods
            self.addItemsToBasket(index: indexPath.row)
            print(self.addedFoods)
        }
        return cell
    }

    func collectionView(_ collectionView: UICollectionView, layout collectionViewLayout: UICollectionViewLayout, sizeForItemAt indexPath: IndexPath) -> CGSize {
        .init(width: 190, height: 190)
    }
}
```

Fig 4. FoodController extension

In the **FoodController**, we add an "Add" button to the cell, allowing the user to add the desired food items to the basket screen by pressing the button. *(Fig. 5)*

Fig 5. Food Controller screen

Creating helper classes

In this project, there are **2 helper classes** and **3 struct models** used. The struct models are **Foods**, **FoodCategory**, and **User**, and they are utilized for data transfer between screens and displaying data on the UI. The helper classes are **FileManagerHelper** and **UserDefaultsManager**. These classes serve different purposes.

• **UserDefaultsManager** is used mainly for handling small-scale data, such as checking whether the user is logged in or not.

• **FileManagerHelper** is used for storing the user's data in a file when they register.

However, there's an important nuance here: both **UserDefaults** and **FileManager** store data inside the application, meaning that if the app is deleted, all the stored data will be wiped out. In such cases, using **Keychain** is more appropriate because it stores data on the phone itself, not within the app. Keychain is better suited for storing larger data and handling transformations. The best approach for using **UserDefaults** is to create a dedicated class for

it. The class mentioned above is designed to handle this. Inside the class, **enums** and functions are used, with the enum simplifying the creation of instances. This makes the code more readable and easier for other developers to understand. This class will be used mainly in the **SceneDelegate** and **Profile screen**. In the **SceneDelegate**, we check if the user is logged in using **UserDefaults**. If they are, this information is saved in **UserDefaults**. When the user clicks the login button, the information will be saved in memory. At this point, the root screen of the app changes. The **root** determines which screen the user will see when they open the app for the first time or the second time. Logically, if the user is already logged in or registered, these screens will not be shown again. Therefore, when the user clicks the login button, the root will change to the **Home screen**. From then on, whenever the user enters the app, they will be greeted with the Home screen. *(Fig. 6)*

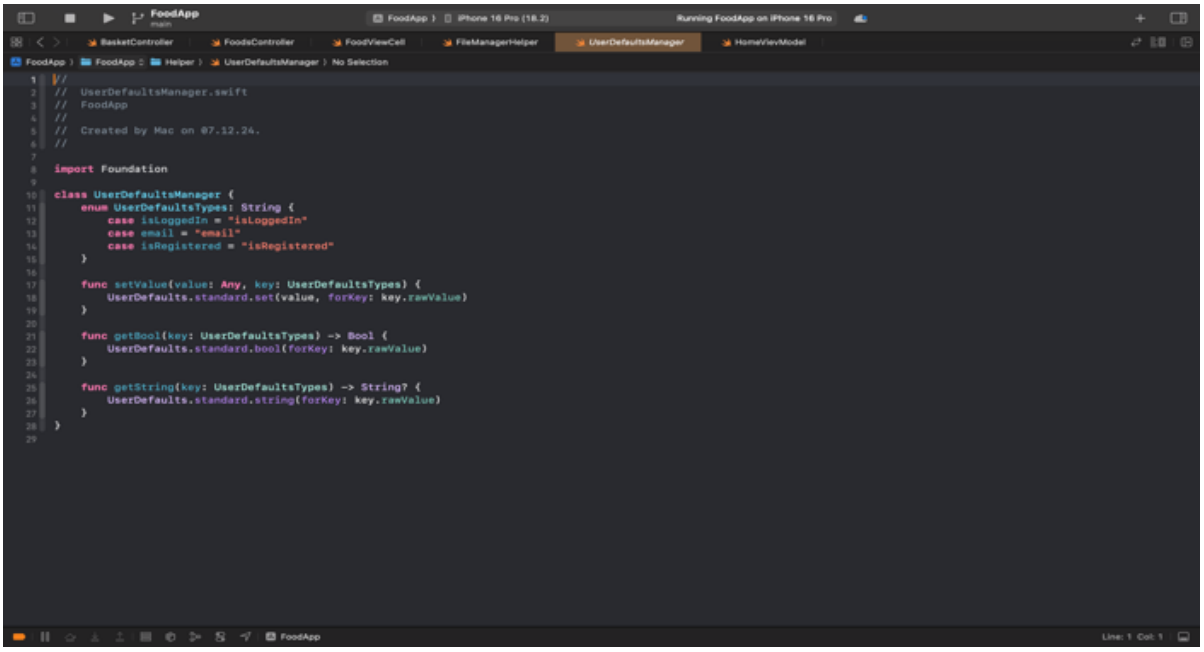

Fig 6. UserDefaultsManager class

Using JSON file

JSON files are typically used when fetching data from APIs. However, in this current project, you can also use a JSON file to display data, but you will have to manually input the data into the JSON file. The data inside the JSON file must match the structure of the struct models so that the data can be transferred from the JSON file to the struct model. If they do not match, no data will be displayed on the screen, and an error message will be shown in the console. There is a common method to transfer data from JSON to the struct model, which is widely used. *(Fig. 7)*

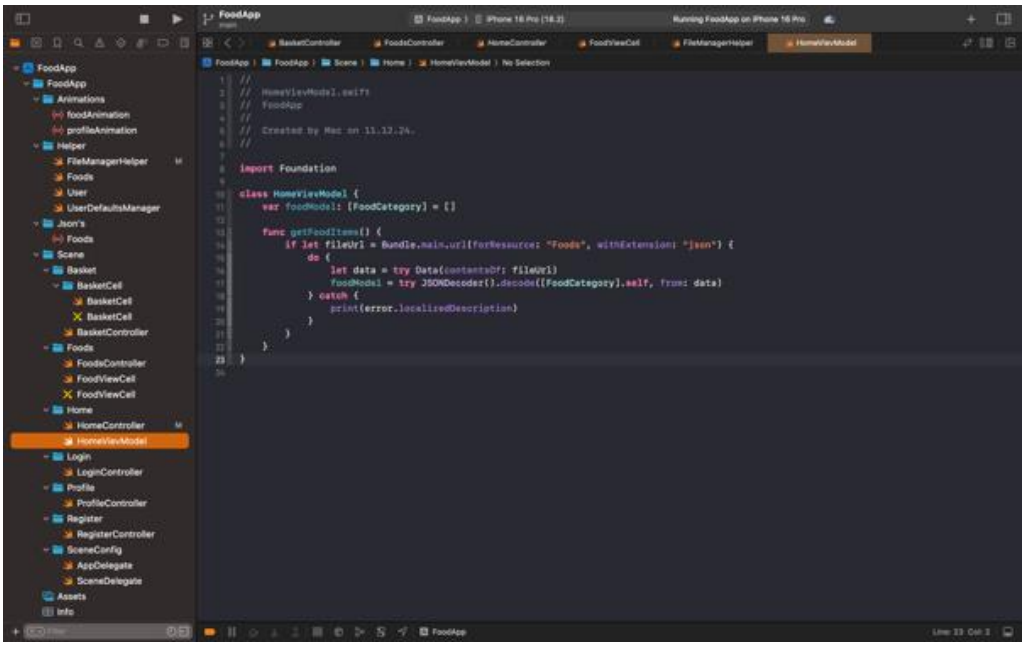

Fig 7. Reading from JSON file

As seen, data is read from the JSON file using the **JSONDecoder** function. We assign the decoded struct to the instance we created. For this, the instance must be of a variable type. If it were a **let** constant, the compiler would throw an error.

Creating the basket and profile screens using navigation items

If you want to navigate to other screens from the home screen using the navigation item, you first need to assign a button to the navigation item in the code. When the user clicks on a button, the navigation controller will ensure the transition between screens and display the content of the respective screen. For navigation items, system-provided images are used to make the user interface more visually appealing. The basket button will be on the right side, and the profile button will be on the left. Thus, by assigning Objective-C-style selector functionality to each button, we define which screen will be shown when the user clicks on each button. This is how the navigation item is provided in the code. (Fig 8).

```
class HomeController: UIViewController {
    @IBOutlet private weak var homeCollection: UICollectionView!

    let homeViewModel = HomeVievModel()
    let foods = FoodsController()
    let manager = FileManagerHelper()
    override func viewDidLoad() {
        super.viewDidLoad()

        configureUI()
        homeViewModel.getFoodItems()
    }

    func configureUI() {
        title = "Home"

        homeCollection.dataSource = self
        homeCollection.delegate = self

        homeCollection.register(UINib(nibName: "FoodViewCell", bundle: nil), forCellWithReuseIdentifier: "FoodViewCell")

        navigationItem.rightBarButtonItem = UIBarButtonItem(image: UIImage(systemName: "basket.fill"), style: .plain, target: self,
            action: #selector(basketController))
        navigationItem.rightBarButtonItem?.tintColor = .black
        navigationItem.leftBarButtonItem = UIBarButtonItem(image: UIImage(systemName: "person.crop.circle.fill"), style: .plain, target:
            self, action: #selector(profileController))
        navigationItem.leftBarButtonItem?.tintColor = .black
    }
}
```

Fig 8. Navigation Items

Thus, each button has its own functionality.

In the **Basket screen**, a **TableView** is used, and for the table, a custom class and xib file are created. In the xib file, the design is structured according to the data to be displayed on the screen. Inside the cell, **UIImageView** and **UILabels** are used. Three main labels will be used here: one will display the name of the added food, one will show the quantity of the food, and the other will show the total price of the food based on the quantity. Some mathematical functionalities are also applied here. Below the **TableView**, a **TableFooter** is used. The TableFooter will remain fixed at the bottom of the table, even as the table is scrolled down. The footer will calculate the total amount of the added foods. (Fig 9).

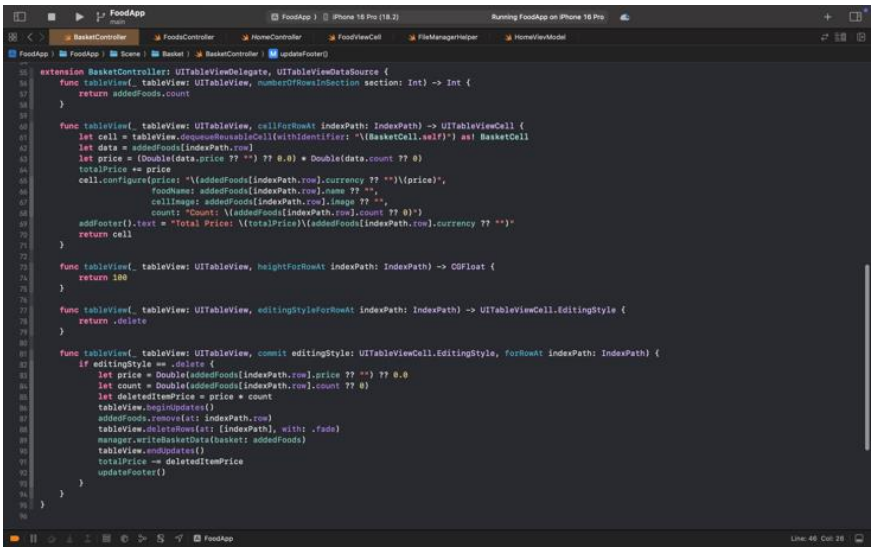

```
extension BasketController: UITableViewDelegate, UITableViewDataSource {
    func tableView(_ tableView: UITableView, numberOfRowsInSection section: Int) -> Int {
        return addedFoods.count
    }

    func tableView(_ tableView: UITableView, cellForRowAt indexPath: IndexPath) -> UITableViewCell {
        let cell = tableView.dequeueReusableCell(withIdentifier: "\(BasketCell.self)") as! BasketCell
        let data = addedFoods[indexPath.row]
        let price = (Double(data.price ?? "") ?? 0.0) * Double(data.count ?? 0)
        totalPrice += price
        cell.configure(price: "\(addedFoods[indexPath.row].currency ?? "")\(price)",
                       foodName: addedFoods[indexPath.row].name ?? "",
                       cellImage: addedFoods[indexPath.row].image ?? "",
                       count: "Count: \(addedFoods[indexPath.row].count ?? 0)")
        addFooter().text = "Total Price: \(totalPrice)\(addedFoods[indexPath.row].currency ?? "")"
        return cell
    }

    func tableView(_ tableView: UITableView, heightForRowAt indexPath: IndexPath) -> CGFloat {
        return 100
    }

    func tableView(_ tableView: UITableView, editingStyleForRowAt indexPath: IndexPath) -> UITableViewCell.EditingStyle {
        return .delete
    }

    func tableView(_ tableView: UITableView, commit editingStyle: UITableViewCell.EditingStyle, forRowAt indexPath: IndexPath) {
        if editingStyle == .delete {
            let price = Double(addedFoods[indexPath.row].price ?? "") ?? 0.0
            let count = Double(addedFoods[indexPath.row].count ?? 0)
            let deletedItemPrice = price * count
            tableView.beginUpdates()
            addedFoods.remove(at: indexPath.row)
            tableView.deleteRows(at: [indexPath], with: .fade)
            manager.writeBasketData(basket: addedFoods)
            tableView.endUpdates()
            totalPrice -= deletedItemPrice
            updateFooter()
        }
    }
}
```

Fig 9. Calculation of the total quantity and price of the food.

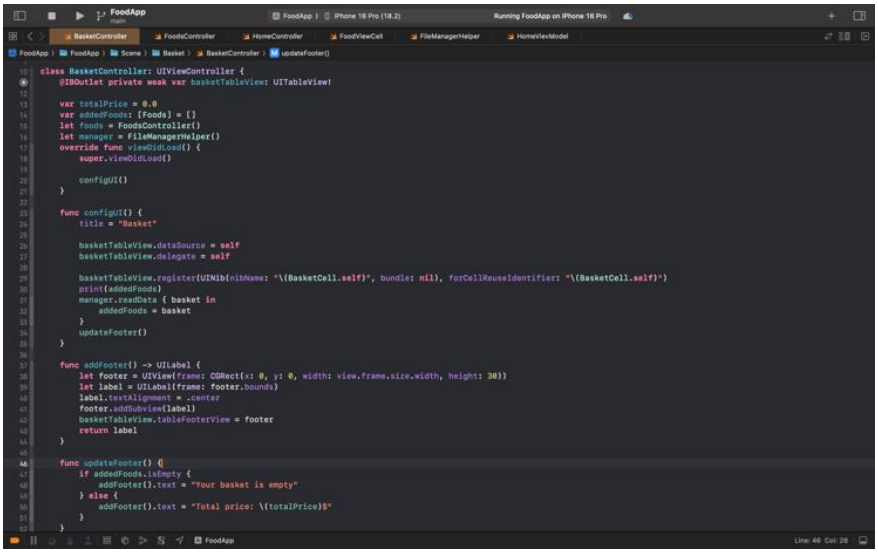

```
class BasketController: UIViewController {
    @IBOutlet private weak var basketTableView: UITableView!

    var totalPrice = 0.0
    var addedFoods: [Foods] = []
    let foods = FoodsController()
    let manager = FileManagerHelper()
    override func viewDidLoad() {
        super.viewDidLoad()

        configUI()
    }

    func configUI() {
        title = "Basket"

        basketTableView.dataSource = self
        basketTableView.delegate = self

        basketTableView.register(UINib(nibName: "\(BasketCell.self)", bundle: nil), forCellReuseIdentifier: "\(BasketCell.self)")
        print(addedFoods)
        manager.readData { basket in
            addedFoods = basket
        }
        updateFooter()
    }

    func addFooter() -> UILabel {
        let footer = UIView(frame: CGRect(x: 0, y: 0, width: view.frame.size.width, height: 30))
        let label = UILabel(frame: footer.bounds)
        label.textAlignment = .center
        footer.addSubview(label)
        basketTableView.tableFooterView = footer
        return label
    }

    func updateFooter() {
        if addedFoods.isEmpty {
            addFooter().text = "Your basket is empty"
        } else {
            addFooter().text = "Total price: \(totalPrice)$"
        }
    }
```

Fig 9. Configuration of basket screen

As seen here, the register function is also used for the TableView. By registering, we specify that the xib file will be inside that TableView. The user can delete the foods they have added to the basket at any time. When this happens, the price of the deleted item will be subtracted from the total amount. If we express the calculation of the foods in a mathematical formula, it would look like this:

count = addedFoods.count

price = addedFoods.price * count

deletedItemPrice = price * count

totalPrice = totalPrice – deletedItemPrice

it can be shown as follows. (Fig. 10).

Fig 10. Basket screen

In the profile screen, the data associated with the email the user logged in with will be displayed. To achieve this, when the user clicks the login button on the login screen, we use **UserDefaults**. We store the logged-in email in the app's memory using **UserDefaults**. Thus, in the profile screen, the data corresponding to the logged-in email will be displayed. This data will be shown on the screen using a filter function. (Fig 11).

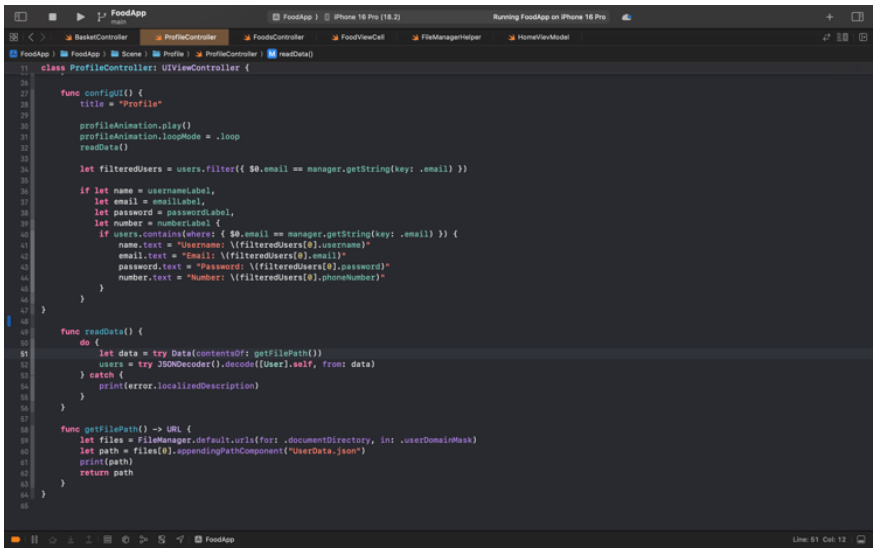

Fig 11. Configuration of profile screen

With the filter function, we filter from the existing instance and assign the filtered result to a new instance. During the filtering process, we retrieve the data by matching the email from **UserDefaults**. This way, the user will be able to see the account details of the last login. (Fig 12).

Fig 12. Profile screen

III. PERFORMANCE IMPROVEMENT

The article presents an analysis of the development of a mobile application for the food ordering process. While the proposed system is functionally appropriate, the following suggestions could be made to further improve performance and user experience:

• **Use of Database Instead of User Defaults and FileManager**: Transition from using User Defaults and FileManager to a more robust database solution like Core Data or SQLite to handle large volumes of data more efficiently.

• **Increase Asynchronous Processes**: Enhance the app's responsiveness by utilizing asynchronous processes for tasks such as network requests, image loading, and database operations, ensuring smoother performance and a better user experience.

• **Optimize Memory Usage**: Use memory efficiently by implementing strategies like data caching and minimizing memory leaks, which can improve the overall performance of the app.

• **Improve Network Performance**: Optimize network operations by implementing techniques like data compression, background fetching, and error handling to reduce latency and enhance the speed of data transfers.

• **Testing and Monitoring**: Incorporate extensive testing (unit tests, UI tests) and continuous monitoring to identify potential issues early, ensuring the app works seamlessly across different devices and network conditions.

This article not only addresses the technical aspects of app development but also focuses on solutions aimed at enhancing user experience. Each suggested feature highlights effective methods used in iOS programming for better performance and user satisfaction.

Conclusion and discussions

Using FileManager and UserDefaults as a small-scale database is aimed at simplifying the user's experience and making the food ordering process more accessible. This ensures that user data is neither lost nor altered unintentionally. By leveraging FileManager, a secure environment is created, which is crucial for safely storing and accessing user data. This approach ensures that the information is protected and easily retrievable when needed, contributing to a more reliable and secure app experience.

REFERENCES

1. 1.Khruleva N.D. Features of programming in the Swift language. International journal of Professional Sceince No 11-2021, p 115-119.
2. Scott, Susan V. and Zachariadis, Markos (2012) Origins and development of SWIFT, 1973–2009. Business History, 54 (3). pp. 462-482. ISSN 0007-6791.
3. Martin, R. C. (2008). Clean Code: A Handbook of Agile Software Craftsmanship. Prentice Hall.
4. Tian, Y., Liu, X., & Zhang, X. (2021). "Performance Optimization Techniques for Mobile Applications: A Survey." Journal of Software Engineering and Applications, 14(3), 156-170.
5. Gupta, S., & Singh, R. (2020). "Cloud-Based Food Delivery Applications: Challenges and Future Trends." International Journal of Computer Applications, 182(45), 12-18.
6. Hossain, M. T., & Hossain, M. S. (2022). "Design and Performance Analysis of a Scalable Food Ordering System Using Microservices." IEEE Access, 10, 12345-12360.
7. Data Structures & Algorithms in Swift Implementing Practical Data Structures with Swift By the raywenderlich Tutorial Team Kelvin Lau & Vincent Ngo
8. Data Structures and Algorithms in Swift - Implementing practical data structures with Swift 4
9. Swift Programming: The Big Nerd Ranch Guide by Matthew Mathias and John Gallagher
10. Learn Swift by examples Beginner level SIMPLE INTRODUCTION SERIES

2025. Volume 9, Number 1 ***Pages 29-37***

UOT: 621.91; 621.923; 621.95; 684.4
DOI: https://doi.org/10.30546/09085.2025.01.015

FEATURES OF DEFORMATİON OF DİSC CUTTER TEETH IN PROCESSİNG RECTANGULAR GROOVES ON CHİPBOARD

V.A. ABBASOV
Azerbaijan Technical University, H.Javid ave 25, Baku, AZ 1073 Azerbaijan
vaqif.abbasov@aztu.edu.az

M.S. NASIROV
Baku Engineering University, Khirdalan city, Hasan Aliyev str., 120 AZ0101, Absheron, Azerbaijan
munasirov@beu.edu.az

B.H. ALIYEV
Baku Engineering University, Khirdalan city, Hasan Aliyev str., 120 AZ0101, Absheron, Azerbaijan
baeliyev@beu.edu.az

ARTICLE INFO

Article history:
Received: 2025-03-05
Received in revised form: 2025-03-05
Accepted: 2025-04-02
Available online

Keywords: rectangular grooves; deformations; runout, cutting forces; wood materials.

JEL Classification: L60, O33

ABSTRACT

This paper presents the deformation of the teeth of disk cutters when milling rectangular grooves on chipboards depending on the processing modes. Since, depending on the cutting modes of the grooves, a significant cutting force occurs, under the influence of which deformations of the cutting teeth occur in the direction parallel to the axis of the cutter, which affects the quality of manufacturing rectangular grooves and the choice of the allowance for sharpening the teeth of the cutter. And, to develop a new technology for sharpening disk cutters, ensuring with minimal removal of the allowance, the identity of the tool profile and the elimination of its runout.

I. INTRODUCTION

Wood materials are widely used in the production of furniture for various consumer purposes, with chipboard being the leading material. Depending on the furniture design, grooves of various shapes and geometric dimensions are milled on wood boards. Most often, rectangular grooves with a depth of up to 10 mm are milled on chipboard boards. Milling rectangular grooves on chipboards uses disc cutters with different diameters and numbers of teeth. Rectangular grooves 3–10 mm wide and up to 10 mm deep are milled with disc cutters with a diameter of 100–125 mm and a count of teeth is 24.

The deformation of the cutting teeth of the cutter, along with other factors, largely depends on the choice of the tool body material. The body of the disc cutter of the KÖNİG brand, type WZ TUNGSTEN HARTMETALL with a diameter of 100 mm, having 24 teeth, which is used for cutting rectangular grooves on furniture parts, produced according to GOST 14959-79 or to GOST 5950-73, the disk hardness is 40-45 HRCэ. The material of the cutting part of the disk cutters is made according to GOST 3882-74. The shape and dimensions of the carbide plates

choosen according to GOST 13833-77. The thickness of the cutter is 3.0 mm. Carbide plates of various shapes are soldered to the top of the teeth of the cutter body, after which the cutter is sharpened and the necessary geometry is ensured [5].

When milling grooves wider than 3 mm, the cutter forms it in several passes. During the first pass, the cutting teeth of the cutter on the front, rear and both end surfaces at a high rotation speed (20–100 m/s) contact the processed wood material and chips are formed. Such a pattern of contact of the teeth of disk cutters creates complex contact and force pressures on their surfaces. Therefore, at a high cutting speed, large forces arise that affect the deformation of the cutting teeth [6].

It is known that [1] in the production of furniture using wood-based materials, which are made by pressing plasticized and glued laminated mass in the form of chipboard and MDF. Therefore, when processing such materials, the deformation of the teeth of disk cutters depends on their structure and indicators of physical and mechanical properties. Since, depending on the properties of wood, the density of its structure and humidity significantly fluctuates within wide limits. Therefore, the teeth of disk cutters when milling rectangular grooves under the influence of cutting forces are subject to uneven deformation, leading to beating of the cutting tool. Analysis of the process of milling rectangular grooves with disk cutters shows that the cutting teeth of the cutter when processing chipboard are also subject to varying degrees of wear both cutting edges and on the front and back surfaces of the tool. Uneven wear of the cutting teeth leads to a change in the nature of the cutting forces, its direction, action, and trajectory, which differently affect the resulting deformations of the cutting teeth of the cutter [7].

It is known that wood materials subjected to milling have a pronounced parallel-layered structure, in which the anisotropy of mechanical properties acts on the cutting tool in two directions, i.e., parallel, and perpendicular to the planes. Therefore, when milling chipboard, its non-uniform structure leads to varying degrees of wear of the working surfaces of the cutter, under the influence of which the wear and deformation of the cutting teeth of the cutter separately differ from each other. Based on the research work carried out on milling rectangular grooves on chipboard, it was found that the study of the deformation of the cutting teeth of the cutter when processing rectangular grooves will allow us to establish the direction of reducing the deformation of the cutting teeth of the cutter to improve the quality of the processed groove [2].

II. RESEARCH METHODS

The experimental study was conducted at the furniture factory "HASANOGLU" on a machining center with a CNC portal "profi line BHT 500", the processing was carried out with KÖNİG brand cutters, type WZ TUNGSTEN HARTMETALL with a diameter of 100 mm and 24 teeth. The dimensions of the milled groove were hxb = 10x3.0 mm, the grooves were milled with a length of 50,000 m. The depth on each pass was 5 mm. The longitudinal feed rate was taken as S_{feed} = 12 m/min (S_0 = 125 mm/tooth), the rotation speed of the cutter was 20 m / s. The milling power was measured using a special setup consisting of an ACTDN24685 wattmeter, a UTT5 type current transformer and an additional resistor DV30 μA, 5000 Ohm. After measuring the milling power of chipboards, the cutting force P_z is calculated and, on its basis, the forces P_y and P_x are calculated [24,25,26,27,28].

The method of measuring the deformation of individual teeth on the side surfaces, i.e. in the axial direction of the cutter, is that the cutter is installed on the shaft of a special installation, which is shown in Fig. 1,

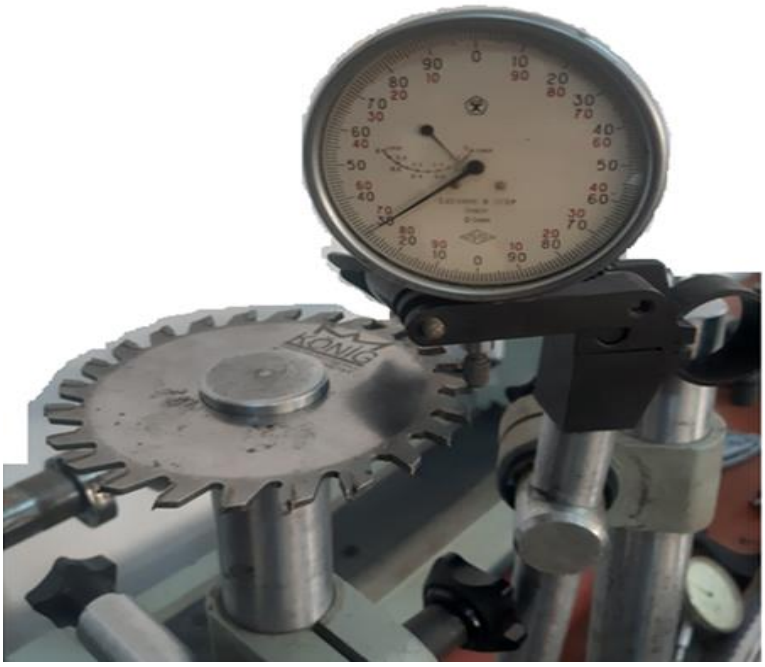

Fig.1. Device for measuring the deformation of the teeth of a disc cutter

and an indicator with micron accuracy, fixed on a tripod, touches the side surface of one tooth, the indicator readings are set to zero, after which the cutter is turned to the next tooth and the indicator measures the magnitude of its deformation. In this case, the difference in the indicator readings when measuring the next teeth is applied to the table and their deformation is calculated. After measuring the deformation of all teeth, the runout of the disk cutters is calculated to develop a technology for sharpening the cutter teeth [3,9,11]. (fig. 1).

As is known, when processing rectangular grooves with disk cutters, the cutting teeth are affected by the cutting forces that arise during the chip formation process. In this case, the cutting teeth of the disk cutters form chips within the rectangular grooves, a process that occurs in a closed milling condition. In this case, the position of the processed surface and the feed direction relative to the wood fibers are along the fibers. The scheme of milling rectangular grooves with a milled disk cutter on a machining center with a CNC portal "profi line BHT 500" is shown in Fig. 2, from which the tangential (tangent) cutting force P_z at point "0" acts along the front surface of the cutting teeth of the cutter, where the chip is formed. In this case, a normal cutting force P_y arises, which is directed perpendicularly to the cutting surface along the vertical axis of the cutter. The force P_x, which is the axial cutting force, acting along the horizontal axis of the cutter, depending on the anisotropy of the cut wood, affects the end surfaces of the cutting teeth and leads to the appearance of deformation of the cutter teeth in the axial direction (O - O) [18,19,20,21,22,23].

Since when processing rectangular grooves on chipboards, the workpiece is installed and secured on the machine table and the spindle with the tool, along with the rotational movement, performs longitudinal feed, therefore, the accuracy of the formed surface and the dynamics of the process are affected not only by the cutting forces, but also by the kinematic movements of

the spindle unit of the machine. As noted above, the deformation of the cutting teeth of disk cutters when processing rectangular grooves on chipboards occurs due to the kinematics of the rotational and longitudinal movement of the machine spindle [8,13,14,15,16,17].

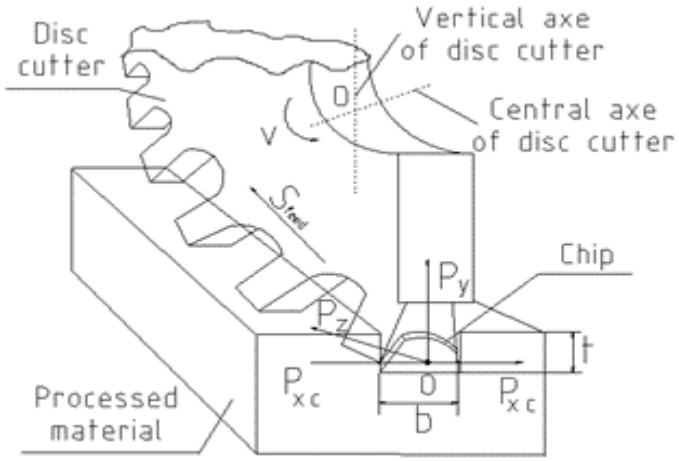

Fig. 2 Scheme of milling rectangular grooves on the machining center with CNC portal "profi line BHT 500" (the drawing was made using the LibreCAD program)

It is known that when processing rectangular grooves on furniture parts, the cutting teeth of disc cutters are affected by the cutting force "P", which consists of the following components: tangential (tangent) P_z, radial P_y and axial P_x. Considering these components of the cutting forces, the total cutting force "P" when milling with a disc cutter can be determined from the following equation [10,12]:

$$P = \sqrt{P_x^2 + P_y^2 + P_z^2},\ N \qquad (1)$$

Analysis of the process of milling rectangular grooves shows that depending on the cutting depth, the length of the arc of contact of the cutter with the surface being machined changes. Depending on the length of the arc of milling L (Fig. 3) and the depth of groove processing, the number of teeth simultaneously participating in the milling process will be different. Therefore, the value of the tangential force P_z will be determined by the following formula [4]:

$$P_z = P_{zt} * z_{cut.} \qquad (2)$$

where, P_{zt} – tangential force acting on one tooth of the cutter,

$z_{cut.}$ - the number of simultaneously cutting teeth.

$z_{cut.}$ – can be determined from the following formula:

$$z_{cut.} = \frac{L}{t_{teeth}} \qquad (3)$$

t_{teeth} – the value of the axial pitch of the teeth.

Arc length at milling rectangular grooves we determine from Fig. 3 as follows [4,8,9]

$$L = \frac{2\pi R}{360} * (\varphi_{cont} + \varphi_{out}) \qquad (4)$$

where, φ_{cont} – contact angle of the tooth of the disk cutter

$$\varphi_{cont} = \varphi_{out} - \varphi_{in} \qquad (5)$$

φ_{in} – angle of tooth entry into the material

φ_{out} – angle of tooth exit from the material.

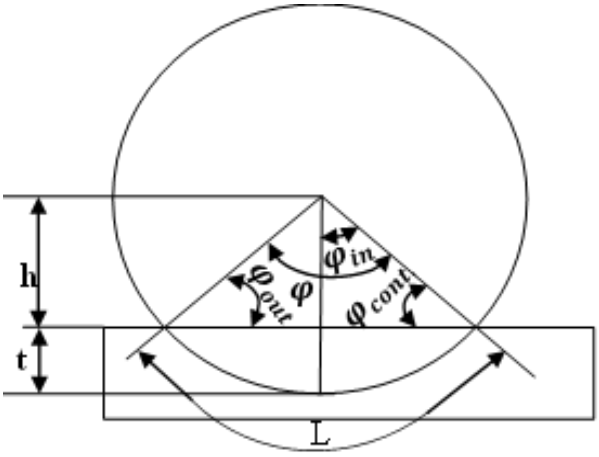

Fig. 3 Parameter diagram for cutting rectangular grooves.

III. RESEARCH RESULTS AND THEIR DISCUSSION

A rectangular groove on chipboard is milled with a disc cutter with a diameter of 100 mm, the number of teeth is 24. Considering the parameters of the cutter, the following can be calculated:

$$t_{tooth} = \frac{\pi D}{z} = \frac{3.14 * 100}{24} = 13.08mm$$

$$\varphi_{in} = arccos\frac{h}{R} \qquad (6)$$

where h – is the distance from the center of the disc cutter to the processing surface

$$h = R - t \qquad (7)$$

where, t – milling depth, mm

R – cutter radius, mm.

When processing rectangular grooves, t=10mm is taken, while

$h = 50 - 10 = 40$ мм

then from here $\varphi_{in} = arccos\frac{40}{50} = arccos0{,}8\varphi_{in} =$

$$= 36{,}87°$$

Also $\varphi_{out} = arccos\frac{h-t}{R} = arccos\frac{40-10}{50} =$

$$= arccos0{,}6 = 53{,}13°$$

We determine the number of cutting teeth simultaneously involved in cutting as follows:

$$z_{cut} = \frac{L}{t_{tooth}} \qquad (8)$$

where L is the length of the contact arc

$$L = \frac{2\pi R}{360} * (\varphi_{cont} + \varphi_{out}) == \frac{2 \cdot 3{,}14 \cdot 50}{360} * (53{,}13 + 16{,}26) == 0{,}8722 \cdot 69{,}39 = 60{,}523 \text{ мм}$$

Then $z_{cut} = \frac{60,523}{13,08} = 4,63$ tooth is taken as 5 teeth.

Thus, when processing chipboards with cutters of 100 mm diameter, with a processing depth of 10 mm, 4.63 teeth are simultaneously involved in cutting. We determine the quantities tangential (tangent) cutting force on the arc of contact. We determine the average tangential force on the arc of contact of the blade with the workpiece F_{xt} and the average cyclic F_{xy}:

$$F_{xt} = F_{x1} \cdot b \cdot a_{cor.} \qquad (9)$$

where, F_{x1} is the tabular tangential force for particle boards, a_{med}=0.16; density of chipboard is 700 kg/m^3, F_{x1}=8.1 N/mm^2 [4].

b – milling width per pass, equal to 3 mm,

a_{cor} – general correction factor, determined from the following equation [4]:

$$a_{cor.} = a_{tw} * a_w * a_\rho * a_\delta * a_v * a_t \qquad (10)$$

where a_{tw} –correction factor for the type of wood used to make the particleboard (on average, we take it equal to 1)a_{tw}=1;

a_w – correction factor for particleboard humidity (with humidity of 5-8% equals 0.9) a_w=0.9

$a_ϱ$ – correction factor for blade dullness, $a_ϱ$ = 1.7

$a_δ$ – correction factor for the cutting angle, $a_δ$ = 0.86

a_v – correction factor for cutting speed, a_v = 1.07

a_t – correction factor for the processing depth, a_t = 0.8

Thus $a_{cor} = a_{tw} * a_w * a_\rho * a_\delta * a_v * a_t = 1 *$

$$* 0,9 * 1,7 * 0,86 * 1,07 * 0,8 = 1,1263$$

$F_{xt} = F_{x1} \cdot b \cdot a_{cor} = 8,1 \cdot 3 \cdot 1,126 = 27,362$N

Total tangential cutting force is

$F_{xy} = F_{xt} * z_{cut} = 27,362 \cdot 5 = 136,81$N

F_{xy} – cutting forces are designated as the total tangent force equal to P_z. Then the normal cutting force during groove milling can be determined from the following equation

$$P_y = P_z * cos\varphi_{out} = 136,81 * cos53° = 136,81 *$$

$$* 0,6018 = 82,333\text{N}$$

The axial force when milling a rectangular groove 3 mm wide will be:

$P_x = P_z * cos\varphi_{in} = 136,81 * cos37° = 136,81 \cdot 0,7986 = 109,261$N

Thus, the total cutting force coming per 1 mm^2 of area during milling will be

$$P = \sqrt{P_z^2 + P_y^2 + P_x^2} == \sqrt{136,81^2 + 82,333^2 + 109,261^2} == \sqrt{18716,9761 + 6778,722 + 11937,966 =}$$

$$= \sqrt{37433,664} = 193,478\ N$$

If we take into account that rectangular grooves with a width of 3 mm and a depth of 10 mm are milled, at the same time in this case the total area of the cut layer was . Based on this, when cutting a given groove, the cutting forces that arise will be: $P = b \cdot t = 3 \cdot 5 = 15\ mm^2$

$P_0 = P \cdot b \cdot t = 193{,}478 \cdot 3 \cdot 5 = 2952{,}17$ N

We calculate the total cutting forces proportionallyP_{ztot}, P_{ytot} and P_{xtot}

$P_{\text{ztot}} = P_z \cdot b \cdot t = 136{,}81 \cdot 3 \cdot 5 = 2052{,}15$N

$P_{\text{ytot}} = P_y \cdot b \cdot t = 82{,}333 \cdot 3 \cdot 5 = 1234{,}95$N

$P_{\text{xtot}} = P_x \cdot b \cdot t = 109{,}261 \cdot 3 \cdot 5 = 1638{,}93$N

As noted above, under the influence of cutting forces, the cutting teeth of disc cutters are subject to deformation, which increases the runout of the cutter, which has a negative impact on the quality and accuracy of the cuts. rectangular grooves. The deformation value of individual teeth of the disk cutter in the direction of its axis was investigated. The results of the deformation measurement of all teeth of the cutter are shown in Table 1.

Table 1. THE VALUES OF DEFORMATION OF THE TEETH OF A DISC CUTTER

Parameters of a disc cutter		Parameters of a disc cutter	
Teeth No.	The magnitude of deformation, microns	Teeth No.	The magnitude of deformation, microns
1.	0	13.	44
2.	12	14.	8
3.	16	15.	-9
4.	20	16.	25
5.	-8	17.	-33
6.	-40	18.	-11
7.	30	19.	41
8.	40	20.	-8
9.	23	21.	-2
10.	-21	22.	2
11.	30	23.	5
12.	-40	24.	-4

The measurement scheme is shown as graph in fig4.

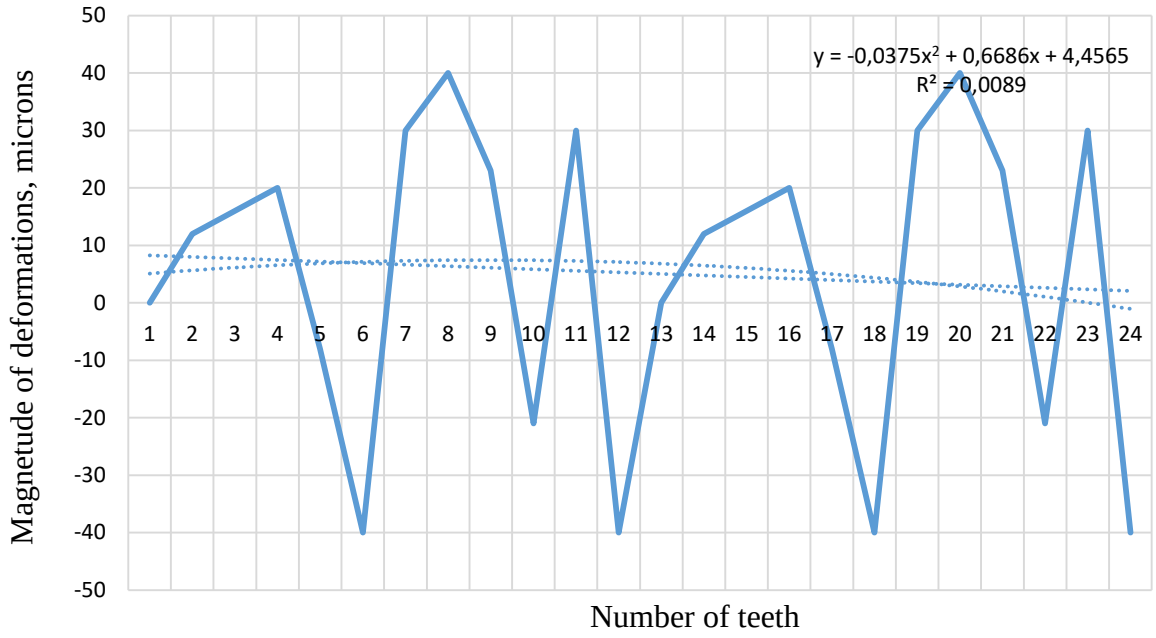

Fig4. The measurement scheme of deformation

IV. CONCLUSION

1. It has been established that when processing rectangular grooves on chipboard, the deformation of the cutter teeth along the axial direction of the tool is uneven, which shows the complexity of the process of milling wood materials, which is associated with the kinematics of the cutting process, the influence of cutting forces and the properties of the cutter material, etc.

2. When processing rectangular grooves with disk cutters, it was found that the size and signs of deformation of the cutting teeth of the cutter require the development of a new technological process for sharpening the tool to ensure the identity of the profile and eliminate the runout of the cutter, ensuring the milling of rectangular grooves with the required accuracy of the product.

ACKNOWLEDGMENT

Authors deeply thankful to managers and workers of "HASANOGLU" firm, for their support on technical areas of the furniture producing plant.

REFERENCES

1. Krilek, Jozef, Ján Melicherčík, Tomáš Kuvik, Ján Kováč, Arkadiusz Gendek, Monika Aniszewska, and Jan Mareček. 2023. "Analysis of Cutting Forces in Cross-Sawing of Wood: A Study of Sintered Carbide and High-Speed Steel Blades" Forests 14, no. 7:1395. https://doi.org/10.3390/f14071395
2. Kováč, Ján & Harvánek, Pavol & Krilek, Jozef & Kuvik, Tomáš & Melicherčík, Ján. (2020). Analysis of cutting conditions in the process of cross-cutting wood by circular saws. BioResources. 16. 1029-1041. https://doi.org/10.15376/biores.16.1.1029-1041
3. V.A. Abbasov, R.C. Bashirov. Production technology of metalworking tools. Textbook. Baku. AzTU, 2018–380p. (In Azerbaijan)
4. Lyubchenko, G. F. Druzhkov. Machines and tools for furniture production. Textbook for technical schools. Moscow: Lesnaya Promyshlennost, 1990–360 pp. ISBN5 – 7120–0249–3. (In Russian).
5. J. Nordström, J. Bergström, Wear testing of saw teeth in timber cutting, Wear, 13th International Conference on Wear of Materials, Volume 250, Issues 1–12, 2001, Pages 19-27, ISSN 0043-1648, https://doi.org/10.1016/S0043-1648(01)00625-1
6. Glebov I. T. Fundamentals of wood cutting: a textbook for secondary vocational education / I. T. Glebov. - 3rd ed., reprinted. - St. Petersburg: Lan, 2022. - 112 p. (In Russian).
7. Glebov I. T. Woodcutting machines and tools. Preparation for testing: a textbook for universities / I. T. Glebov. - 2nd ed., Stereotype. - St. Petersburg: Lan, 2021. - 252 p. (In Russian).
8. Glebov I. T. Calculation of wood cutting modes: Monograph. – Ekaterinburg: Ural. state forestry university, 2005. – 155 p. ISBN 5-230-25725-3. (In Russian).
9. Abbasov V.A., Bashirov R.J. Features of ultrasound application in plasma-mechanical processing of parts made of hard-to-process materials. Obrabotka metallov (tekhnologiya, oborudovanie, instrumenty) = Metal Working and Material Science, vol. 24, no. 3, pp. 53–65. https://doi.org/10.17212/1994-6309-2022-24.3-53-65 (In Russian) (2022)
10. Grinevich S. A., Lukash V. T. Geometric modeling of wood cutting tool blunting. Proceedings of BSTU. Forestry, nature management and processing of renewable resources. Ser. 1, No. 2 (210). Minsk. (2018). P. 275–279.
11. Mohammadian A., Sadeqi BM, Investigation on the Cutting Force and Surface Quality in Harmonically Vibrated Broaching (HVB).Advances in Tribology. 1-11. (2023).https://doi.org/10.1155/2023/9917497
12. M. S. Bajestani, B. Moetakef-Imani, and A. Hosseini, "Effects of harmonic vibrations of cutting speed on cutting force and surface quality in Al 7075-T6 broaching," IFAC-Papers OnLine, vol. 52, no. 10, (2019). pp. 276–281. DOI:10.1016/j.ifacol.2019.10.042
13. Trejo, J., Polli, M.L., Da Rocha, M.P. etc. Working limit of the circular saws in the cutting of high density fiberboard (HDF) through a nonlinear model and differential equations. Eur. J. Wood Prod. 78, 1183–1194 (2020). https://doi.org/10.1007/s00107-020-01596-9

14. Kang J., Zhang H., Zhang Z. and etc. Investigating damage mechanisms of honeycomb cores machined with PCD circular saw blades. Journal of Materials Processing Technology, Volume 327, 2024,
15. https://doi.org/10.1016/j.jmatprotec.2024.118381
16. Sandak J, Orlowski K. Machine vision detection of the circular saw vibrations. Journal of Machine Engineering, 2018, Vol. 18, No. 3, 67–77 https://doi.org/10.5604/01.3001.0012.4617 https://www.researchgate.net/publication/327524393_Machine_vision_detection_of_the_circular_saw_vibrations
17. R. Licow, D. Chuchala, M. Deja and etc. Effect of pine impregnation and feed speed on sound level and cutting power in wood sawing. Journal of Cleaner Production, Volume 272, 2020. https://doi.org/10.1016/j.jclepro.2020.122833
18. Muhammed, M.; Javidani,M.; Heidari, M.; Jahazi, M. Enhancing the Tribological Performance of Tool Steels for Wood-Processing Applications: A Comprehensive Review. Metals 2023, 13, 1460. https://doi.org/10.3390/met13081460
19. Al-Asadi M. M., Al-Tameemi H. A.. A review of tribological properties and deposition methods for selected hard protective coatings, Tribology International, 2022,Volume 176. https://doi.org/10.1016/j.triboint.2022.107919
20. Melekhov V.I., Soloviev I.I., Ponomareva N.G. Formation of coaxial fields of residual stresses in a circular saw blade // Izvestia VUZov. Forest magazine. 2022. No. 2. (In Russian).
21. URL: https://cyberleninka.ru/article/n/formirovanie-koaksialnyh-poley-ostatochnyh-napryazheniy-v-polotne-krugloy-pily
22. Melekhov V.I., Solovyov I.I., Tyurikova T.V., Ponomareva N.G. Increasing the stability of wood-cutting saws by thermoplastic influence on the distribution of residual stresses in the blade. Izv. universities Forest magazine 2020. No. 6. pp. 172–181. (In Russian). https://doi.org/10.37482/0536-1036-2020-6-172-181
23. Konstantinov V.F., Borisov V.A., Pakhomov P.K. Reducing the wear rate of wood cutting tools. Resources and Technology, 2020. 17(3), 111–123. (In Russian). https://cyberleninka.ru/article/n/snizhenie-intensivnosti-iznashivaniya-rezhuschego-instrumenta-dlya-drevesiny
24. Zhusupov K., Kozbagarov R., Kaliev E. et al. Research on the mechanisms of wear and destruction of carbide tools with multicomponent nanostructured systems. Vestnik KazATK, 126(3), 2023. 65–73. (In Russian). https://doi.org/10.52167/1609-1817-2023-126-3-65-73
25. Wang Y., Chang M., Huang X. et al. Cutting tool wear prediction based on the multi-stage Wiener process. The International Journal of Advanced Manufacturing Technology. 129, 5319–5333 (2023). https://doi.org/10.1007/s00170-023-12648-8
26. Guoqiang Z., Lin Y. "Tribological Properties of Micro-Groove Cemented Carbide by Laser Processing" Micromachines 12, 2021. no.5:486. https://doi.org/10.3390/mi12050486
27. Torkghashghaei M., Shaffer W., Ugulino B. etc. "Improvement of the Wear Resistance of Circular Saws Used in the First Transformation of Wood through the Utilization of Variable Engineered Micro-Geometry Performed on PVD-Coated WC-Co Tips" Applied Sciences 12, no. 23: 12213. 2022. https://doi.org/10.3390/app122312213
28. Miran M. (2020). Influence of Temperature Distribution on Circular Saw Blade Natural Frequencies during Cutting. Bioresources. https://doi.org/10.15376/biores.16.1.1076-1090
29. Yu M., Wang B., Ji P. etc. "Study on the dynamic stability of circular saw blade during medium density fiberboard sawing process with thermo-mechanical coupling." Computers and Electronics in Agriculture, Volume 211, 108042, ISSN 0168-1699, 2023 https://doi.org/10.1016/j.compag.2023.108042
30. Krilek J., Ťavodová M., Kováč J., Tichý B. "Impact of irregular tooth pitch of circular saw blades on power for wood cross-cutting," Drvna Industrija 71(1), 3-11. 2020. https://doi.org/10.5552/drvind.2020.1824

UOT: 669.18
DOI: https://doi.org/10.30546/09085.2025.01.019

INVESTİGATİON OF THE EFFECT OF ACİDİTY AND ALKALİNİTY OF THE ASH ON THE CORROSİON OF THE REFRACTORY PART OF THE FURNACE

V. F. GAHRAMANOV
Baku Engineering University, Hasan Aliyev str., 120, Baku, AZ0102, Azerbaijan
vqahremanov@beu.edu.az

A.H.GULIYEV
Baku Engineering University, Hasan Aliyev str., 120, Baku, AZ0102, Azerbaijan
asquliyev@beu.edu.az

O.H. MIRZAYEV
Baku Engineering University, Hasan Aliyev str., 120, Baku, AZ0102, Azerbaijan
omirzayev@beu.edu.az

ARTICLE INFO

Article history
Received: 2025-03-15
Received in revised form: 2025-03-18
Accepted:2025-04-02
Available online

Keywords:
Basic rust;
Viscosit;
chemical composition;
boiling point;
rust composition;
natural gas.
JEL Classification: O32

ABSTRACT

The acid open-hearth process allows steel to be produced with a lower gas content compared to the basic process. However, depending on the melting process factors and the type of process used (active or silicon-reducing), the hydrogen content in the resulting steel fluctuates from 2.5 to 6.5 sm³ /100 g, and nitrogen – from 0.006%. This was the reason for a lengthy discussion between [1] and [4] about the behavior of gases in the bath of an acid open-hearth furnace. For a long time, it was believed that the main reason determining the behavior of gases in the metal of an acid open-hearth furnace was the rate of silicon reduction from high-silica materials into metal. [2] was the first to draw attention to the significant influence of the gas-protective properties of the slag cover. However, in the study [5], based on several melts with one acid slag, carried out in an induction furnace, the opinion was expressed that acid slags are impermeable to hydrogen and reliably isolate the molten metal from the water vapor of the open-hearth furnace atmosphere.

Introduction

Hydrogen permeability of acid steelmaking rust. The process of hydrogen transfer from the furnace atmosphere through acid slag into metal includes the stage of dissolution of water vapor in the rust melt without considering in detail the data available in the literature on the solubility of water vapor in the rust melt, it can be noted that they were first obtained in a study the results of which have recently been mainly confirmed by the work of American and Japanese scientists. The degree of acidity of the slag melt can be described by the equations of hydrogen mass transfer through the rust melt layer to the rust and metal interphase surface and the transition of hydrogen from the rust to the metal.

$$H_2O_r + 0^{2-}_{ru.} = 2OH^-_{ru.}; \qquad (1)$$

$$H_2O_r + 2Si0^{4-}_{4ru.} = 20H^-_{d.} + Si_2\ 0^{2-}_{7ru.} \quad (2)$$

$$H_2O_r + Si_2\ 0^{6-}_{7} = 20H^-_{ru.} + 2Si0^{2-}_{3ru.} \quad (3)$$

The last stage, depending on the process conditions and the degree of oxidation of the metal, can proceed in different ways. For example, the decomposition of hydroxyl into oxygen and hydrogen can proceed with the participation of iron atoms of the surface layer of the metal or without the participation of iron atoms.

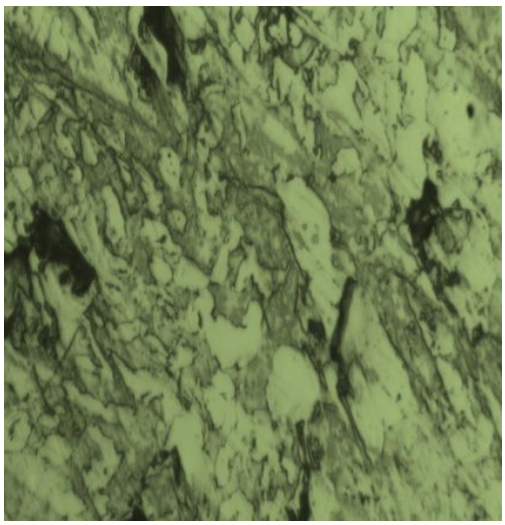

Fig. 1. Inclusions in steel 30KhGSNA. X500: a, b, aluminum additive after alloying steel with silicon; c-aluminum additive before alloying steel with silicon

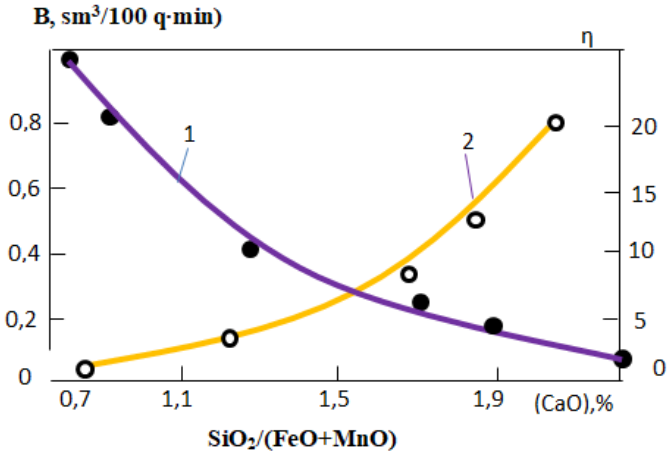

Fig. 2. The effect of the Si2O /(FeO + MnO) ratio on the hydrogen permeability (1) and viscosity (2) of acidic open-hearth rust at 1650 ^{0}C and p_(H2O)= 150 mm Hg.

THEORETİCAL PART

In the conditions of experiments on studying the hydrogen permeability of slag melts, all the above-mentioned stages of hydrogen movement took place. Some researchers claimed that with an increase in the basicity of the slag, the hydrogen content in the steel increases, while others reported a decrease in the hydrogen concentration in the metal with an increase in the basicity of the rust melt [6]

Therefore, in the first series of experimental melts, the effect of the basicity (CaO/SiO_2) of electric steel-making rust on their hydrogen permeability was studied. The technique was similar to that previously described in as applied to the main electric steel-making rust. With the method used for supplying the steam-nitrogen mixture (see Fig. 1), which primarily washes the crucible with molten metal and rust, the gas permeability of the crucible could greatly affect the results obtained.

$$I = SAT^2e^{-\varepsilon f/\kappa T,} \qquad (5)$$

where I - is the emission current;

S - is the cathode area;

A - is a constant;

ε - is the electron charge.

Accordingly, the activation energy of the process of hydrogen transition from the gas phase to the slag increases. Comparison of hydrogen permeability of basic and acid steel-making slags shows that the hydrogen permeability of the latter is four to five times lower than that of the basic rust.

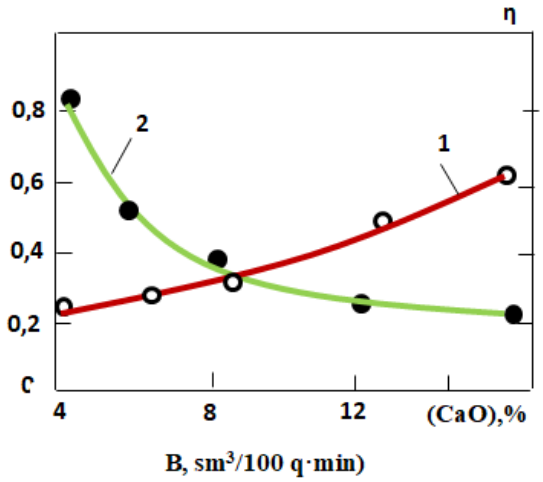

Fig. 3. Effect of CaO on hydrogen permeability (1) and viscosity (2) of acidic open-hearth

Slags of the silicon-reducing process contain up to 4.0% calcium oxide, and in the active process the concentration of this component reaches 15.0%. In this regard, it is extremely important to know the effect of calcium oxide on the hydrogen permeability of acid steel-making rust [7], The chemical composition of the melts studied for this purpose is given in Table 1 (Group II rust). The results obtained are presented in Fig. 4, from which it is evident that an increase in the calcium oxide content in the acid rust is accompanied by a significant increase in its hydrogen permeability. Such an effect of calcium oxide on the hydrogen permeability of acid rust is explained by the strong thinning effect of this component under these conditions and a decrease in the viscosity of the melt (see Fig. 3). In addition, with an increase in the calcium oxide content in silicate melts, the activity of oxygen anions increases, which promotes the dissolution of water vapor in the rust.

The effect of alumina content in acid slags on their hydrogen permeability is shown in Fig. 4. Alumina present in the acid slag increases its hydrogen permeability not only due to a

decrease in the viscosity of the melt, but also due to an increase in the solubility of water vapor in the rust, since one weight unit of alumina binds a smaller amount of oxygen anions compared to silica.

$$SiO_2 + 2O^{2-} \rightarrow SiO_4^{4-};\ Al_2O_3 + O^{2-} \rightarrow 2AlO_2^{-}. \qquad (6)$$

Depending on the fuel used (blast furnace, generator, natural gas or fuel oil) and its humidity, the amount of water vapor in the atmosphere of the open-hearth furnace varies widely.

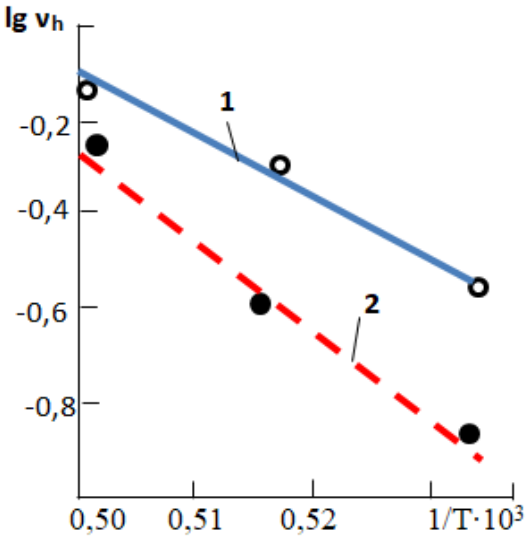

Fig. 4. Influence of temperature on hydrogen permeability of acidic rust 1 – 49,0% SiO_2; 2- 54,2% SiO_2

To do this, we represent the equation ($\upsilon_H = \beta_H S(C_1\text{-}C_2)$) in the following form:

$$\upsilon_H = AB_0\, e^{-E/RT}(C_1\text{-}C_2) \qquad (7)$$

$$lg = \upsilon_H = A_0 - B_0/T \qquad (8)$$

Where,

$$A_0 = lg\ AB_0 \qquad (9)$$

$$B_0 = E/R\ lg\ e = E/4{,}575 \qquad (10)$$

Table 2. Chemical composition of synthetic slags and their hydrogen permeability

Rust	Contents of components, %				SiO_2/FeO+MnO	Hydrogen permeability, sm³ /100 q-min at 1650 ⁰ C and different values of p_{H_2O}= 150 mm Hg.			
	SiO_2	FeO	MnO	Al_2O_3		55	100	170	260
1	62,12	7,64	18,73	10,60	2,36	-	-	0,18	-
2	57,20	7,40	21,30	13,40	2,00	-	-	0,30	-
3	50,60	22,10	15.25	12,70	1.36	-	0,37	0,43	0,52
4	45,60	11,90	29,10	13,50	1,11	-	0,43	0,54	0,63
5	44,00	36,80	9,20	12,00	0,95	0,36	0,55	0,74	0,90
6	46,40	27,75	14,00	13,60	1,12	0,30	0,37	0,42	0,51
7	46,00	19,82	21,56	13,55	1,11	-	0,38	0,45	0,55
8	46,00	14,30	26,20	13,50	1,13	0,32	0,40	0,50	0,58

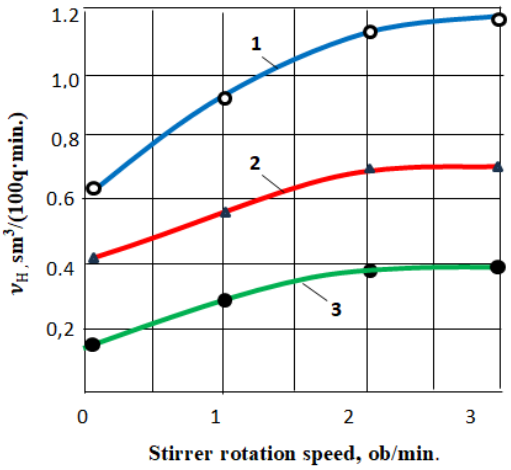

Fig. 5. Effect of mixing intensity on hydrogen permeability of rust with different compositions:

1 - 52,2% SiO_2 ; 14,6 % CaO; 11,6 % FeO; 16,8 % MnO; 2 – 49,0 % SiO2; 4,9 % CaO; 22,2 % FeO; 15,6 % MnO; 3 – 59,4 % SiO_2 ; 4,3 % CaO; 1,1-2,0 % FeO; 19,6 % MnO

In this case, the tangent of the angle of inclination of the straight line to the abscissa axis (Fig. 4) will characterize the apparent activation energy of the slag hydrogen permeability process. For the rust containing 49.0% silica, this value was equal to 56.8 kcal/mol, and for the melt with 54.20% silica, 74.6 kcal/mol [8],

Thus, the study of the hydrogen permeability of unstirred slags showed that the limiting link in the process is the mass transfer of hydrogen in the slag layer, determined mainly by the viscosity of the latter.

$$\upsilon_H = K_{OH^-}\cdot(OH^-) = K_{OH^-}\cdot\sqrt{K_{H_2O}}(O^{2-})P_{H_2O} = K_H\sqrt{P_{H_2O}} \qquad (10)$$

The next series of experimental smeltings was carried out to study the effect of rust mixing intensity on its hydrogen permeability. The slag was stirred with a special molybdenum mixer connected to an electric motor. It was noted (Fig. 6) that with an increase in the slag mixing intensity, the hydrogen mass transfer rate increases only to a certain limit and then remains unchanged at a certain level, depending only on the slag composition (for given values of p_{H_2O} in the gas phase and slag temperature) [9]. The rate of hydrogen transition from the gas phase through the slag to the metal is expressed as the rate of the first-order reaction and is proportional to the square root of the partial pressure of water vapor in the furnace atmosphere:

The activation energy of the process of hydrogen transfer from slag to metal was found to be equal to 70.0% kcal/mol for slag containing 49.0% silica and 97.0 kcal/mol for melt containing 59.4% silica.

The kinetic mode of hydrogen transfer through intensively stirred slags to metal is also confirmed by the peculiar influence of the MnO/FeO ratio in slags on their hydrogen permeability. This part of the study was carried out by us on synthetic rust melted from chemically pure reagents (Table 2).

The first series of experiments was carried out with unstirred slags. From the obtained data (Fig. 7, curve 1) it follows that with an increase in the MnO/FeO ratio from 0.50 to 2.42, the hydrogen permeability of rust increases from 0.42 to 0.54 **sm**³/(100 q·min). Under conditions

of mixed slags [10], the MnO/FeO ratio has a dual effect on the rate of hydrogen transfer from the slag to the metal (Fig. 7, curve 2).

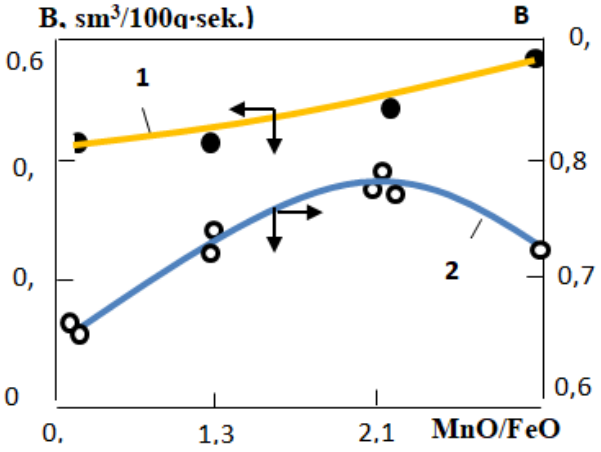

Fig. 6. Effect of the MnO/FeO ratio in slags on their hydrogen permeability at 1650 ^{0} C 1 – unstirred slags; 2 – intensively stirred slags;

using the "narrowing" method when processing experimental data on the hydrogen content in the slag and metal, he determined the equilibrium constants of the latter reactions (12) and (13). The values of the changes in the isobaric potential under standard conditions for these reactions are expressed respectively

$$\Delta G = 118000 - 61{,}5T \qquad (14)$$

$$\Delta G = 192800 - 91{,}0\ T \qquad (15)$$

These equations allow us to conclude that the reactions of hydrogen transfer from slag to metal are sharply endothermic, and the reaction involving iron cations is of greatest importance in the process of hydrogen transfer from slag to metal, because it requires less energy. It is evident from this that at a high value of the MnO/FeO ratio (from 1.85 and above), hydrogen transfer from slag to metal occurs mainly due to manganese cations. This process requires a large energy expenditure, therefore, the hydrogen permeability of slags, starting from the MnO/FeO ratio of 1.85, decreases. After laboratory studies, the effect of the slag regime on the behavior of hydrogen in the metal of acid open-hearth and electric steelmaking furnaces under industrial conditions was studied. The smelting was carried out using an active and silicon-reducing process. The open-hearth furnaces at both plants (Baku Steel Company) had the same capacity (90 t) with a hearth area of 30.0 and 28.0 m2 and were heated with fuel oil. The electric furnace had a capacity of 5 t.

Table 3. Hydrogen behavior in metal during melting carried out by silicon-reducing and active processes using recycled slag.

Melt number	Sample number	[C], %	[Mn], %	Rust composition, %						(H), sm³/100q	υ, sm³/(100 r·c)
				SiO_2	Al_2O_3	FeO	CaO	MgO	MnO		
	1	0,94	0,14	56,30	5,34	15,67	3,56	0,17	16,77	2,60	
1	2	0,46	0,25	57,54	4,54	12,48	3,73	0,14	19,47	2,48	
	3	0,33	0,25	58,80	4,32	10,94	4,14	0,15	19,42	2,70	0,18
	4	0,36	0,35	60,56	4,08	9,86	3,77	0,16	19,44	3,90	
	1	1,04	0,12	50,93	5,50	21,18	4,41	0,12	13,67	4,63	
2	2	0,44	0,31	57,37	3,92	12,48	4,36	0,13	18,91	4,18	
	3	0,36	0,27	61,34	3,44	10,15	3,40	0,13	18,91	3,09	0,14
	4	0,36	0,45	61,46	3,04	9,72	4,02	0,14	17,84	4,54	
	1	0,90	0,28	55,96	4,13	13,78	7,36	0,12	15,75	3,91	0.19
3	2	0,36	0,30	59,41	3,10	10,59	4,64	0,13	18,62	3,26	
	3	0,25	0,27	61,74	3,32	10,61	4,13	0,13	15,24	2,84	
	4	0,27	0,27	60,80	3,76	10,01	4,30	0,14	18,46	4,40	
	1	0,96	0,07	50,82	4,32	19,81	5,02	0,13	17,84	5,02	0,11
4	2	0,45	0,16	57,52	4,40	13,54	5,18	0,15	17,91	2,90	
	3	0,35	0,23	60,02	4,30	12,33	4,70	0,13	17,52	2,70	
	4	0,38	0,50	59,92	4,24	12,19	4,58	0,14	18,11	4,30	
	1	1,01	0,10	54,20	5,82	16,68	7,41	0,15	13,37	3,50	0,15
5	2	0,47	0,29	56.08	4,18	13,06	5,83	0,14	19,03	2,81	
	3	0,32	0,20	58,32	4,46	10,83	5,65	0,14	19,61	2,80	
	4	0,33	0,31	58,48	4,48	10,60	5,77	0,13	19,59	4,06	

Samples were taken: 1 - after melting; 2 - at the end of ore boiling; 3 - at the end of clean boiling; 4 - before tapping.

Silicon reduction smelts were carried out by a duplex process (the main one was acid open-hearth furnaces). The data on these smelts are given in Table 3 (the first six smelts). The last four smelts (see Table 3) were carried out by an active process on a solid charge using 3.5% recycled slag and 0.5% iron ore. The smelts presented were carried out by an active process on a solid charge without the use of recycled rust.

In view of this, the issue of rust formation in an acid steel-making furnace, which has been discussed in detail in various works, is of extreme importance. Early slag formation in an acid steel-making furnace also plays a positive role in preserving the furnace bottoms and slopes from corrosion by rust rich in iron and manganese acids.

Comparison of the hydrogen content in the metal of the studied melts (Table 3). It can be noted that when using recycled slag in the charge, the average hydrogen content in the metal after melting and during the melting process is lower than in the metal of melts carried out without using recycled rust.

To obtain a lower hydrogen content in the metal after melting, it is necessary to have a rust in this period with a SiO_2 (FeO + MnO) ratio of 1.07 - 1.20 (Fig. 10). For melts carried out by the silicon-reducing process, this ratio can have a higher value

During the period of ore and pure boiling, the hydrogen content in the metal decreases and the more so, the higher the value of the ratio in the rust SiO_2 /(FeO + MnO + CaO) (Table 3). When the billet is transferred from the main furnace to the acid furnace in a liquid state, when using recycled rust in the charge, the average hydrogen content in the steel during the entire smelting is lower than in smelts on a solid charge and without recycled slag additives (Fig. 7). Additions of manganese ore instead of ferromanganese to the metal bath give a

lower hydrogen content in the steel (melts 1-5 in Table 3). This is explained by the rapid increase in the silica content in the ruls due to the interaction of manganese ore with the lining of the slopes.

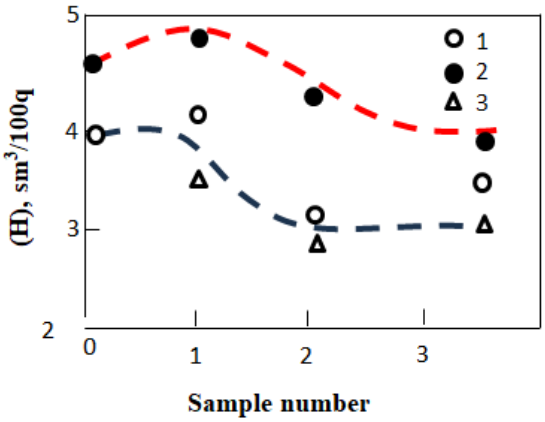

Fig. 7. Behavior of hydrogen in metal the course of acid open-hearth smelting (zero) sample - 1 hour before ore boiling, numbers - number of heats 1 - active process with additives turnover- a lot of rust; 2- without slag additives; 3- cream- recovery process

In an acid electric furnace, due to the lower content of water vapor in the gas phase, the concentration of hydrogen in the metal is significantly lower than in open-hearth steel. But even under these conditions, the rust is not a complete insulator of the metal from the hydrogen-containing atmosphere. Based on our data on the study of the behavior of hydrogen in the metal bath during 60 melts in an acid electric furnace, 14 of which are described in detail, the following pattern was revealed for the melting periods As a result of this study, it was established that in order to obtain a low hydrogen content in acid electric steel upon melting and throughout the entire melting process, it is necessary to obtain a silica content in the slag upon melting of at least 45–48%, for which it is advisable to add calcined sand or recycled rust.

Melting period	**Hydrogen content in steel, sm³/100 q**
Half an hour before melting	2,10 – 3,50
By melting	2,54 – 5,40
By melting	1,40 – 1,93
Before release	1,96 -2,94

Conclusions

1. By reducing the acidity of the slag, the service life of refractory materials with basic properties was increased

2. By creating a basic slag, the service life of furnaces built from basic refractory materials increased from approximately 1 to 3-3.5 times

3. It was found that the quality of the produced steel also depends on the nature of the slag created.

4. The chemical composition of the steel obtained during the smelting process also has a significant effect

References

[1]. V.F.Gakhramanov, A.H.Guliyev, N.S.Rzayev, Z.S.Musayev, "Effect of increasing electrical resistance of alloys of various compositions" İnternational Journal on "Technical and Physical Problems of Engineerin" Volume 16, Number 4, 2024,Pages 355-361

[2]. V.F.Gakhramanov, "Improving the properties of abrasive steels by chemical-thermal treatment". XIX republican conference of doctoral students and young researchers, pp. 167-169, Baku, 2016.

[3]. V.F.Gakhramanov, E.A.Aslanov,"Influence of preliminary oxidation on the process of nitriding of iron alloys", Mechanics of Machines, Mechanisms and Materials. Scientific and technical journal, No. 2(55). pp. 33-38, Baku, 2021

[4]. S.N. Namazov, V.F.Gakhramanov, A.A. Dzhafarova "Structural characteristics of powdered iron graphite with subsequent oxidation" International scientific practical conference, pp. 91-94, Yurga, 2016

[5] V.F.Gakhramanov, "Diffusion chroming and carbochroming of stamping steels", Oil and gas business. Scientific and technical journal, Founder: FGBOU VO Ufa State Petroleum Technical University, Vol. 3, No. 19, pp.121-127, 2021

[6]. M.Hill, "Materials Protection and Performance", Technology and organization of production,Vol. 11, No. 1, pp. 1-19 , 1995

[7]. J.J.Mistuo, "İron and Steel " İnsnt. Japan, 2015, v 48, №2, p 97.

[8]. G.S. Ershov and others. "Black metallurgy", 2020

[9]. V.I. Javanese. "Сталь", 2018Ю №3-4, p. 17.

[10]. P.Ya. Ageev, V.G. Chernov «New technology technology in welding production» issue 253, 2022

2025. Volume 9, Number 1 Pages 47-50

UOT: 621.89
DOI: https://doi.org/10.30546/09085.2025.01.017

PHYSICAL MODELING OF THE EFFECT OF ADHESION ON THE FRICTION PROCESS IN MACHINES AND PARTS

N.Z. ABDULLAYEVA[1], Y.A.ABDULAZIMOVA[*], A.M.YARIYEVA[2]

[1]*Azerbaijan Technical University, Baku, Azerbaijan*

** Baku Engineering University, Khirdalan, Azerbaijan*

[2] *Azerbaijan Technical University, Baku, Azerbaijan*

[*]*Corresponding author*

yabdulazimova@beu.edu.az (Abdulazimova Yegana Ayyub)

ARTICLE INFO

Article history
Received: 2025-03-14
Received in revised form: 2025-03-14
Accepted:2025-04-15
Available online

Keywords:
Friction; deformation; tension; adsorption; adhesion.
JEL Classification: O33, L60, C61

ABSTRACT

This article investigates the effect of adhesion on the friction process of mechanisms in machines and their components. The research indicates that adhesion has a significant influence on the mechanism of the friction process. It is evident that factors such as the adhesion layer formation mechanism, its strength, dynamic conditions, surface tension, molecular forces, and the surface condition of the adhesion layer all affect the friction process. Furthermore, the work expended on frictional adhesion varies depending on surface tension and the wetting angle. The research shows that if adhesion is diffusive, the primary controlling factor is the energy generated between crystal defects. This energy varies based on the inter-defect distance and inter-defect electrification. If adhesion during friction is of a diffusive nature, the nature of diffusion around any axis and the speed of diffusion can be mathematically described. If adhesion during friction is deformational, deformation occurs in different directions.

1. Introduction

The mechanism of friction in machines and the factors that influence it remain a critical research topic. Finding an optimal solution to this problem requires examining it from nanotribological, microtribological, and macrotribological perspectives [1].

From a nanotribological standpoint, understanding the adhesion mechanism and its effect on friction allows for a more comprehensive analysis of the issue. During friction, one material exerts force on another, and at the points of contact, atomic interactions occur as the atoms attract each other [2]. A key aspect of this phenomenon is the behavior of atoms in frictional contact and the physical modeling of adhesion effects, which can help address the problem.

The impact of adhesion on friction depends on multiple factors. These include the adhesion layer formation mechanism, the strength of the adhesion layer, the influence of dynamic conditions, the interaction between adhesion and cohesion, and the effect of surface tension on the adhesion layer [3]. Additionally, molecular forces, the nature and variation of these forces, the surface condition of the adhesion layer, and the influence of air humidity on adhesion all play a role in determining friction behavior [4].

2. Research methodology

Initially, the study focuses on the work of adhesion during friction, particularly its relationship with surface tension (θ) and wetting.

$$W_{adg} = \theta_{surface\ tension}(1 + cos\theta) + N \quad (1)$$

The wetting angle plays a crucial role in adhesion, and the first challenge is to control the factors that influence it during friction. One of the most intriguing aspects of adhesion is the mechanism by which it occurs during friction.

From a mechanical perspective, adhesion takes place when the adhesive substance fills the pores of the material. If adhesion follows an adsorption mechanism, it occurs at the molecular level through surface contact. In cases where adhesion follows a chemical mechanism, it results from the formation of chemical compounds between two substances. It is also possible that frictional adhesion occurs through an electrification mechanism.

A key area of interest is how these mechanisms interact. Depending on the conditions of friction, they may replace one another, combine to form a more complex adhesion mechanism, or alter the nature of friction. If adhesion occurs via diffusion, the primary concern is the energy generated between defects in the crystal structure.

$$\mathrm{E} = \frac{q^2}{\varepsilon R} \quad (2)$$

It is clear that if the mechanism of adhesion during friction is diffusion, the distance between R-defects and the electrification between q-defects depend on the dielectric permeability of the ε −material.

$$\mathrm{jx} = \frac{vC(x,\tau)}{vx} \quad (3)$$

When there is friction on the surface, we can write the mechanism of diffusion around any axis as follows:

$$\mathrm{V} = \frac{dq}{d\tau} = DS\frac{vC(x,\tau)}{vx} \quad (4)$$

The rate of diffusion in adhesion during friction is:

$$\mathrm{j} = -\mathrm{D\ grad\ C(x,y,z,}\ \tau) = -\mathrm{D}\nabla C(\mathrm{x,y,z,}\ \tau) \quad (5)$$

If diffusion goes in 3 directions in the process of adhesion during friction, then:

$$\mathrm{f} = F_{slide}/F_n = (F_{dif} + F_{ad}/F_n) \quad (6)$$

If the adhesion during friction is of a diffusion nature, then the basic formula that characterizes the friction is as follows:

$$M_{ir} = \int (F_i X_R - F_R X_i) dV \quad (7)$$

If adhesion during friction is deformational, the friction mechanism will behave as follows: The friction in different directions changes depending on the processes occurring within a single volume. However, if one part of the rubbing surface experiences adhesion deformation while another part follows a diffusion mechanism, the overall friction mechanism will differ. Friction progresses more rapidly in the deformation-dominated region.

On the other hand, if adhesion during friction follows an adsorptive mechanism, the friction mechanism will behave differently. The way adhesion changes during friction depends on various factors, especially when adsorption is involved. In this case, key influencing factors include the integral changes in thermodynamic functions, variations in Gibbs energy, and the mechanism of adsorption change based on surface parameters:

$$W_a = K_1(1-\theta)\mathrm{p} \tag{8}$$

If adhesion during friction follows the adsorption mechanism, the main controlling factors are the speed and pressure of W_a −adsorption. Additionally, one of the key factors in this process is the thermal effect of adsorption. If adhesion during friction is governed by adsorption, the variation in thermal effects plays a crucial role in determining the overall mechanism:

$$\Delta H = \Delta G + T\Delta s \tag{9}$$

3. Discussion of results

The thermal effect of adsorption during friction depends on the mechanism of change in surface enthalpy (H), surface free energy (G), and entropy change (S). However, if we were to physically describe the adsorption mechanism of adhesion during friction:

$$D_s = \frac{S}{V} = \frac{K_{sv}}{q} \tag{10}$$

It is clear that the adhesion $K_{sv}-$ during friction depends on the coefficient characterizing the shape of the particles on the surface and the surface-volume coefficient:

$$\mathrm{S} = 4\pi {R^2}_0 n^{2/3} \tag{11}$$

$$\mathrm{V} = \frac{4}{3}(\pi \mathrm{R^3}_0 \mathrm{n}) \tag{12}$$

It is clear that the radius of atoms and molecules (R_0) varies depending on the surface-to-volume ratio and the number of molecules and atoms in the particle (N). If adhesion during friction is adsorptive, then the surface energy changes depending on the following parameters:

$$G_s = 4\pi v \left|\frac{3\pi}{4\pi}\right|^{\frac{2}{3}} \cdot n^{\frac{2}{3}} \tag{13}$$

It is clear that the mechanism of adsorption-type adhesion during friction depends on surface tension (v), surface area (s), and the volume of v-atoms and molecules. At the same time, the freedom of the mechanism of adsorption-type adhesion during friction is influenced by:

$$G_V = -nK_BTkln\left(\frac{P}{P_s}\right) \tag{14}$$

We can express the effect of energy as follows: If adhesion during friction follows the adsorption mechanism, the free energy (K_B) depends on the Boltzmann constant, the absolute temperature (T), and the vapor pressure (P_1P_s).

If the adhesive deforms during friction, the direction of friction depends on the stresses. It is clear that, in this case, the stresses can change direction depending on various parameters. These stresses are influenced by several factors, including the mechanisms of adhesion and adsorption, as well as the friction mechanism itself.

$$-\oint \theta_{ir} df_R \tag{15}$$

Distribution of the force applied to friction in different directions and coordinates:

$$M_{ir} = \int (F_i X_R - F_R X_i) dV \qquad (16)$$

The stress distribution during friction is:

$$M_{stress\ distrib} = \int \left(\frac{\vartheta \emptyset_{ie}}{\vartheta X_e} X_R - \frac{\vartheta \emptyset_{Re}}{\vartheta X_e}\right) dV = \int \frac{\vartheta (\emptyset_{ie} X_H - \emptyset_{Re} X_{i)}}{\vartheta X_L} dV - \int (\emptyset_{ie} \frac{\vartheta X_R}{\vartheta X_L} - \emptyset_{Re} \frac{\vartheta X_i}{\vartheta X_L}) dV \qquad (17)$$

During friction, if adhesion is deformational, we can express the change in internal energy (dε) as follows: (Provide the equation or description here)

$$\mathrm{d}\varepsilon = Tds + \emptyset_{in} du_{iR} \qquad (18)$$

In general, the processes that occur during friction, the factors that influence them, and the physical modeling of their effects on the mechanism are highly relevant.

4. Conclusion

1. Adhesion has a significant impact on the mechanism of the friction process.

2. The formation mechanism of the adhesion layer during friction directly affects the friction process.

3. The work required for frictional adhesion varies depending on surface tension and the wetting angle.

4. If adhesion is diffusive during friction, the primary controlling factor is the energy generated between crystal defects.

5. If adhesion during friction is deformational, the distribution of deformation and stress changes direction under the influence of various parameters.

REFERENCE LIST

1. Janachmadov A. X., Gurbanov R. A., Aliyev A.M. Basic of tribology. Textbook. Baku. Çashıoğlu, 2001.276 p.
2. Penкin N.S.The basic of tribology and tribotechnikal.M.Mashinostroenie,2008.206 p.
3. Sadixov A.I. The increesing durability of machne detals. Baku. Elm-2001.148p.
4. Garkunov D. N. Tribotechnikal., Preparation and ekport machine/M.Printing press/ MSXA,2002.632 P

JOURNAL OF BAKU ENGINEERING UNIVERSITY- MECHANICAL AND INDUSTRIAL ENGINEERING
2025. Volume 9, Number 1 ***Pages 51-56***

UOT: 539
DOI: https://doi.org/10.30546/09085.2025.01.008

APPLICATION OF THE TAGUCHI METHOD IN PROCESSING EXPERIMENTAL RESULTS

N. S. RZAYEV
Baku Engineering University, Hasan Aliyev str., 120, Baku, AZ0102, Azerbaijan
nzayev@beu.edu.az

M. M. BASHIROV
Baku Engineering University, Hasan Aliyev str., 120, Baku, AZ0102, Azerbaijan
mbashirov@beu.edu.az

N. D. NABIYEV
Baku Engineering University, Hasan Aliyev str., 120, Baku, AZ0102, Azerbaijan
nnabiyev@beu.edu.az

ARTICLE INFO

Article history:

Received: 2025-02-20

Received in revised form: 2025-03-03

Accepted: 2025-04-22

Available online

Keywords:

Taguchi method; experimental results; process optimization; Signal-to-Noise ratio; orthogonal arrays; statistical analysis.

JEL Classification: C15, C61, L60

ABSTRACT

This study examines in detail the application potential of the Taguchi method in processing and optimizing experimental data. The Taguchi method is an effective technique developed to improve manufacturing processes and especially to optimize the effects of controllable parameters, which is widely used in the field of quality engineering. In the study, the optimization of the main parameters that are effective in minimizing surface roughness (Ra) during a material processing process in a manufacturing process is considered as a case study, and how maximum efficiency can be achieved with less experimentation is demonstrated with solutions. As a result, the generalizability of the method in engineering applications and the potential benefits it can offer in different industrial areas are discussed. In addition, in the processing of the results of the experiment, the practical results of the Taquchi method have been processed.

1. Introduction

Experimental designs play an important role in improving quality in production and operational processes, increasing efficiency to high levels and achieving the best results with minimum cost. Traditional experimental design methods generally require a large number of experiments, resulting in high costs in terms of time and resources. In contrast, the Taguchi method allows parameter optimization with a small number of experiments. This method is an effective approach widely used in the field of quality engineering and experimental design.

Studies in the literature on the Taguchi method show the effectiveness of the method in different industrial applications. For example, Ross has shown that the Taguchi method provides a significant cost advantage in quality improvement projects in the automotive sector [1]. Phadke, on the other hand, has emphasized the simple and systematic structure of the method in design

optimization and emphasized how valuable the results obtained with a small number of experiments are in the decision-making process [2]. Similarly, Güllü et al. have shown that the Taguchi method is an effective method in optimizing surface roughness in applications in the steel industry [3]. In [6] and [7], experimental values of wear on shafts subjected to longitudinal bending deformation and shafts with different widths were analyzed using the Taguchi method. The optimal combination of controlled factors for obtaining the smallest wear was determined. The percentage of factors that most affect wear is shown.

The aim of this study is to present the theoretical background of the Taguchi method and an application example to reveal the advantages and application potential of the method.

2. Theoretical Foundation of the Taguchi Method

The Taguchi method, developed by Genichi Taguchi, focuses on robust design to enhance product and process performance by reducing the influence of noise factors. The Taguchi method involves several key concepts that allow for effective experimentation and data analysis. The main components include:

- Factorial Design: This involves selecting a set of factors that may affect a given process and evaluating their interactions. Taguchi typically uses a fractional factorial design to reduce the number of experimental runs.
- Orthogonal Arrays (OAs): These arrays are pre-arranged matrices that allow for the efficient and balanced study of the effects of multiple factors on an experiment. By using OAs, the number of experiments can be minimized, ensuring an optimal combination of factors.
- Signal-to-Noise (S/N) Ratio: The S/N ratio is a crucial metric in the Taguchi method. It quantifies the variability in an experiment, where the "signal" represents the desired output and the "noise" signifies the variability or unwanted influences. Maximizing the S/N ratio leads to improved robustness by minimizing the effects of noise factors.
- Control Factors and Noise Factors: In the Taguchi method, control factors are variables that the experimenter can manipulate, while noise factors represent uncontrollable elements that may affect the outcome. The goal is to identify settings for the control factors that minimize the influence of noise.

Benefits of the Taguchi Method

- Efficiency: Reduces the number of experiments without compromising reliability.
- Simplicity: Straightforward implementation using predefined orthogonal arrays.
- Robustness: Focuses on minimizing variability and achieving consistent performance.
- Cost-effectiveness: Lowers experimental costs and resource requirements.

3. Taguchi Method in Experimental Design

The Taguchi method is an experimental design method used in quality control and product development processes. This method aims to conduct a minimum number of experiments to optimize the performance of a particular process or product. The application steps of the Taguchi method can be summarized as follows:

1. Problem Definition: Targeted quality characteristics and parameters to be improved are determined. The output of the problem (e.g. maximum yield, minimum error) is defined.

2. Determination of Controllable and Uncontrollable Factors: Controllable factors: Process or product parameters (e.g. temperature, speed, pressure). Uncontrollable factors: Environmental effects or external conditions (e.g. humidity, vibration).

3. Determination of Experiment Levels and Factors: Appropriate levels are selected for each controllable factor (e.g. low, medium, high). Levels are important for determining the variety of experiments.

4. Selection of Orthogonal Array: The Taguchi method uses orthogonal arrays in planning experiments. These arrays provide a balanced distribution between factors and levels. A suitable orthogonal array is selected to reduce the number of experiments (e.g. L4, L8, L16).

5. Conducting Experiments: Experiments are performed in accordance with the plan prepared according to the orthogonal array. Process or product performance is measured under each condition.

6. Calculating Signal-to-Noise (S/N) Ratio: S/N ratio is used to evaluate performance variability. The S/N ratio formula is selected according to the targeted quality characteristic:

o Smaller is better: Minimum error is desired.

o Larger is better: Maximum performance is desired.

o Nominal is better: Closeness to a specific target value is desired.

7. Analysis and Optimization: Based on the experimental results, the effects of factors and levels are analyzed. The combination of factors and levels that provides the best performance is determined.

8. Verification Experiment: A verification experiment is performed using the optimized parameters. The obtained results are compared with the predicted results.

9. Interpretation and Application of Results: The effect of the optimum parameter combination on the process or product is evaluated. If necessary, the method is integrated into practical applications.

4. Practical Applications of the Taguchi Method

The Taguchi method has been applied in a wide variety of fields, with notable success in manufacturing, materials processing, and quality control. Some of the key applications include:

- Manufacturing and Process Control: In manufacturing, the Taguchi method helps identify optimal settings for machine parameters, tooling, and operational procedures to reduce defects and improve product consistency. It is commonly used for process optimization in the automotive, electronics, and aerospace industries.
- Quality Improvement: The Taguchi method is instrumental in achieving consistent product quality by identifying factors that contribute to variability and providing solutions to minimize their impact. It has been used in the production of consumer goods, pharmaceuticals, and other sectors where quality is paramount.
- Materials Science: In materials processing, the Taguchi method has been used to optimize the properties of materials such as metals, polymers, and composites. By systematically studying factors such as temperature, pressure, and time, researchers can fine-tune processing parameters to achieve desired material characteristics.

Sample work. Problem: In a production process, it is desired to minimize the surface roughness (Ra) during a material processing operation. Cutting speed, feed rate and depth of cut are determined as process parameters. Taguchi method will be used to analyze the effect of these three factors on surface roughness and to find the most suitable parameter combination.

1. 1. Factors and Levels:

1.1. Cutting Speed (m/min):

o Level 1: 100

o Level 2: 150

o Level 3: 200

1.2. Feed Rate (mm/min):

o Level 1: 0.1

o Level 2: 0.2

o Level 3: 0.3

1.3. Depth of Cut (mm):

o Level 1: 0.5

o Level 2: 1

o Level 3: 1.5

2. Experimental Design: Taguchi method uses orthogonal arrays to minimize the number of experiments. Since there are three factors and three levels in each, L9 array was deemed appropriate. A total of 9 experiments will be conducted in this array.

Table 1. Level values of the factors managed

Experiment No.	Cutting Speed	Feed Rate	Depth of Cut
1	50	0.1	0.5
2	50	0.2	1.0
3	50	0.3	1.5
4	100	0.1	1.0
5	100	0.2	1.5
6	100	0.3	0.5
7	150	0.1	1.5
8	150	0.2	0.5
9	150	0.3	1.0

3. Experimental Results: Surface roughness (Ra, in micrometers) will be used to evaluate the machined quality of the metal surface. Surface roughness (Ra) was measured for each combination and the results were recorded:

Table 2. Measured value of the surface culture

Experiment No.	Cutting Speed	Feed Rate	Depth of Cut	Ra (μm)
1	50	0.1	0.5	1.2
2	50	0.2	1.0	1.5
3	50	0.3	1.5	2.1
4	100	0.1	1.0	1.0
5	100	0.2	1.5	1.4
6	100	0.3	0.5	1.8
7	150	0.1	1.5	0.9
8	150	0.2	0.5	1.3
9	150	0.3	1.0	1.7

3. 2. Analysis of Data: Based on the analysis of the surface roughness values obtained at the end of each experiment, it can be determined which factors and levels provide the lowest roughness (i.e. the highest quality).

Calculation of Signal/Noise Ratio (S/N Ratio): Taguchi method tries to optimize the signal/noise ratio. As a measure of surface roughness, smaller-the-better approach is usually used. In this case, lower roughness is better. Since the surface roughness is to be minimized, the "Smaller-the-Better" criterion is used. The S/N ratio is calculated as follows:

$$S/N = -10 \cdot log_{10}\left(\frac{1}{n}\sum_{i=1}^{n} y_i^2\right) \qquad (1)$$

Interpretation of Results: The effects of factors on surface roughness are calculated. Average S/N ratios are found for each factor and graphs are drawn. It will reveal which factors and levels show better performance.

Result: For example, as a result of the analysis, the following finding can be obtained:

- Cutting speed = 150 m/min
- Feed rate = 0.1 mm/min
- Cutting Depth = 0.5mm

This combination results in the lowest surface roughness (highest quality).

6. Validation Experiment: Experiment is performed with the obtained optimum parameters and the results are compared with the predicted improvement.

This example shows an application and analysis of the Taguchi method, which allows you to quickly assess the effects of factors and determine the conditions that will provide the best performance.

Conclusion and discussions

This study has shown that the Taguchi method is an effective tool for parameter optimization with a small number of experiments. The simple and effective structure of the method has a wide application potential in the field of engineering and quality control. Future studies can contribute to the method becoming more generalizable by examining its applications in different industrial areas.

The Taguchi method provides a powerful and systematic framework for processing experimental results. The Taguchi method, through the use of orthogonal arrays and S/N ratios,

helps identify optimal operating conditions for processes and products efficiently while minimizing the number of trials required. The method's application spans numerous industries, offering valuable insights into process improvement, quality control, and product design. As industries continue to demand higher levels of precision and efficiency, the Taguchi method remains a valuable tool for achieving these objectives.In future applications, the integration of modern statistical software and machine learning techniques could further enhance the power of the Taguchi method, enabling even more precise optimization in complex systems.

The theoretical foundations of the Taguchi method are developed here, and the application areas are shown. In addition, the application sequence of the Taguchi method is developed in the development of the experimental results.

An example of the application of the Taguchi method is shown here. Here, the effect of cutting depth, cutting speed and feed rate on the surface roughness was analyzed using the Taguchi method. As a result of the analysis, the optimal values of cutting depth, cutting speed and feed rate were determined. With these values, the minimum value of surface roughness is obtained.

REFERENCES

1. Ross, P.J. (1996) Taguchi Techniques for Quality Engineering: Loss Function, Orthogonal Experiments, Parameter and Tolerance Design. 2nd Edition, McGraw-Hill, New York, 329p.
2. Phadke, M. S. (1989). Quality Engineering Using Robust Design. Prentice Hall, 334p.
3. Gullu, A., Demir, H., Aydin, M. (2010). Optimization of surface roughness in steel production by Taguchi method. Journal of Metallurgical and Materials Engineering, Vol 45, No 3, pp. 210-215.
4. Taguchi, G., Konishi, S. (1987). Taguchi Methods: Orthogonal Arrays and Linear Graphs. Dearborn, MI: American Supplier Institute.
5. Antony, J. (2003). Design of Experiments for Engineers and Scientists. Butterworth-Heinemann, 261p.
6. Mirzayev H.I, Rzayev N. S. (2022). Experimental study of wear in shafts subjected to longitudinal bending deformation using the Taguchi method. Journal of Baku Engineering University. Mechanical and industrial engineering. Vol 6, No2, pp. 59–66.
7. N.S. Rzaev. (2023). Investigation of the deflection of bars of different width by the Taguchi method, Vestnik RUDN. Series: Engineering research. Volume 24, No. 4, pp. 365-372.

UOT 621.311
DOI: https://doi.org/10.30546/09085.2025.01.025

REGRESSION MODEL OF THE DEPENDENCE OF ARC OVERVOLTAGE ON GROUND FAULT RESISTANCE AND NETWORK PHASE CAPACITANCE RELATIVE TO GROUND

N.I. ORUJOV[1], H.B. GULIYEV[2], S.J. ALIMAMMADOVA[3]

[1]*Baku Engineering University, AZ0101, Hasan Aliyev str. 120, Khirdalan, Azerbaijan*
email: norucov@beu.edu.az
[2]*Azerbaijan Technical University, AZ1073, H. Javid avenue 25, Baku, Azerbaijan*
email: huseyngulu@mail.ru
[3]*Azerbaijan State Oil and Industry University, AZ1010, Azadlig Avenue 16/21, Baku, Azerbaijan*
email: sara_elimemmedova@mail.ru

ARTICLE INFO

Article history
Received:2025-04-07
Received in revised form: 2025-04-15
Accepted: 2025-04-22
Available online

Keywords:
neutral-isolated network; non- stationary ground fault; overvoltage multiplicity; regression equation, 3D modeling.
JEL Classification: O32

ABSTRACT

In neutral-isolated networks, testing insulation under load requires determining the dependencies between parameters characterizing single-phase non-stationary ground faults. Identifying such dependencies is often accompanied by a number of difficulties. Therefore, simple mathematical models that allow understanding the relationships between these parameters in practical conditions must be developed. This paper considers the issue of determining the relationship between the overvoltage arising in a neutral-isolated network as a result of non-stationary ground faults, the ground fault resistance, and the network phase capacitance to ground. For this purpose, a regression equation was obtained to describe the dependence of the overvoltage multiplicity on the ground fault resistance and network phase capacitance to ground, and the corresponding 3D visualization was constructed.

Introduction

Neutral-isolated networks play a significant role in supplying consumers with electrical energy. Such networks primarily perform the distribution of electrical energy among consumers, comprising numerous overhead and cable lines. During operation, the insulation of these lines, especially cable lines, deteriorates due to prolonged electrical, thermal, and mechanical impacts. This results in a decrease in insulation resistance and electrical strength, which can cause sudden damage and disrupt the power supply to consumers. Therefore, timely detection of weak insulation sections in networks and restoration of damaged areas is of great importance. For this reason, network equipment is periodically disconnected and subjected to insulation testing [1,2]. However, such tests are considered inconvenient as they require considerable time and labor. Consequently, methods for testing network insulation without disconnecting equipment have been proposed [3-5]. These methods are based on the principle of creating artificial ground faults under load conditions. However, the devices used in these methods cannot perform regulation and control functions. Therefore, a new method for testing insulation in neutral-isolated networks has been proposed [6]. According to this method, controlled and regulated artificial non-stationary ground faults are created in the network to test the insulation under load

conditions. It is important to note that the overvoltage value arising during such ground faults, based on Petersen's theory, depends on the network's phase-to-ground capacitance, ground fault resistance, and ground fault angle. Hence, determining the test voltage value requires prior identification of the ground fault resistance and ground fault angle. For this purpose, the dependence of arc overvoltage multiplicity on ground fault resistance, ground fault angle, and network phase-to-ground capacitance is determined based on non-stationary ground faults in neutral-isolated networks.

1. Problem statement

To determine the dependence of arc overvoltage multiplicity on ground fault resistance, ground fault angle, and network phase-to-ground capacitance, the numerical solution of the system of differential equations characterizing the transient process of non-stationary ground faults in neutral-isolated networks must be performed using modern computational technologies. However, the numerical solution of the problem is significantly complicated due to the "stiffness" of these differential equations, which in some cases disrupts the stability of the system solution and distorts the results. Therefore, to overcome such difficulties, it is necessary to obtain analytical expressions that define the dependencies between the arc overvoltage multiplicity (k), the ground fault resistance (R_0), the ground fault angle (φ), and the network phase-to-ground capacitance (C_f). It should be noted that analytical expressions for the dependence of arc overvoltage multiplicity on ground fault resistance were previously considered in [7,8], on ground fault angle in [9,10], on network phase-to-ground capacitance in [11,12], and on both ground fault resistance and ground fault angle in [13-16]. As a continuation of these studies, this work focuses on obtaining the regression model of the dependence of arc overvoltage multiplicity on ground fault resistance and network phase-to-ground capacitance.

2. Problem solving

The analytical expression for the dependence of the arc overvoltage multiplicity on the ground fault resistance and the network's phase capacitance relative to the ground in a neutral-isolated electrical network during single-phase ground faults is considered. For this purpose, the results of experimental studies carried out on a low-voltage model of a neutral-isolated network, presented in Table 1, are used $\left(\varphi = 90^\circ\right)$ [6].

Table 1. $k = f\left(R_0, C_f\right)$ **dependence**

R_0, Om	C_f, mkF						
	1	***2***	***3***	***4***	***5***	***6***	***8***
5	3,30	2,99	2,85	2,74	2,66	2,58	2,47
10	2,96	2,74	2,59	2,47	2,39	2,33	2,21
15	2,77	2,54	2,39	2,28	2,20	2,14	2,08
20	2,62	2,38	2,24	2,13	2,06	2,01	1,92
25	2,49	2,25	2,12	2,02	1,95	1,91	1,84
30	2,38	2,15	2,02	1,93	1,88	1,84	1,80

As seen from Table 1, the dependence between the arc overvoltage multiplicity, the ground fault resistance, and the network's phase capacitance relative to the ground can be approximated by the following regression equation [17, p. 133-135]:

$$k = \frac{a}{R_0} + \frac{b}{C_f} + c, \quad (1)$$

Here, $a, b, c -$ is referred to as the regression coefficients.

If we assume the substitutions in equation (1) as $\frac{1}{R_0} = x$ və $\frac{1}{C_f} = y$

$$k = ax + by + c, \quad (2)$$

Thus, the dependence between the arc overvoltage multiplicity (k), the conductance of the ground fault circuit (x), and the reciprocal value of the network's phase capacitance relative to the ground (y) can be approximated by a linear regression equation (Table 2).

Table 2. $k = f(x, y)$ **dependence**

x	y						
	1,00	0,50	0,333	0,250	0,200	0,167	0,125
0,200	3,30	2,99	2,85	2,74	2,66	2,58	2,47
0,100	2,96	2,74	2,59	2,47	2,39	2,33	2,21
0,067	2,77	2,54	2,39	2,28	2,20	2,14	2,08
0,050	2,62	2,38	2,24	2,13	2,06	2,01	1,92
0,040	2,49	2,25	2,12	2,02	1,95	1,91	1,84
0,033	2,38	2,15	2,02	1,93	1,88	1,84	1,80

Regression coefficients are determined by the following expressions [17, p.133-135]:

$$\left.\begin{aligned} a &= \frac{\sigma_k}{\sigma_x} \cdot \frac{r_{kx} - r_{ky} r_{xy}}{1 - r_{xy}^2}; \\ b &= \frac{\sigma_k}{\sigma_y} \cdot \frac{r_{ky} - r_{kx} r_{xy}}{1 - r_{xy}^2}; \\ c &= \bar{k} - a\bar{x} - b\bar{y} \end{aligned}\right\}, \quad (3)$$

Here, $\bar{x}$ – the mean value of the quantity x, $\bar{y}$ – the mean value of the quantity y, $\bar{k}$ – the mean value of the quantity k, σ_x – the root mean square deviation of the quantity x, σ_y – the root mean square deviation of the quantity y, σ_k – the root mean square deviation of the quantity k, r_{xy} – the linear correlation coefficient between the quantities x and y, r_{kx} – the linear correlation coefficient between the quantities k and x, and r_{ky} – the linear correlation coefficient between the quantities k and y are determined based on the correlation table (Table 3). The following notations are adopted according to the correlation table:

$$A_i = (x_i - \bar{x})^2; \; B_i = (y_i - \bar{y})^2; \; C_i = (k_i - \bar{k})^2; \; D_i = (x_i - \bar{x}) \cdot (y_i - \bar{y});$$

$$E_i = (k_i - \bar{k}) \cdot (x_i - \bar{x}); \; F_i = (k_i - \bar{k}) \cdot (y_i - \bar{y}); \; M_i = \left| \frac{ax_i + by_i + c - k_i}{k_i} \right|; \; N_i = (ax_i + by_i + c - k_i)^2.$$

$$n = 42;$$

$$\sum_{i=1}^{n} x_i = 3{,}43; \; \sum_{i=1}^{n} y_i = 15{,}45; \; \sum_{i=1}^{n} k_i = 97{,}62;$$

$$\sum_{i=1}^{n}\left(x_i-\bar{x}\right)^2=0{,}13747222;\ \sum_{i=1}^{n}\left(y_i-\bar{y}\right)^2=3{,}35869048;\ \sum_{i=1}^{n}\left(k_i-\bar{k}\right)^2=5{,}259829;$$

$$\sum_{i=1}^{n}\left(x_i-\bar{x}\right)\left(y_i-\bar{y}\right)=0;\ \sum_{i=1}^{n}\left(k_i-\bar{k}\right)\left(x_i-\bar{x}\right)=0{,}6259;\ \sum_{i=1}^{n}\left(k_i-\bar{k}\right)\left(y_i-\bar{y}\right)=2{,}5669524;$$

$$\bar{x}=\frac{\sum_{i=1}^{n}x_i}{n}=0{,}082;\ \bar{y}=\frac{\sum_{i=1}^{n}y_i}{n}=0{,}368;\ \bar{k}=\frac{\sum_{i=1}^{n}k_i}{n}=2{,}324;$$

Table 3. Correlation table

i	x_i	y_i	k_i	A_i	B_i	C_i	D_i	E_i	F_i	M_i	N_i
1	0,200	1,000	3,30	0,01400278	0,39960459	0,952018	0,07480357	0,1154595	0,6167908	0,013993	0,002132
2	0,100	1,000	2,96	0,00033611	0,39960459	0,404133	0,01158929	0,0116548	0,4018622	0,023350	0,004777
3	0,067	1,000	2,77	0,00022500	0,39960459	0,198661	-0,00948214	-0,0066857	0,2817551	0,011148	0,000954
4	0,050	1,000	2,62	0,00100278	0,39960459	0,087447	-0,02001786	-0,0093643	0,1869337	0,016503	0,001870
5	0,040	1,000	2,49	0,00173611	0,39960459	0,027461	-0,02633929	-0,0069048	0,1047551	0,051289	0,016310
6	0,033	1,000	2,38	0,00233611	0,39960459	0,003104	-0,03055357	-0,0026929	0,0352194	0,087125	0,042997
7	0,200	0,500	2,99	0,01400278	0,01746173	0,443176	0,01563690	0,0787762	0,0879694	0,008682	0,000674
8	0,100	0,500	2,74	0,00033611	0,01746173	0,172818	0,00242262	0,0076214	0,0549337	0,084398	0,053477
9	0,067	0,500	2,54	0,00022500	0,01746173	0,046533	-0,00198214	-0,0032357	0,0285051	0,072053	0,033494
10	0,050	0,500	2,38	0,00100278	0,01746173	0,003104	-0,00418452	-0,0017643	0,0073622	0,041553	0,009781
11	0,040	0,500	2,25	0,00173611	0,01746173	0,005518	-0,00550595	0,0030952	-0,0098163	0,006412	0,000208
12	0,033	0,500	2,15	0,00233611	0,01746173	0,030376	-0,00638690	0,0084238	-0,0230306	0,025684	0,003049
13	0,200	0,333	2,85	0,01400278	0,00119189	0,276376	-0,00408532	0,0622095	-0,0181497	0,004680	0,000178
14	0,100	0,333	2,59	0,00033611	0,00119189	0,070604	-0,00063294	0,0048714	-0,0091735	0,080552	0,043526
15	0,067	0,333	2,39	0,00022500	0,00119189	0,004318	0,00051786	-0,0009857	-0,0022687	0,067110	0,025726
16	0,050	0,333	2,24	0,00100278	0,00119189	0,007104	0,00109325	0,0026690	0,0029099	0,038516	0,007443
17	0,040	0,333	2,12	0,00173611	0,00119189	0,041733	0,00143849	0,0085119	0,0070527	0,005568	0,000139
18	0,033	0,333	2,02	0,00233611	0,00119189	0,092590	0,00166865	0,0147071	0,0105051	0,028635	0,003346
19	0,200	0,250	2,74	0,01400278	0,01389031	0,172818	-0,01394643	0,0491929	-0,0489949	0,012034	0,001087
20	0,100	0,250	2,47	0,00033611	0,01389031	0,021233	-0,00216071	0,0026714	-0,0171735	0,061668	0,023201
21	0,067	0,250	2,28	0,00022500	0,01389031	0,001961	0,00176786	0,0006643	0,0052194	0,050036	0,013015
22	0,050	0,250	2,13	0,00100278	0,01389031	0,037747	0,00373214	0,0061524	0,0228980	0,018763	0,001597
23	0,040	0,250	2,02	0,00173611	0,01389031	0,092590	0,00491071	0,0126786	0,0358622	0,012132	0,000601
24	0,033	0,250	1,93	0,00233611	0,01389031	0,155461	0,00569643	0,0190571	0,0464694	0,043603	0,007082
25	0,200	0,200	2,66	0,01400278	0,02817602	0,112704	-0,01986310	0,0397262	-0,0563520	0,028105	0,005589
26	0,100	0,200	2,39	0,00033611	0,02817602	0,004318	-0,00307738	0,0012048	-0,0110306	0,046248	0,012217
27	0,067	0,200	2,20	0,00022500	0,02817602	0,015447	0,00251786	0,0018643	0,0208622	0,032862	0,005227
28	0,050	0,200	2,06	0,00100278	0,02817602	0,069847	0,00531548	0,0083690	0,0443622	0,003970	0,000067
29	0,040	0,200	1,95	0,00173611	0,02817602	0,140090	0,00699405	0,0155952	0,0628265	0,028868	0,003169
30	0,033	0,200	1,88	0,00233611	0,02817602	0,197390	0,00811310	0,0214738	0,0745765	0,051032	0,009204
31	0,200	0,167	2,58	0,01400278	0,04047761	0,065390	-0,02380754	0,0302595	-0,0514473	0,050110	0,016714
32	0,100	0,167	2,33	0,00033611	0,04047761	0,000033	-0,00368849	0,0001048	-0,0011497	0,032622	0,005777
33	0,067	0,167	2,14	0,00022500	0,04047761	0,033961	0,00301786	0,0027643	0,0370765	0,017651	0,001427
34	0,050	0,167	2,01	0,00100278	0,04047761	0,098776	0,00637103	0,0099524	0,0632313	0,008132	0,000267
35	0,040	0,167	1,91	0,00173611	0,04047761	0,171633	0,00838294	0,0172619	0,0833503	0,037077	0,005015
36	0,033	0,167	1,84	0,00233611	0,04047761	0,234533	0,00972421	0,0234071	0,0974337	0,060035	0,012202
37	0,200	0,125	2,47	0,01400278	0,05897959	0,021233	-0,02873810	0,0172429	-0,0353878	0,083983	0,043031
38	0,100	0,125	2,21	0,00033611	0,05897959	0,013061	-0,00445238	-0,0020952	0,0277551	0,005496	0,000148
39	0,067	0,125	2,08	0,00022500	0,05897959	0,059676	0,00364286	0,0036643	0,0593265	0,004624	0,000092
40	0,050	0,125	1,92	0,00100278	0,05897959	0,163447	0,00769048	0,0128024	0,0981837	0,038803	0,005550
41	0,040	0,125	1,84	0,00173611	0,05897959	0,234533	0,01011905	0,0201786	0,1176122	0,059224	0,011875
42	0,033	0,125	1,80	0,00233611	0,05897959	0,274876	0,01173810	0,0253405	0,1273265	0,065899	0,014070
⚜	**3,430**	**15,450**	**97,62**	**0,13747222**	**3,35869048**	**5,259829**	**0,00000000**	**0,6259000**	**2,5669524**	**1,520226**	**0,448307**

$$\sigma_x=\sqrt{\frac{\sum_{i=1}^{n}\left(x_i-\bar{x}\right)^2}{n}}=0{,}057;\ \sigma_y=\sqrt{\frac{\sum_{i=1}^{n}\left(y_i-\bar{y}\right)^2}{n}}=0{,}283;\ \sigma_k=\sqrt{\frac{\sum_{i=1}^{n}\left(k_i-\bar{k}\right)^2}{n}}=0{,}354;$$

$$r_{xy}=\frac{\sum_{i=1}^{n}\left(x_i-\bar{x}\right)\left(y_i-\bar{y}\right)}{n\sigma_x\sigma_y}=0;\ r_{kx}=\frac{\sum_{i=1}^{n}\left(k_i-\bar{k}\right)\left(x_i-\bar{x}\right)}{n\sigma_k\sigma_x}=0{,}736;\ r_{ky}=\frac{\sum_{i=1}^{n}\left(k_i-\bar{k}\right)\left(y_i-\bar{y}\right)}{n\sigma_k\sigma_y}=0{,}611.$$

$$\sum_{i=1}^{n}\left|\frac{ax_i+by_i+c-k_i}{k_i}\right|=1{,}520226;\ \sum_{i=1}^{n}\left(ax_i+by_i+c-k_i\right)^2=0{,}448307.$$

Based on the expressions (3), the regression coefficients are:

$$a=4{,}55;\ b=0{,}76;\ c=1{,}67.$$

Thus, after determining the regression coefficients, the dependency (2) between the overvoltage multiplicity caused by non-stationary earth faults in isolated neutral networks and the inverse value of the phase capacitance of the network relative to the ground, along with the conductivity of the earth fault circuit, can be explicitly written as follows:

$$k=4{,}55x+0{,}76y+1{,}67 \quad (4)$$

Let us verify the adequacy of the obtained regression equation (4) between the overvoltage multiplicity during non-stationary earth faults, the conductivity of the earth fault circuit, and the inverse value of the phase capacitance of the network relative to the ground. To do this, the value of the multiple correlation coefficient can be calculated and its significance can be verified using the Fisher criterion [17, p. 133-135].

The value of the multiple correlation coefficient is determined by the following known expression:

$$R=\sqrt{\frac{r_{kx}^2+r_{ky}^2-2r_{kx}r_{ky}r_{xy}}{1-r_{xy}^2}}=0{,}96.$$

The fact that the multidimensional correlation coefficient is close to unity $\left(R=0{,}96\to 1\right)$ indicates that the dependence between the conductivity of the ground closing cycle and the inverse value of the network's phase capacitance relative to the ground, with the variation of extreme voltage, can be considered a strong linear correlation.

We check the significance of the multidimensional correlation coefficient using the $F-$Fisher criterion. It is known that, at the significance level α, the regression equation is considered adequate if the condition $F>F(\alpha,q_1,q_2)$ is met [18, p.50], where q_1,q_2- the degrees of freedom.

The calculated value of the $F-$Fisher criterion is determined based on the data as follows:

$$F=\frac{R^2}{1-R^2}\cdot\frac{n-m-1}{m}, \quad (5)$$

Here, $n-$is the number of experiments, $n=42$; $m-$is the number of factors, $m=2$. Then, based on expression (5), $F=229{,}22$.

$F-$ Fisher criterion table value, is taken from the table depending on the significance level (α) and degrees of freedom (q_1,q_2) [18, p.370]:

$$\alpha = 0{,}05;\ q_1 = m = 2;\ q_2 = n - m - 1 = 42 - 2 - 1 = 39;\ F(\alpha, q_1, q_2) = 3{,}24.$$

$F = 229{,}22 > F(\alpha, q_1, q_2) = 3{,}24$ thus confirming the statistical significance of the multivariate correlation coefficient $(R = 0{,}96)$ and the regression equation.

The mean relative and mean square errors of the approximation are determined by the following corresponding expressions:

$$\bar{\varepsilon} = \frac{1}{n}\sum_{i=1}^{n}\left|\frac{ax_i + by_i + c - k_i}{k_i}\right| \cdot 100\% = 3{,}62\%;$$

$$\sigma = \sqrt{\frac{\sum_{i=1}^{n}(ax_i + by_i + c - k_i)^2}{n}} = 0{,}103.$$

The determination index of $R^2 = 0{,}96^2 = 0{,}9216$ indicates that $92{,}16$ % of the change in the arc overvoltage multiplier (k) is due to the changes in the ground fault current (x) and the inverse value of the network's phase capacitance relative to ground (y), while the remaining $7{,}84$ % is caused by the changes in other factors not considered.

The average elasticity coefficients are determined by the following well-known expressions [18, p.102]:

$$\bar{E}_x = \frac{\partial k}{\partial x}\frac{\bar{x}}{\bar{k}} = a\frac{\bar{x}}{\bar{k}} = 0{,}16;$$

$$\bar{E}_y = \frac{\partial k}{\partial y}\frac{\bar{y}}{\bar{k}} = b\frac{\bar{y}}{\bar{k}} = 0{,}121.$$

From this, it can be concluded that a 1% increase in the ground fault current (x) results in a 0.16% increase in the arc overvoltage multiplier (k), while a 1% increase in the inverse value of the network's phase capacitance relative to ground (y) causes a 0.121% increase in the arc overvoltage multiplier (k). Since $\bar{E}_x = 0{,}16 > \bar{E}_y = 0{,}121$, the ground fault current (x) has a greater effect on the arc overvoltage multiplier (k) compared to the inverse value of the network's phase capacitance relative to ground (y). The fact that the average elasticity coefficients are smaller than 1% indicates that the arc overvoltage multiplier (k) is not elastic to changes in the ground fault current (x) and the inverse value of the network's phase capacitance relative to ground (y).

Thus, the dependency (1) between the arc overvoltage multiplier (k), ground fault resistance, and the network's phase capacitance relative to ground, resulting from non-stationary ground faults in neutral-isolated networks, can be expressed as follows:

$$k = \frac{4{,}55}{R_0} + \frac{0{,}76}{C_f} + 1{,}67, \quad (6)$$

Using the OriginLab [19] program, based on the regression equation (6) obtained, a 3D (spatial) plot was created showing the dependence of the arc overvoltage deflection on ground fault resistance and the network phase capacitance relative to ground (Figure 1).

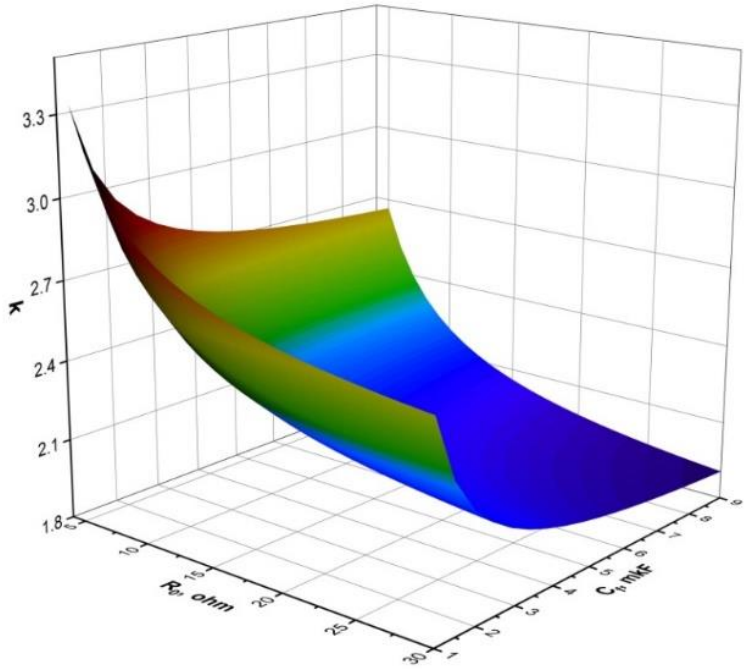

Figure 1. 3D plot of the dependence of arc overvoltage on ground fault resistance and network phase capacitance relative to ground.

3. Conclusion

Based on Petersen's theory, a regression model was developed, which shows the relationship between the overvoltage deflection of the arc due to non-stationary ground faults in neutral-isolated networks, the fault circuit's conductivity, and the inverse value of the network's phase capacitance relative to the ground. This model can be easily implemented in practice. The analytical dependence proposed between the mentioned parameters can be considered a strong linear correlation.

The obtained results can be used during the insulation testing of neutral-isolated networks in the Azerbaijani power system under load conditions.

REFERENCES

1. Khazieva, R.T., Vasiliev, P.I., Aflyatunov, R.R. (2022). A study to establish the isolization of electrical equipment in the pierced area. *Electrical technology in passing*, *3*(56), 65-69.
2. Patsch, R. (2018). Dielectric diagnostics of power transformers and cables – Return voltage measurements, theory and practical results. *VDE High Voltage Technology, ETG Symposium. https://www.vde-verlag.de/proceedingsde/454807130.html*
3. Şalıt, Q.M. (1985). Profilaktiçeskie ispıtaniya kabelnıx setey 6-10 kV pod naqruzkoy.- *Elektriçeskie stantsii, 8*, 66-70.
4. Baranov, B.M. (1961). O Profilaktiçeskix ispıtaniyax izolyatsii kabelnıx setey. - *Elektriçeskie stantsii, 2*, 55-59.
5. Dudarev, L.E. (1978). Profilaktiçeskie ispıtaniya izolyatsii setey pod naqruzkoy metodom iskustvenno sozdannıx perenapryajeniy. *Elektriçestvo, 8*, 69-72.
6. Orucov, N.İ. (1998). Süni qeyri-stasionar yerlə qapanmalar əsasında neytralı izolə olunmuş şəbəkələrdə

izolyasiyanın sınaq üsullarının işlənməsi və tədqiqi. *Texnika elmləri namizədi alimlik dərəcəsi almaq üçün təqdim edilən dissertasiya*. Bakı, 139 s.

7. Orucov, N.İ., Orucov, A.O. (2013). Qövs ifrat gərginliyin dəfəliyi ilə yerlə qapanma müqaviməti arasındakı asılılığın təyini, *Elmi əsərlər. AzTU*, *3*, 83-86.
8. Orucov, N.İ. (2019). Qövs ifrat gərginliyin yerlə qapanma müqavimətindən asılılığının reqressiya modeli. *"Azərbaycanın innovariv inkişafında mühəndisliyin rolu: hədəflər və perspektivlər" beynəlxalq elmi-praktiki konfransı, Bakı: BMU, - 29-30 noyabr*, 285-287.
9. Orucov, N.İ., Orucov, A.O. (2014). Qövs ifrat gərginliyi ilə yerlə qapanma bucağı arasındakı asılılığın təyini. *Energetikanın problemləri*, *2*, 36-39.
10. Orucov, N.İ., Mirili, T. (2021). Qövs ifrat gərginliyin yerlə qapanma bucağından asılılığının reqressiya modeli. *Gənc tədqiqatçıların V beynəlxalq elmi konfransı, - Bakı, Kitab 1. BMU, 29-30 aprel*, 113-116.
11. Orucov, N.İ. (2018). Qövs ifrat gərginliyin dəfəliyi ilə şəbəkənin yerə nəzərən faza tutumu arasındakı asılılığın təyini. *Azərbaycan Xalq Cümhuriyyətinin 100 illik yubileyinə həsr olunmuş "Təhsil - tədqiqat - istehsalat mexanizminin qurulması" mövzusunda Respublika Elmi-texniki konfransının materialları, Bakı: AzTU, - 4-5 aprel,* 254-257
12. Orucov, N.İ. (2021). Qövs ifrat gərginliyin şəbəkənin yerə nəzərən faza tutumundan asılılığının reqressiya modeli. *II beynəlxalq elm və texnologiya konfransı, - Bakı: BMU, - 26-27 noyabr*, 333-335.
13. Orucov, N.I., Guliyev, H.B., Alimammadova, S.J. (2024). Regression model of arc overvoltage during single-phase non-stationary ground faults in neutral isolated networks. *Reliability: Theory & Applications*, *19*(78), 425-433.
14. Orucov, N.İ., Quliyev, H.B., Əliməmmədova, S.C. (2024). Qövs ifrat gərginliyin yerlə qapanma müqaviməti və yerlə qapanma bucağından asılılığının reqressiya modeli. *Elmi əsərlər. AzTU, 1*, 43-48.
15. Orucov, N.İ., Quliyev, H.B., Əliməmmədova, S.C. (2024). Qövs ifrat gərginliyin yerlə qapanma müqaviməti və yerlə qapanma bucağından asılılığının 3D modelləşdirilməsi. *Energetikanın problemləri*, *2*, 9-17.
16. Orujov, N.I., Guliyev, H.B., Alimammadova, S.J. (2024). Arc Overvoltage Regression Model. *Proceeding of he 9th International Conference on Control and Optimization with Industrial Applications (COIA-2024), Istanbul, Turkiye, 27-29 August*, 64-67.
17. Məmmədov, N.R..Məmmədov, B.M. (2005). *Eksperimentin nəticələrinin riyazi işlənməsi.* Bakı: Elm.
18. Orucov, E. (2018). *Ekonometrika* Bakı: Elm.
19. Origin (Pro), "Version 2022". OriginLab Corporation, Northampton, MA, USA.

2025. Volume 9, Number 1 ***Pages 65-74***

UOT: 621.039.58
DOI: https://doi.org/10.30546/09085.2025.01.032

ENHANCING VVER1000 EFFICIENCY THROUGH GAS TURBINE INTEGRATION

ABDULRABBIN MAMMADOV[1], MEHDI BASATI PANAH[2]

[1] *SPbPU, Saint Petersburg, Russia*

[2] *SPbPU, Saint Petersburg, Russia*

amemmedov12@std.beu.edu.az

ARTICLE INFO

Article history
Received:2025-05-11
Received in revised form: 2025-05-24
Accepted: 2025-06-10
Available online

Keywords:
Combined Cycle Power Plant (CCPP);
Energy Efficiency;
Thermodynamic Simulation;
Sustainable Power Generation4
Energy Optimization.
JEL Classification: Q42, O33, L94

ABSTRACT

The development of sophisticated, effective, and sustainable power generation technologies is required to meet the expanding energy demands of modern society. Despite their benefits in generating electricity without direct greenhouse gas emissions, conventional nuclear power plants (NPPs) have relatively poor efficiency. This study investigates a new setup that combines a VVER1000 NPP with MGT-80 Gas Turbine Units (GTUs): a Combined Cycle Power Plant (CCPP). The third energy recovery loop in the integration uses the Supercritical Carbon Dioxide (sCO_2) Brayton Cycle or the Organic Rankine Cycle (ORC). The goal is to improve the NPP's steam cycle by utilizing the thermal potential of GTU exhaust gases, which will raise system efficiency overall. The Engineering Equation Solver (EES) program was used to create thermodynamic models, which were verified against operational data. Compared to standalone plant operations, the research shows that the suggested system structure offers greater efficiency and economic viability.

Introduction

Although humanity hasn't reached Type 1 civilization status, our position on the Kardashev scale is rapidly advancing. Scientific and industrial revolutions have speeded up the development of our technology. Recent breakthroughs in artificial intelligence have further increased this demand. For example, a single ChatGPT query consumes about 0.0029 kWh—nearly ten times that of a Google search—collectively, ChatGPT uses roughly 2.9 million kWh daily. This is equivalent to the daily energy use of 100,000 average U.S. households. Therefore, our energy consumption has increased not only linearly but also exponentially from the early 1800s, as we can see in Figure 1 [1]. In addition to this exponential increase in energy demand, limited fossil fuel supplies, and climate change push the global energy industry to adopt more efficient and sustainable technology. To achieve that we need to build new eco-friendly power plants or increase the power and efficiency of the current ones. Building new facilities is expensive and takes much more time than increasing the current ones` capacity and efficiency. Previous studies [2, 3] showed that the efficiency of the VVER1000 of the Bushehr nuclear power plant can be increased. In this study, we aim to increase the efficiency of Bushehr NPP, as well as the capacity, by adding Gas Turbines.

Due in large part to lower operating pressures and temperatures than fossil-fueled systems, nuclear power's moderate thermal efficiency of about 33% limits its potential as a substantial part of the low-carbon energy mix.

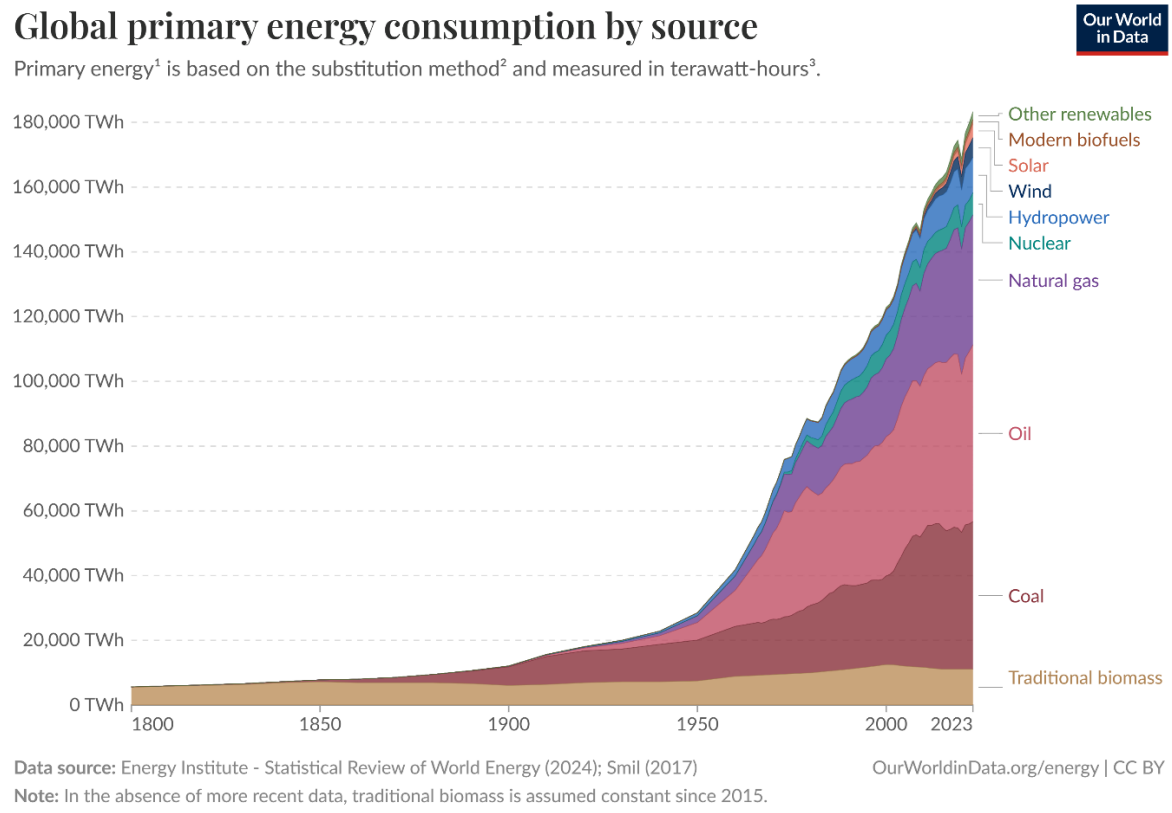

1. **Primary energy**: Primary energy is the energy available as resources – such as the fuels burnt in power plants – before it has been transformed. This relates to the coal before it has been burned, the uranium, or the barrels of oil. Primary energy includes energy that the end user needs, in the form of electricity, transport and heating, plus inefficiencies and energy that is lost when raw resources are transformed into a usable form. You can read more on the different ways of measuring energy in our article.

2. **Substitution method**: The 'substitution method' is used by researchers to correct primary energy consumption for efficiency losses experienced by fossil fuels. It tries to adjust non-fossil energy sources to the inputs that would be needed if it was generated from fossil fuels. It assumes that wind and solar electricity is as inefficient as coal or gas. To do this, energy generation from non-fossil sources are divided by a standard 'thermal efficiency factor' – typically around 0.4 Nuclear power is also adjusted despite it also experiencing thermal losses in a power plant. Since it's reported in terms of electricity output, we need to do this adjustment to calculate its equivalent input value. You can read more about this adjustment in our article.

3. **Watt-hour**: A watt-hour is the energy delivered by one watt of power for one hour. Since one watt is equivalent to one joule per second, a watt-hour is equivalent to 3600 joules of energy. Metric prefixes are used for multiples of the unit, usually: - kilowatt-hours (kWh), or a thousand watt-hours. - Megawatt-hours (MWh), or a million watt-hours. - Gigawatt-hours (GWh), or a billion watt-hours. - Terawatt-hours (TWh), or a trillion watt-hours.

Figure 1. Global primary energy consumption. [1]

In the meantime, NPPs and Gas Turbine Units (GTUs), renowned for their quick deployment and adaptability, can be strategically combined. When coupled with heat exchangers, their high-temperature exhaust gases offer a chance for enhanced heat recovery and steam production. The possibilities of merging several MGT-80 GTUs with a VVER1000 NPP. Using sophisticated simulation in EES software, the integration seeks to maximize operational performance and thermal efficiency. The study evaluates the technical and thermodynamic viability of each component cycle by modelling it separately and then in combination.

The characteristics of the NPP

The commercially available NPPs are PWR, BWR, and PHWR known as CANDU. The steam generated to drive the steam turbines in these NPPs is almost saturated steam of relatively low pressure, compared to that in fossil power plants. With technological advancements, fourth-generation nuclear reactors can achieve efficiency levels of approximately 45%. However, commercially operated reactors typically exhibit efficiency levels ranging from 33% to 37%. In the previous studies, the NPP of the Bushehr nuclear power plant using PWR, known as VVER1000 was discussed and a detailed exergy analysis has been made.

Table 1. Principal features of the VVER1000 NPP. [3]

Reactor core thermal power output (MW_{th})	3000
Coolant flowrate (kg/s)	16800
Net thermal efficiency (%)	33.33
The pressure of the coolant at the core outlet (MPa)	15.7
The temperature of the coolant at the reactor outlet (°C)	321
Coolant heating in the reactor (°C)	30
The difference in the pressure in the reactor (MPa)	0.381
Number of loops (pcs)	4
Feedwater temperature at steam generator inlet (°C)	224
Steam temperature after steam generator (°C)	280
Steam pressure (MPa)	5.88
Steam flow rate (kg/s)	1661.11
Enrichment of the fuel - UO_2 (%)	3.6-4.95

To meet the Soviet Union's increasing demand for reliable and effective electricity sources in the 1970s, the VVER1000 nuclear power station was built. It is an improved version of the VVER440 NPP, which was created in the 1960s. The VVER1000 transfers heat from the core to the steam generators, which create the steam that powers the turbines and generates electricity, using a pressurized water system. Compared to other NPP models, the VVER1000's architecture enables it to function at higher temperatures and pressures, which increases efficiency. [4] The main characteristics of the VVER1000 NPP steam cycle are given in Table 2. The VVER-type nuclear power plant has gained widespread adoption in various countries, including Belarus, China, the Czech Republic, Finland, Germany, Hungary, India, Iran, Russia, and Turkey. This widespread adoption is due to the plant's reputation for reliability, efficiency, and advanced safety features.

Several cutting-edge safety features are included with the VVER1000. These include an emergency core cooling system to prevent fuel rods from overheating and melting in the event of a coolant loss accident and a double containment system to prevent the escape of radioactive material in the event of an accident. The reactor also has a passive heat removal system that may release heat from the core in an emergency without the need for outside power or assistance.

To improve the efficiency of the NPP cycle, the hot gases released from these GTs can be used to superheat the steam produced in the NPP before it enters the steam turbines. Additionally, by preheating the feed water that returns from the condenser to the NPP's steam generators, these gases can boost the plant's power output. More power will be produced by utilizing the steam drawn from the NPP steam turbine for the feed heaters. To put it briefly, the efficiency and power production of both cycles may be greatly increased by combining the gas turbine GT cycle with the NPP.

The steam cycle of the suggested VVER1000 NPP

Figure 2 shows a schematic diagram of the VVER1000. The first loop of VVER1000 transfers heat from fission in the reactor to the steam generators. The steam produced is then sent to the steam turbine through a secondary loop. The steam cycle includes high-pressure turbines, low-pressure turbines, a moisture separator, a reheater, closed-feed water heaters, a deaerator, a condenser, and an electric generator. The produced steam has a mass flow rate of 1661.11kg/s and is nearly a saturated vapour at a pressure of 5.88MPa and a temperature of 274.3C. In the high-pressure turbine, the steam expands to a mid-pressure level (P10), aiming for a steam quality (x10) of more than 0.86. The extracted steam from the high-pressure turbine is directed to the high-pressure feed water heater 5 and the deaerator. The isentropic efficiency is 0.957 for the high-pressure turbine and 0.8637 for the low-pressure turbine. At the exit of the high-pressure turbine, the steam conditions are as follows: P10=770KPa, T10=168.8C, x10=0.861, and h10(enthalpy)=2482.4kJ/kg. Following its expansion in the high-pressure turbine, the steam proceeds through a reheater and a moisture separator. Moisture is extracted in the moisture separator and sent to a low-pressure feed water heater running at 741KPa. The reheater generally has a 33KPa pressure loss, resulting in a steam pressure of P14=708KPa. In order to raise the steam temperature, there is also a direct steam supply from the steam generator to the reheater, and the condensed steam is directed to the reheat cooler (RHC). Three steam extraction lines from the low-pressure turbine are directed to the low-pressure feed water heaters 3, 2, and 1, operating at pressures of 196, 86.2, and 35.3 KPa, respectively. After the low-pressure turbine, the steam goes to the condenser with a pressure of 7.5KPa, 40.3C, and 2328.7kJ/kg enthalpy. [4, 5]

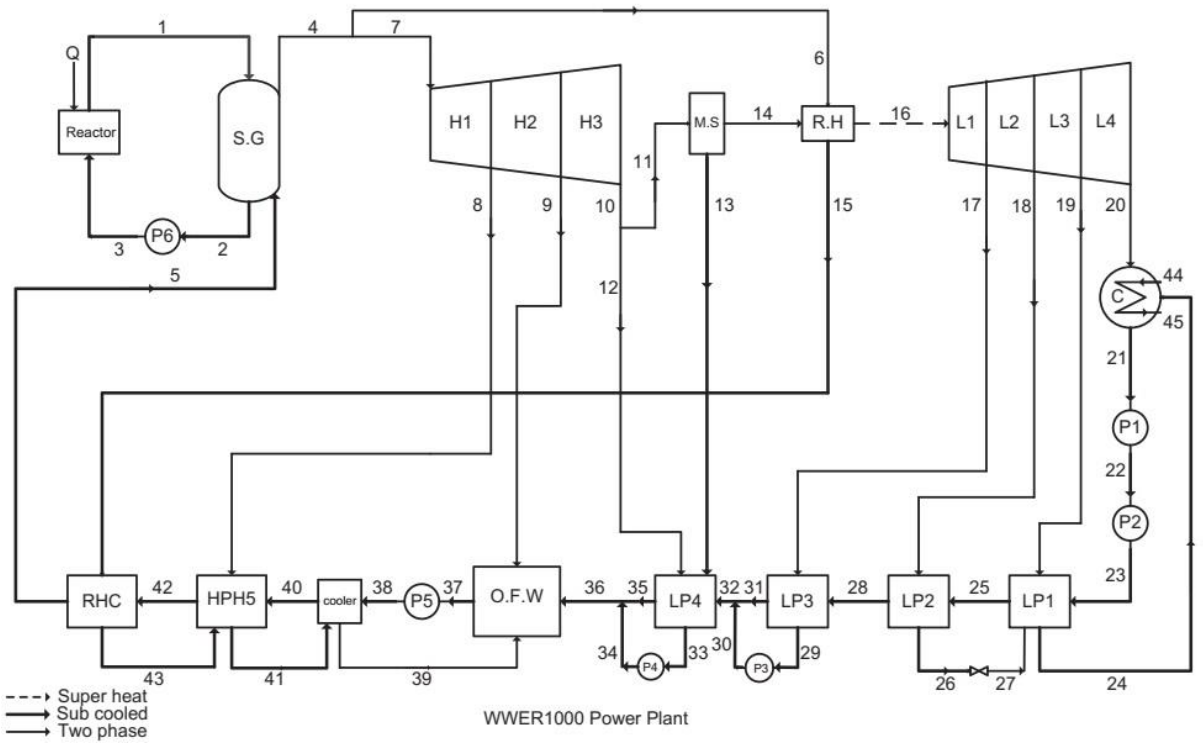

Figure 2. A schematic diagram of the VVER1000 steam cycle. [2]

Gas turbine unit

The gas turbine selected for this study, the MGT-80, is manufactured and developed by the Iranian technical company MAPNA Group. This heavy-duty gas turbine has a gross efficiency of up to 40% and a significant nominal power output of 308 MW. The MGT-80 has a 15-stage axial flow compressor, a dry low-emission combustor with 24 burners, a 4-stage axial power turbine, and a generator.

Atmospheric air enters the compressor with a particular mass flow rate ($\dot{m}_{air}$), temperature, and pressure. After passing through the compressor with a pressure ratio (PR) of 19, the air exits the compressor at a determined pressure. Fuel is injected, ignited, and burned in the combustor downstream of the compressor at a specific fuel flow rate ($\dot{m}_{fuel}$).

The turbine inlet temperature (TIT), which represents the highest temperature (T_2) in the cycle, is achieved when the combusted mixture of air and fuel, at a specific flow rate ($\dot{m}_{gas}$), exits the combustor and enters the turbine. The turbine transforms the energy of the expanding hot mixture into work. The expanded gases leave the gas turbine as exhaust at a particular temperature and pressure.

If the gas turbine is equipped with a heat recovery steam generator (HRSG), it can recover waste heat at this stage and produce steam. This steam can then be utilized for process heat, space heating, or to drive a steam turbine for additional power generation. The performance data of the gas turbine unit are outlined in Table 2.

Table 2. The performance data of MGT-80 gas turbine. [5]

Gross Power Output (MW)	308
Gross Efficiency (%)	40.1
Turbine Inlet Temperature (°C)	1265
Exhaust Gas Temperature (°C)	581
Exhaust Mass Flow Rate (kg/s)	724
No. of Compressor Stages (EA)	15
No. of Turbine Stages (EA)	4
Pressure Ratio	19
Type of Combustors	Annular, 24 Burners

Modified combined NPP-GT analysis

This chapter examines the technical feasibility and potential benefits of integrating gas turbine units into a nuclear power plant. The goal is to increase the nuclear facility's overall efficiency and power-producing capabilities. We used modern modelling techniques and thorough analysis based on relevant books and scientific journals.

Using the EES software package, we developed a trustworthy computational model to analyse and simulate the proposed integrated system. This model took into account several important factors, such as thermodynamics, heat transfer, fluid dynamics, and system dynamics. The simulation model was created to accurately replicate the behaviour of integrating gas turbine units with a nuclear power station in the actual world by utilizing empirical data and previous research findings.

We assessed several crucial performance metrics using the simulation, including the system's overall efficiency, power output, and long-term viability. To quantify these characteristics and determine the potential advantages and disadvantages of the integrated system, we carried out a

comprehensive analysis. The technological feasibility, and operational characteristics of integrating gas turbine units with a nuclear power station are explained in this paper.

The study's findings contribute to the body of scientific knowledge already available on nuclear power generation and offer wise counsel to academics, decision-makers, and industry experts who wish to explore innovative strategies for enhancing the sustainability and effectiveness of nuclear energy systems.

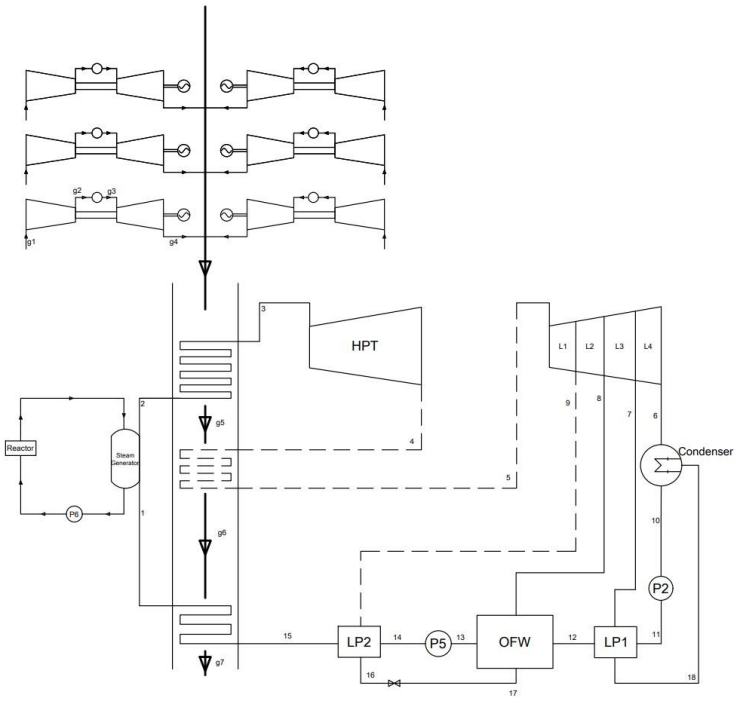

Figure 3. A simplified illustration of the GT-NPP combined cycle.

A possible strategy to increase power generation efficiency is the integration of gas turbine units into nuclear power plants, often known as a GT-NPP combined cycle. The gas turbine's exhaust waste gases raise the steam temperature after the nuclear power plant's steam generator in this combined cycle. This enables a more effective utilisation of the heat produced by the nuclear reactor, as the gas turbine's exhaust gas can complement the reactor's heat generation. Figure 3 presents a simplified illustration of the GT-NPP combined cycle.

The nuclear reactor and the gas turbine operate as independent systems in the GT-NPP combined cycle. Whereas the nuclear reactor creates heat by fissioning uranium or other nuclear fuels, the gas turbine uses natural gas or other fuels to produce electricity. A steam generator is used to boil feed water and create steam by transferring the heat from the nuclear reactor's core to a seperate circuit. This steam then drives multiple steam turbines that, in turn, generate electricity. The temperatures of the steam after the steam generator (around 250-300) and the exhaust gases (around 550-600) of the GTU differ significantly. So, in an additional stage of CCPP, the exhaust gas from the gas turbines passes through another section of the heat exchanger to increase the steam temperature further before expansion in the turbines, thereby optimising the use of the nuclear reactor's heat. [6]

When compared to traditional power plants, the VVER-1000's present thermal efficiency of about 33% is rather low. This is mainly because the steam does not enter the turbine in a superheated state. Furthermore, around 30% of steam extraction must come from the steam turbines to heat

the feed water coming back from the condenser to the steam generator and to reheat the steam leaving the high-pressure turbine before it enters the low-pressure turbine. As a result, the main flow's mass flow rate is lowered, which lowers the overall work output. So, integrating gas turbine units (GTUs) and nuclear power plants (NPP) is an effective way to increase efficiency and power output significantly. This can enhance the availability of steam, thereby increasing the work output of the steam turbine, by elevating the steam temperature delivered to the high-pressure turbine of the NPP.

The waste heat from the GTUs' exhaust gas can be used to increase the steam's temperature by using a superheater, which is comparable to the heat recovery steam generator (HRSG) of combined cycle power plants (CCPPs). As exhaust gases maintain their relatively high temperatures after the superheater section (around 300°C), this waste heat can also be used as a reheater between high- and low-pressure turbines and as an economizer to heat the feed water delivered to the NPP's steam generator (SG) from the steam condenser. When feedwater heaters, a moisture separator, and a reheater are eliminated from the nuclear power plant's steam cycle, steam is not extracted from turbines. This allows more steam to expand in the turbine and produce more power.

The proposed GT-NPP combined cycle, illustrated in Figure IV.8, incorporates six MGT-80 gas turbine units and the VVER1000 with its stream cycle. This modified design utilised two low-pressure-closed feedwater heaters and a deaerator (open feed water heater). Unlike the original VVER1000 setup, we excluded the reheat cooler, a high-pressure-closed feedwater heater, a cooler, and two low-pressure-closed feedwater heaters. We used hot gases from the six MGT-80 gas turbines to superheat the steam before the high-pressure turbine, reheat it in between the turbine's two stages, and preheat the condenser's feed water to the steam generator. Only the installation of heat recovery steam generators (HRSG), which are a superheater, reheater, and economizer, was necessary to do this without changing the NPP steam-generating process.

Table 3. Given data from previous research papers. [3, 4, 6]

T_{g4}	Gas temperature at gas turbine outlet (°C)	581
P_1	Steam pressure at steam generator inlet (MPa)	5.88
T_1	Steam temperature at steam generator inlet (°C)	224
T_2	Steam temperature at steam generator outlet (°C)	280
P_6	Steam pressure at extraction 6 (MPa)	0.196
P_7	Steam pressure at extraction 7 (MPa)	0.0862
P_8	Steam pressure at extraction 8 (MPa)	0.0353
P_9	Steam pressure at extraction 9 (MPa)	0.0075
η_{HPT}	HP turbine	95.72
η_{LPT}	LP turbine	86.37
η_{p2}	Main condensate pump 2	92.08
η_{p5}	Main condensate pump 5	96.9

Data from previous sources was used to model this configuration, and some assumptions have been made, shown in Table 3 and Table 4, respectively. The turbine and pump efficiency, the steam generator's inlet and outlet temperatures (from the nuclear reactor's safety perspective), and the pressure readings are identical to those found in earlier studies [3, 4, 6]. At the same time, all heat exchangers are taken to be isolated devices (η=1) and small kinetic and potential energy differences are ignored. The temperature difference between the hot medium's inlet and the cold medium's outlet is mainly considered 10°C in closed feedwater heaters (LP1 and LP2),

while in HRSG, this difference is 15°C. It is worth to note, T_{g7} is used when n={3,4,5} and T_3 is used when n={6,7}.

Table 4. Assumptions made to simulate.

T_{g4}	Gas temperature at gas turbine outlet (°C)	581
T_{g7}	Gas temperature at ecomoniser outlet (°C)	120
T_3	Steam temperature at superheater outlet (°C)	565
T_5	Steam temperature at reheater outlet (°C)	T_{g5}+15
T_{12}	Water temperature at outlet of LP1 (°C)	66
T_{17}	Steam temperature at outlet of LP2 (°C)	T_{14}+10
T_{19}	Steam temperature at outlet of LP1 (°C)	T_{11}+10

The superheater section's inlet temperatures of steam (280) and exhaust gases (581) and their mass flow rates are known. To maximize heat transfer while taking technological constraints into account, the ideal output temperatures for steam and exhaust gases are acknowledged to be 565°C and 300°C, respectively. Thus, we can find the minimum number of GTUs:

$$n * \dot{m}_{gas} * \left(h_{g4} - h_{g5}\right) = \dot{m}_{steam} * (h_3 - h_2)$$

where n is the number of GTUs, $\dot{m}_{gas}$ and $\dot{m}_{steam}$ are mass flow rates of a single gas turbine and NPP, $h_{g4}, h_{g5}, h_3 \; and \; h_2$ are enthalpy values of those points on the cycle. By solving this equation, we can found n as 5.327. This means we should have a minimum of 6 GTUs to achieve maximum heat transfer in the superheater section. Even though this configuration needs a minimum of 6 GTUs for the maximum heat transfer in the superheater section, to find the optimal number of GTUs for the cycle efficiency, we have simulated the same cycle with n={3,4,5,6,7}. Knowing the effectiveness of the reheater and LP2 at the same time is preferable. We should have enough heat supply to the system to add a reheater section. However, when n<6, we can neither reach the possible maximum temperature (565) for the steam entering the turbine (T3) nor decrease the exhaust gases` temperature after the superheater section until 300. The need for an economiser can explain the main reason for this issue. Due to the removal of several components from the cycle, which were heating steam entering the steam generator, an economiser needs more heat input. According to this information, we did not perform a simulation, where we have reheater, for the cases n<6. You can see the generated data in

Table 0.

Table 0. Results of the simulation.

n	RH	LP2	T_3 (°C)	T_{g5} (°C)	T_{g7}(°C)	W_{net} (MW)	◎ (%)
7	+	-	565	317.9	162.6	4418	45.88
	+	+		317.9	193.2	4358	45.54
	-	-		367.2	211.9	4289	44.54
	-	+		367.2	240.8	4259	44.23
6	+	-		298.4	117.3	4040	46.54
	+	+		298.4	152.1	4009	46.18
	-	-		331.5	150.4	3970	45.72
	-	+		331.5	184.1	3940	45.38
5	-	+	529.5	314.2	120	3551	45.91
	-	-	504.5	337.3		3512	45.40
4	-	+	431.1	362.8		3014	44.41
	-	-	407.5	391.6		2981	43.91
3	-	+	341.7	443.7		2503	42.86
	-	-	322.1	482.2		2476	42.40

Analysis and Discussion

With a stunning 46.5% gain in thermal efficiency while using six GTUs, the integration of VVER1000 with MGT-80 gas turbine units has produced a much more efficient system. Comparing this to the respective efficiencies of MGT gas turbines (34%) and commercial nuclear power reactors (33%), there is a noticeable improvement. Several changes are responsible for the efficiency gain. A superheater has been installed in the GT-NPP combined power plant to raise the steam temperature from 280°C to 565°C, improving the steam availability. In addition to increasing the overall output work, reheating steam between high- and low-pressure turbines assisted in bringing the exhaust gas temperature down to about 120C. The HRSG's economizer now manages the process of heating the returning feed water from the condenser to the steam generator, doing away with the requirement to extract steam from the high-pressure turbine. Additionally, more steam expands in the turbines as a result of the removal of a reheater, a moisture separator, and feedwater heaters, producing greater power.

The power output of the improved VVER1000 has increased by an impressive 112.5% to 2125 MW. Consequently, the GT-NPP combined power plant's total power production is 4040 MW, which is 41.9% higher than the combined power output of the individual power plants, which comes to 2848 MW (1000 MW + 6 x 308 MW).

Better use of high-temperature exhaust, reduced thermal losses, and optimal load distribution among system components were credited with the efficiency increases. These findings were corroborated by energy analysis, which showed that the improved system has less irreversibility.

Conclusion

This study offers a solid framework for strategically integrating gas turbines and low-grade heat recovery cycles to increase the sustainability and efficiency of nuclear-based power generation. Significant gains in thermal efficiency and economic performance can be made by combining five MGT-80 GTUs with a VVER1000 NPP.

The suggested system layout provides a scalable answer to today's energy problems, especially in areas looking to increase nuclear capacity while reducing their environmental impact. The EES-based modelling and simulation demonstrated the approach's practical viability and offered precise thermodynamic insights.

The power output of the improved VVER1000 has increased by an impressive 112.5% to 2125 MW. Consequently, the GT-NPP combined power plant's total power production is 4040 MW, which is 41.9% higher than the combined power output of the individual power plants, which comes to 2848 MW (1000 MW + 6 x 308 MW).

According to our baseline models, each MGT-80 GTU produces roughly 308 MWe at 34% efficiency, while a solo VVER-1000 generates about 1,050 MWe at about 33% thermal efficiency. The total net production increases to 4,040 MWe and the thermal efficiency rises to 46.5% when six GTUs are integrated with the NPP's steam cycle, rerouting their combined exhaust through economizers and superheaters to elevate steam conditions. Without using more fuel, this results in a power output increase of 41.9% and an efficiency gain of 13 percentage points compared to separate operation.

In terms of operation, the hybrid plant seamlessly responds to peak demand by combining the GTUs' quick start-up (±30 MW/min) and load-following capabilities with the NPP's steady base load. Environmental benefits include lower water use through closed-loop cooling in the tertiary cycles and the avoidance of almost 2.2 million tons of CO_2 annually when compared to simple-cycle GTUs.

The findings support the idea that combining various thermal cycles into a single power-generating platform can be crucial to the shift to more efficient and sustainable energy systems. Future studies should include dynamic load-cycle simulations, and real-world integration issues such waste-heat management, safety procedures, and regulatory compliance. To validate model predictions, pilot-scale demonstrations or experimental validation would be crucial.

In conclusion, the suggested GT-NPP combined cycle shows notable gains in output, economic performance, efficiency, and environmental effect. This arrangement presents a viable route toward more flexible, and sustainable power generation by efficiently recovering GTU waste heat to superheat nuclear steam.

References

1. "Our World in Data," May 2025. [Online]. Available: https://ourworldindata.org/grapher/global-energy-substitution. [Accessed 2 May 2025].
2. A. Naserbegi, M. Aghaie, A. Minuchehr, Gh Alahyarizadeh, "A novel exergy optimization of Bushehr nuclear power plant by gravitational search algorithm (GSA)," *Energy,* pp. 373-385, 2018.
3. H. Ebrahimgol, M. Aghaie, A. Zolfaghari, A. Naserbegi, "A novel approach in exergy optimization of a WWER1000 nuclear power plant using whale optimization algorithm," *Annals of Nuclear Energy,* vol. 145, 2020.
4. "The VVER today," ROSATOM Overseas.
5. Mapna Group, 2024. [Online]. Available: https://mapnagroup.com/mgt-80-gas. [Accessed 8 May 2024].
6. C. A. Alaçam, "Feasibility study of implementing and integrating gas turbines in a commercial nuclear power plant," Peter the Great St. Petersburg Polytechnic University, Saint Petersburg, 2023.
7. M.A. Darwish, Fatimah M. Al Awadhi, Anwar O. Bin Amer, " Combining the nuclear power plant steam cycle with gas turbines," *Energy,* pp. 4562-4571, 2010.
8. Sanford KLEIN, Gregory NELLIS, THERMODYNAMICS, New York: Cambridge University Press, 2012.
9. M. P. Boyce, Gas Turbine Engineering Handbook, 3rd ed., Elsevier Inc., 2006.
10. "Dry Air - Thermodynamic and Physical Properties," Engineering ToolBox, 2005. [Online]. Available: https://www.engineeringtoolbox.com/dry-air-properties-d_973.html. [Accessed 4 2025].
11. "EES Engineering Equation Solver," F-Chart Software, [Online]. Available: http://www.fchart.com/ees/. [Accessed April 2025].
12. A. Durmayaz and H. Yavuz, "Exergy analysis of a pressurized-water reactor nuclear power plant," *Applied Energy,* pp. 39-57, 2001.
13. K. A. B. Pathiranthna, "Gas Turbine Thermodynamic and Performance Analysis Methods Using Available Catolog Data," 2013.
14. D. J. Ciafone, Gas Turbines: Technology, Efficiency and Performance, UK ed., Nova Science Publishers Inc., 2013.
15. "Mapna Group," [Online]. Available: https://mapnagroup.com/mgt-80-gas-turbine/. [Accessed 10 April 2024].
16. W. Wang, J. Zhang and W. B. Zhao, "Thermodynamic Calculation of Moisture Separator Reheater in Nuclear Power Plant," January 2010.
17. A. R. Navaie, "Thermal Design and Optimization of Heat Recovery Steam Generators and Waste Heat Boilers," Technische Universität Berlin Institut für Energietechnik, Berlin, 2017.
18. J. Kotowicz, M. Job, M. Brzęczek, K. Nawrat and J. Mędrych, "The methodology of the gas turbine efficiency calculation," pp. 20-32, 2016.
19. "World Nuclear Association," 2022. [Online]. Available: https://www.world-nuclear.org/information-library/nuclear-fuel-cycle/nuclear-power-reactors/nuclear-power-reactors.aspx. [Accessed April 2024].
20. YUNUS A.ÇENGEL, MICHAEL A. BOLES, THERMODYNAMICS: AN ENGINEERING APPROACH, 8 ed., New York: McGraw-Hill Education, 2015.
21. "https://www.rosenergoatom.ru/," Rosenergoatom JSC, [Online]. Available: https://www.rosenergoatom.ru/en/npp/leningrad-npp/. [Accessed June 2024].

INSTRUCTIONS FOR AUTHORS

1. "The Baku Engineering University Mechanical and Industrial engineering" accepts original unpublished articles and reviews in the research field of the author.
2. Articles are accepted in English.
3. File format should be compatible with **Microsoft Word** and must be sent to the electronic mail (**journal@beu.edu.az**) of the Journal. The submitted article should follow the following format:

- Article title, author's name and surname
- The name of workplace
- Mail address
- Abstract and key words

4. The title of the article should be in each of the three languages of the abstract and should be centred on the page and in bold capitals before each summary.
5. **The abstract** should be written in **9 point** type size, between **100** and **150** words. The abstract should be written in the language of the text and in two more languages given above. The abstracts of the article written in each of the three languages should correspond to one another. The keywords should be written in two more languages besides the language of the article and should be at least three words.
6. .**UDC** and **PACS** index should be used in the article.
7. The article must consist of the followings:

- Introduction
- Research method and research
- Discussion of research method and its results
- In case the reference is in Russian it must be given in the Latin alphabet with the original language shown in brackets.

8. **Figures, pictures, graphics and tables** must be of publishing quality and inside the text. Figures, pictures and graphics should be captioned underneath, tables should be captioned above.
9. **References** should be given in square brackets in the text and listed according to the order inside the text at the end of the article. In order to cite the same reference twice or more, the appropriate pages should be given while keeping the numerical order. For example: [7, p.15].

Information about each of the given references should be full, clear and accurate. The bibliographic description of the reference should be cited according to its type (monograph, textbook, scientific research paper and etc.) While citing to scientific research articles, materials of symposiums, conferences and other popular scientific events, the name of the article, lecture or paper should be given.

Samples:

a) ***Article:*** Demukhamedova S.D., Aliyeva İ.N., Godjayev N.M.. *Spatial and electronic structure af monomerrik and dimeric conapeetes of carnosine üith zinc,* Journal of structural Chemistry, Vol.51, No.5, p.824-832, 2010

b) ***Book:*** Christie ohn Geankoplis. *Transport Processes and Separation Process Principles*. Fourth Edition, Prentice Hall, p.386-398, 2002

c) ***Conference paper:*** Sadychov F.S., Aydın C., Ahmedov A.İ.. Appligation of Information – Commu-nication Technologies in Science and education. II International Conference."*Higher Twist Effects In Photon- Proton Collisions", Bakı, 01-03 Noyabr, 2007, ss 384-391*

References should be in 9-point type size.

10. The margins sizes of the page: - Top 2.8 cm. bottom 2.8 cm. left 2.5 cm, right 2.5 cm. The article main text should be written in Palatino Linotype 11 point type size single-spaced. Paragraph spacing should be 6 point.
11. The maximum number of pages for an article should not exceed 15 pages
12. The decision to publish a given article is made through the following procedures:

- The article is sent to at least to experts.
- The article is sent back to the author to make amendments upon the recommendations of referees.
- After author makes amendments upon the recommendations of referees the article can be sent for the publication by the Editorial Board of the journal.